Stochastic analysis of clear timber as a structural material

THÈSE N^{O} 6944 (2016)

PRÉSENTÉE LE 17 MAI 2016

À LA FACULTÉ DE L'ENVIRONNEMENT NATUREL, ARCHITECTURAL ET CONSTRUIT
LABORATOIRE DE CONSTRUCTION EN COMPOSITES
PROGRAMME DOCTORAL EN GÉNIE CIVIL ET ENVIRONNEMENT

ÉCOLE POLYTECHNIQUE FÉDÉRALE DE LAUSANNE

POUR L'OBTENTION DU GRADE DE DOCTEUR ÈS SCIENCES

PAR

Alireza FARAJZADEH MOSHTAGHIN

acceptée sur proposition du jury:

Prof. Ph. Thalmann, président du jury
Dr A. Vasilopoulos, Prof. S. Franke, directeurs de thèse
Prof. A. Frangi, rapporteur
Prof. J. Köhler, rapporteur
Prof. E. Brühwiler, rapporteur

ÉCOLE POLYTECHNIQUE
FÉDÉRALE DE LAUSANNE
Suisse
2016

To my parents

Preface

As a non-toxic, renewable natural material, that does not leak chemicals, can be safely handled, while usually, it is widely available within a short distance between production and construction sites, wood/timber is nowadays widely used as an important construction material in structures such as houses, bridges, domes, and piers. The embodied energy in timber is one of the lowest between all common construction materials; timber stores the carbon from the atmosphere and reduces the greenhouse effect. It is also a good thermal insulator reducing the energy necessary for heating and operating a building.

Nevertheless, timber has a complex mechanical behaviour, presenting a high degree of anisotropy in its, inherently, highly variable mechanical properties. This variability includes statistical and spatial variabilities and leads to randomness in the response of timber structural components.

To obtain an accurate estimation of the reliability of timber structures under external loading, probabilistic/stochastic approaches, capable of properly taking into account the random spatial variability of the material properties, are needed.

The Thesis of Alireza addresses new topics concerning the variability of the mechanical properties of clear timber along and transverse to the grain and the way it affects the structural integrity of timber structures. In addition to the extensive experimental program and the database that has been provided, a new computational framework was developed for the modelling of the failure of timber structures taking into account the effect of size and variability. A numerical/analytical size effect model has also been developed taking into account the random spatial variability in the strength field by using the theory of random fields.

It is obvious that further analysis is necessary in order to derive a well-established model, however, this Thesis introduces for the first time such procedure for timber structures' design with random spatial variability and could be the basis for additional developments in the field.

I would like to acknowledge the financial support of this Thesis by the Swiss National Science Foundation through the NRP 66 "Research Wood" research framework, (Grant No. 406640_136680).

Dr. Anastasios P. Vassilopoulos

EPFL/CCLab

Abstract

Wood/timber has been widely used for house and bridge construction. It is a widely available natural material that necessitates low energy for the production, following simple processes. The environmentally friendliness, together with the low cost of raw material makes it an efficient building material. Moreover, timber possesses attractive mechanical properties such as high specific strength and stiffness. In contrast, timber constructions have, to a large extent, been based on experience and craftsmanship, which prevents taking full advantage of this material. There are several reasons for this. Timber has a complex mechanical behavior being a natural highly anisotropic fiber composite, with properties that are also affected by moisture content. For specific species, geographical location, local growth conditions and moisture content, the material properties depend, among others, on the age, the structural imperfections, the location of timber within the tree, and load history. Consequently, the mechanical properties of timber are, inherently, highly variable. Variability of timber properties includes statistical and spatial variabilities, referred to as random spatial variability (RSV). This entails adopting a probabilistic/stochastic approach to analysis of timer structures.

The aim of this research is to understand and model the effect of the RSV on the clear timber mechanical properties, as well as the experimental characterization of RSV for clear timber, and also to develop a stochastic finite element framework for random response assessment of clear timber components.

A size effect model was developed which takes into account the RSV in the strength field. The theory of random fields was used for this purpose. Using the spectral representation scheme, realizations of strength field in each specimen were generated. The stochastic response was obtained via the Monte Carlo method. The model results was compared to the existing experimental data in the literature. Also, an analytical expression was provided to facilitate the application of the model.

Clear timber specimens of different lengths were fabricated for longitudinal tensile tests. Local deformations along the lengths of the specimens were recorded during the tests in order to characterize the RSV in longitudinal properties. A connection between the mesostructure of the clear wood and its local elastic modulus was observed. Statistics concerning the elastic modulus, strength and strain to failure and the effect of length change on these properties were extracted. The correlations between the strength, the elasticity and the density were obtained.

Transverse properties were also investigated which are of particular importance in some applications such as mechanical and adhesively-bonded timber joints. Regularly positioned and randomly positioned specimens were cut from different timber boards. Statistics and size effects concerning the elastic modulus, strength and strain to failure as well as the correlation between the properties were studied. The spatial variability in the transverse elastic modulus, the tensile strength and the failure strain was also experimentally studied. Mesostructural patterns of clear timber were shown to have a direct effect on the local elastic modulus.

Finally, a stochastic finite element framework was established by combining the spectral representation scheme for RSV modelling and the finite element software ABAQUS in a non-intrusive manner. This framework can be used for the stochastic structural response assessment of timber structural components made of clear timber. To show the applicability of the model in real applications, the failure of adhesively bonded double-lap timber joints were simulated under tensile loading. The effect of size on the strength was also taken into account. The results were in a fairly well agreement with the available experimental data in the literature.

Keywords: Clear timber; Experimental characterization; Mechanical properties; Random spatial variability; Size effect; Mechanical tests; Stochastic finite element; Bonded joints; Monte Carlo

Résumé

Le bois a été largement utilisé dans la construction de bâtiments et de ponts. Il est largement disponible dans la nature et nécessite une faible quantité d'énergie pour sa production. Le bois est ainsi un matériau écologique et économique ce qui le rend très attractif dans le domaine de la construction. Le bois a des propriétés mécaniques très intéressantes comme une haute résistance et une haute rigidité spécifique. Pourtant, jusqu'à nos jours la majorité des constructions en bois ont été réalisées sur la base de l'expérience et du savoir-faire, ce qui limite l'exploitation des performances de ce matériau. De nombreuses raisons expliquent cette réalité. Le bois a un comportement mécanique complexe, il s'agit d'un matériau composite naturel, fortement anisotrope et dont les propriétés sont influencées par son taux hygroscopique. Ses propriétés mécaniques dépendent de l'âge, des défauts structuraux, de sa position dans le tronc de l'arbre et de l'historique de chargement. Par conséquent, les propriétés mécaniques du bois sont extrêmement variables. La variabilité des propriétés du bois comprend la variabilité spatiale et statistique, connue comme random spatial variability (RSV). Ceci entraine l'adoption d'une approche probabiliste/stochastique pour l'analyse du bois.

L'objectif de cette recherche est la compréhension et la modélisation l'influence que la RSV sur les propriétés mécaniques bois sans défaut et la caractérisation expérimentale de la RSV du bois sans défaut d'éléments structuraux en bois sans défaut.

Un modèle de l'effet de taille a été développé en considérant la RSV dans le champ de contraintes et en appliquant la théorie des champs aléatoires. Les champs de contraintes ont été générés pour chaque échantillon en utilisant le plan de représentation spectral. La réponse stochastique a été obtenue par la méthode Monte Carlo. Les résultats du modèle ont été comparés aux valeurs expérimentales présentes dans la littérature. De plus, une expression analytique a été établie afin de faciliter l'application du modèle.

Des échantillons de bois pur de longueurs différentes ont été sollicités en traction dans la direction longitudinale. Les déformations locales tout au long des échantillons ont été mesurées afin de caractériser la RSV des propriétés longitudinales. Une relation entre la mésostructure du bois pur et le module d'élasticité local a été observée. Des valeurs statistiques du module d'élasticité, de la résistance et de la déformation à la rupture ainsi que l'effet de la longueur sur ces propriétés ont été extraites. Les corrélations entre la résistance, le module d'élasticité et la densité du bois ont été établies.

Les propriétés dans la direction transversal, importantes pour certaines applications telles que les assemblages mécaniques et les assemblages collés ont été analysées. Des échantillons ont été découpés de manière régulière et de manière aléatoire dans différentes planches en bois. Des valeurs statistiques du module d'élasticité, de la résistance et de la déformation à la rupture, les effets liés aux dimensions des échantillons ainsi que la corrélation entre ces diverses propriétés ont été étudiées. La variabilité spatiale du module d'élasticité, de la résistance à la traction et de la déformation de la rupture dans la direction transversale a été étudié de façon expérimentale. Les résultats ont montrés que la mésostructure du bois sans défauta une influence directe sur le module d'élasticité local.

Finalement, un modèle stochastique d'éléments finis a été établi en combinant le schéma de la représentation spectral utilisé pour la simulation de la RSV et le logiciel d'éléments finis Abaqus. Il permet d'évaluer la réponse structurale stochastique d'éléments structuraux en bois sans défaut. Afin de montrer l'application du model aux situations réelles, la rupture d'assemblages à double recouvrement collés solicités en traction a été simulée. L'effet de taille sur la résistance a été pris en considération. Les résultats obtenus étaient en accord avec les valeurs expérimentales présentes dans la littérature.

Mots clés: Bois sans défaut, Caractérisation expérimentale, Propriétés mécaniques, Variabilité spatial aléatoire, Effets de taille, Essais mécaniques, Eléments finis stochastiques, Joints collés, Monte Carlo.

Acknowledgments

During the past three years and a few months, many people have encouraged and supported me to complete my doctoral studies. I would like to acknowledge all those who provided me with the circumstances for this accomplishment.

First of all, I would like to express my gratitude toward my thesis directors: Dr. Anastasios Vassilopoulos for giving me the opportunity to work on this research project, his support, his guidance and our fruitful discussions and Prof. Steffen Franke, from Bern University of Applied Sciences, for his continuous support and recommendations. I would also like to give special thanks to Prof. Thomas Keller for his co-supervision role, contributions and instructions, and our rich discussions during the course of this PhD thesis.

I wish to acknowledge the exceptional sources of support from the National Research Program NRP 66 of the Swiss National Science Foundation (Grant No. 406640-136680).

I also wish to express my thanks to the thesis defense committee for devoting the time and effort to read and evaluate my thesis and for their constructive suggestions: Prof. Eugen Brühwiler, head of the Structural Maintenance and Safety Laboratory (MCS), EPFL; Prof. Andrea Frangi, Department of Civil, Environmental and Geomatic Engineering, ETH Zürich; Prof. Jochen Köhler, Department of Structural Engineering, Norwegian University of Science and Technology, Norway; and Prof. Philippe Thalmann, Head of the Laboratory of Environmental and Urban Economics (LEURE), EPFL, the president of the jury.

I am thankful to the professional team in the laboratory (IIC-EPFL) for their help and support, Sylvain Demierre for his technical coordination and advice; Gilles Guignet for his help with conducting the experiments and using video-extensometry system, Patrice Gallay, Roland Gysler, Gérald Rouge, Léa Frédérique Dubugnon and François Perrin for their help and support. I would also thank Antoine Gagliardi and his colleagues from Atelier Maquettes, EPFL, for discussions on specimen design and fabricating specimens.

I would also like to thank those who provided technical and administrative support, Prof. Andreas Müller, from Bern University of Applied Sciences, Biel, Switzerland, for his great administrative coordination and support, Ms. Margaret Howett for the professional English corrections of the thesis, Ms. Magdalena Schauenberg and especially Ms. Saira Banu Mohamed-Kanani for all their administrative coordination and support, and Kyriaki Goulouti and Dr. Julia de Castro for translating the English abstract into French (Résumé).

I am also thankful to my current colleagues at CCLAB, EPFL, Dr. Julia de Castro, Dr. Chao Wu, Sonia Yanes Armas, Kyriaki Goulouti, Haifeng Fan, Maria Savvilotidou, Myrsini Angelidi, Abdolvahid Movahedirad, Aida Cameselle Molares and Joao Sousa for their support and providing a friendly environment as well as my ex-colleagues Dr. Roohollah Sarfaraz Khabbaz, Dr. Moslem Shahverdi, Dr. Michael Osei-Antwi, Dr. Carlos Pascual Agullo and Dr. Wei Sun.

I greatly appreciate my friends for their support, and last but not least, my sincere gratitude goes to my family for their continuous support and love, particularly my parents for their extraordinary sacrifices throughout my life.

Alireza Farajzadeh Moshtaghin

Table of contents

1 Introduction

1.1 Motivation

Wood/timber has been widely used traditionally as an important construction material in structures such as houses, bridges, domes, and piers. In 2014, the total consumption of industrial roundwood, sawnwood and wood-based panels was estimated as being 560 million m^3 [1]. There are several reasons for considering timber as an efficient material for construction. Timber is a non-toxic, renewable natural material, does not leak chemicals, can be safely handled with bare hands, while, usually, it is widely available within a short distance between production and construction sites. Relatively very little energy is used to convert the wood from trees to construction timber. The embodied energy in timber is one of the lowest all common construction materials. Timber stores the carbon from the atmosphere and reduces the greenhouse effect. Timber is also a good thermal insulator reducing the energy necessary for heating and operating a building, while it is versatile and also it is easy to work with, even with simple tools. It is also considered as a low-cost material. Finally, timber possesses attractive mechanical properties such as a high strength to weight ratio.

Nevertheless, timber has a complex mechanical behavior as a highly anisotropic fiber composite material. Given specific species, geographical location, local growth conditions and moisture content, the material properties depend on factors such as age, structural imperfections, location of timber within the tree, and load history. Consequently, the mechanical properties of timber are, inherently, highly variable. For these reasons, a high level of expertise is needed to take full advantage of timber.

In current practice, design codes are normally used as guidelines for constructing timber structures. These codes, often, are outdated and have not evolved by incorporating new information regarding the design of timber structures. In some cases, such as for the design of adhesively-bonded timber joints, there is no available code at all. One main concern, which has recently received attention from researchers, is the high scatter/variability in the mechanical properties of timber and its incorporation in design codes [2]. This variability includes statistical and spatial variabilities and is sometimes referred to as random spatial variability (RSV) [3]. This variability leads to randomness in the response of structures and components made of timber. To obtain an accurate estimation of the reliability of timber structures under external loading, probabilistic/stochastic approaches, capable of properly taking into account the RSV of the material properties, are needed.

On the other hand, following a deterministic approach often results in overdesigned structures and increases expenses [4]. Also, as highlighted in a recent study on the random failure analysis of unidirectional composites [5], designs based on deterministic material properties can also overestimate the reliability of structures significantly.

The probabilistic design allows the estimation of reliability by incorporating the stochastic uncertainty in the data using probability density functions (PDFs) and correlations between parameters, based on which designs are certified to offer a given reliability level [6]. The performance is generally evaluated by means of a variable such as the displacement of a point, the maximum stress, maximum allowable load etc., or by a set of them. Variability in the performance of timber structures arises mainly from the variability in the mechanical properties, i.e. stiffness and strength parameters, and also from the variability of the external loading. Efforts have also been made to develop probabilistic/reliability based safety factors in order to minimize the difference between probabilistic design and classical deterministic design [2,6]. These are normally derived based on the available formulas for the limit states of structural components.

The mean value of timber strength, in its brittle failure modes such as those under longitudinal and transverse tensile loadings, decreases as its volume increases, which is known as the size effect on the strength. This is because the probability of occurrence of a weakest material point with a lower strength value increases with volume increase, due to the RSV in the strength field. Pure tensile tests on clear specimens of different sizes have been carried out in [7,8] in the case of longitudinal strength and [9-14] for transverse strength (solid timber and laminated timber specimens) to investigate the size effect. The results have shown an obvious size effect. Concerning finite element simulations, the effect of size in small volumes is important. In the context of this thesis, 'small volume' refers to the scale of a few millimeters or mesoscale. The reason is that the failure initiation occurs at a material point, to which the volume of a small element or the volume around an integration point is normally assigned. There is very limited experimental information on this in the literature.

The classical Weibull size effect law (CWSEL) [15] is commonly used in the literature for modeling this effect on clear timber strength [10,11,16-21]. Very few works in the literature have adopted any other approach than CWSEL to investigate the size effect in timber, especially in the transverse direction. In the case of transverse strength, Pedersen et al. [13] and Astrup et al. [14] conducted transverse tensile tests on bulk specimens with a double symmetry. They developed a deterministic model for the size effect observed from experiments. In [21], after reviewing size effect models, it is noted that "Although no conclusive evidence has yet arisen concerning the accuracy of probabilistic strength theories to describe the size effect in the strength of timber, the existence of significant size effects is largely accepted within the scientific community."

Random variable-based studies, i.e. not considering spatial variability, have been undertaken for different structures; however, the significance of spatial variability for the accurate estimation of the stochastic structural response has been only highlighted in recent studies [22-25]. The theory of random fields has been used in these studies for the representation of RSV. As a numerical method to model the RSV effect on the structural response, stochastic finite element (SFE) modeling has received special attention [26], in spite of being computationally demanding. The consideration of spatial variability, within a stochastic finite element framework, may bring advantages in terms of material utilization, and would result in more accurate estimations of reliability. A recent comprehensive review of different aspects of the SFE method can be found in [26].The focus of the current study is on the experimental characterization of size effects and RSV for mechanical properties of clear timber and development of size effect and SFE models for analysis of clear timber components such as bonded joints.

1.2 Wood as a structural material

Wood is produced by trees in nature. Over million years, its structure has evolved into an optimized efficient system to support the crown, conduct mineral solutions and store food materials. There are about 30,000 different species in the world [27].

Different products made of timber can be classified into three groups. The first is solid timber, and the objective is to produce as efficiently as possible timber with specific dimensions having a quality of surface suitable for the intended use. The second includes board materials such as Chipboard, oriented strand board and fiber board. The third is laminated timber which consists of products such as glulam and laminated veneer lumber. Some of the advantages of the second and third groups over solid timber are lower degrees of variability, lower anisotropy and higher dimensional stability.

Unlike many other materials used in construction industry, solid timber cannot be manufactured to a particular specification. Instead, the best use should be made of the material already produced, although the type of timber can be selected from the wide range available. Timber as a material is a low-density, cellular, hygroscopic, viscoelastic, inhomogeneous, anisotropic polymeric composite. Regarding its high strength to weight ratio and low cost, timber is the most successful fiber composite in the world [27].

Woods from different trees are usually classified into two general groups: hardwood and softwood. Hardwood trees are generally broad-leaved deciduous trees which carry their seeds in seedcases such as beech and maple, while softwoods are generally coniferous trees such as Douglas-fir, spruce and larch. The wood from a tree can be divided into two parts, heartwood and sapwood. Heartwood surrounds the central part of the tree trunk and sapwood surrounds

the heartwood. From a structural-botanical point of view, wood contains many cells. These cells have different functions depending on their location in the tree. Inner cells, located in the heartwood and in which the reserve materials, e.g. starch, have been removed or converted into resinous substances, are mostly dead and provide mechanical support for the tree. Heartwood is generally darker than sapwood, although the two are not always clearly differentiated [27]. Cells located in the sapwood store nutrients and act as conduits for water. Each year, a ring of small width is added to the wood in the tree. As a result of different conditions during the growing season, there are usually two distinguishable parts within each ring, earlywood and latewood, which are more distinguishable in softwoods.

Figure 1.1 shows different parts of cross section of a cut tree trunk, also known as log. At the center of the section, there is a small core of soft, spongy tissue called pith. A few growth rings around the pith have often higher width and lower density and mechanical properties, which are named juvenile wood. Surrounding the juvenile wood are heartwood and sapwood. A thin layer of living reproductive cells called cambium surrounds the sapwood and forms a new growth rings and bark cells. Bark is the outer part of a tree trunk composed of inner living and outer dead bark.

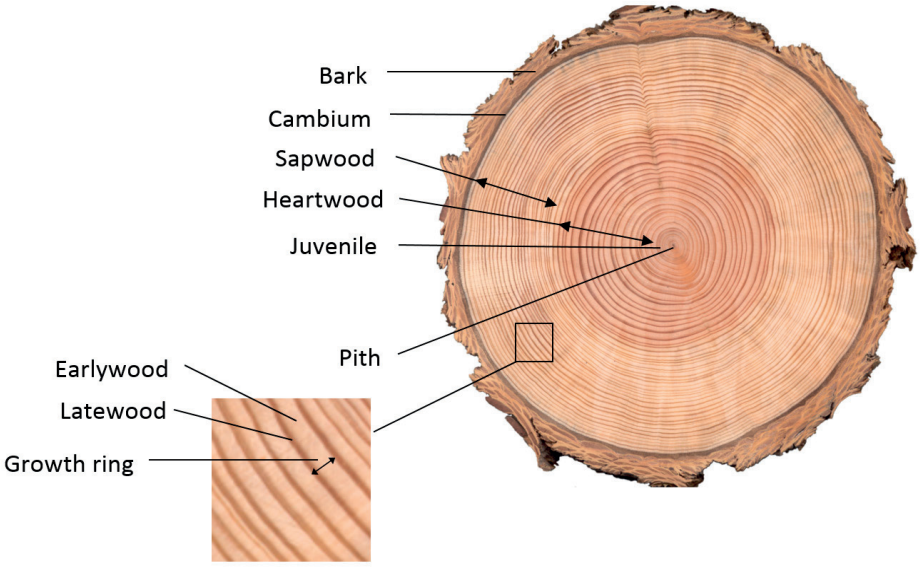

Fig. 1.1: Different parts of a tree in a cross-sectional view of trunk

A schematic illustration of the three main structural planes in a tree trunk is shown in Fig. 1.2. As can be seen, there are three principal directions, longitudinal L, radial R and tangential T, in each tree trunk, and correspondingly, three principal planes which are called cross-sectional or TR plane, radial of LR plane and tangential or LT planes. Most of the cells which contribute to the stiffness and strength of timber are aligned in the longitudinal (axial) direction. Therefore, timber has superior mechanical properties in the axial direction. Also, the mechanical properties

are higher in the radial direction than in the tangential direction. Timber is usually considered to be an orthotropic material in mechanical studies [28-30].

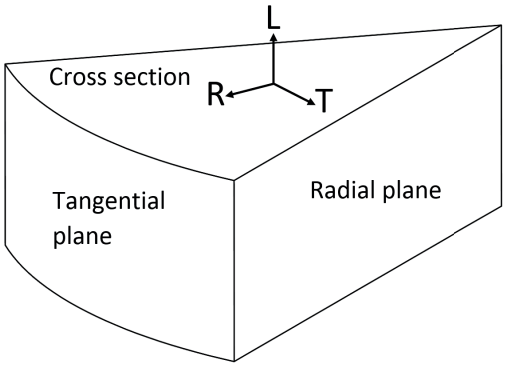

Fig. 1.2: Schematic illustration of a wedge-shaped segment of a tree showing the principal directions and planes

Irregular patterns of wood mesostructure that can be seen in timber pieces in Fig. 1.3, as one might intuitively understand, lead to spatially different local mechanical properties. Also, timber pieces like in Fig. 1.3 can be cut from different positions in a tree and have different overall properties as well.

Fig. 1.3: Irregular structural patterns in timber pieces

1.2.1 Factors affecting mechanical properties of timber

Factors affecting mechanical properties of timber are as follows:

Grain direction: The term ‘grain’ usually refers to the arrangement of aligned cells in the tree longitudinal direction. As already mentioned, the mechanical properties change largely from longitudinal direction (parallel to grain) to transverse (perpendicular to grain) direction. Due to being a natural material, the grain direction always oscillates around the nominal direction of tree stem, which also affects the properties [27].

Reaction wood: Action of wind on a tree or a sloping ground can cause an inclination in the tree stem with respect to the vertical/gravitational axis [27]. This changes the distribution of growth hormones in the tree and an abnormal tissue called reaction wood is formed. In hardwoods, this tissue is formed on the side of the trunk that is under tension, known as tension wood. In tension wood, tensile strengths are higher and compression strengths are lower than normal wood. In softwoods, this tissue is formed on the side of the trunk that is under compression, referred to as compression wood. Its compression strength is higher and its tensile strength and toughness are lower than in normal timber.

Spiral grain: A tree is said to have spiral grain when the average direction of its grain has an obvious difference with respect to the nominal axis of the trunk, which looks like a spiral. The mechanical properties of pieces of sawn timber are negatively affected by spiral grain [32].

Localized defects: Knots are the most common defects in pieces of timber caused by branching in trees. They are imperfections associated with gain distortion. They also cause grain deviation in the surrounding area. Since the mechanical properties are changed with grain direction, knots can have a major negative effect on the properties. The level of this effect is a function of their size, distribution and the type of the knot. Larger knots and more frequently distributed knots are more influential. The deformation and failure behavior of knot clusters have been studied in [33,34]. Also, dead knots, which cause discontinuity in timber are more critical than green knots, which are completely connected to the surrounding timber. Other localized defects are checks, shakes and splits. These cause discontinuities in timber [31].

Decay: Wood, as a product of nature, is biodegradable. Different natural agents such insects can cause decay, but fungi, some low forms of plant life, can causes the highest damage [31]. Decay deteriorates the mechanical properties.

Density: Density is considered as the best indicator for the mechanical properties [27]: the higher the density, the higher the elastic modulus and strength. Density of wood can vary significantly even within a single tree. At mesoscale, in which the material can be considered as a continuous medium, the density of clear timber is a function the ratio between late wood and earlywood. The latewood is denser than earlywood. Also, the density of each one can change from one growth ring to another [27].

Factors which are independent of the structure of wood itself, but can affect the mechanical properties are moisture content, temperature and time (rate and duration of loading) [27].

1.2.2 Small clear timber specimens versus structural-sized lumber

Clear timber refers to defect-free wood from a tree. Small clear specimens are normally tested to specify the characteristic properties of each species. These specimens are usually considered to be homogeneous in mechanical analyses of wood [35,36]. Nevertheless, it will be

experimentally shown in this thesis that there are significant changes in the local mechanical properties within clear timber specimens.

Structural-sized solid timber known as lumber may contain different kind of defects such as knots, checks and spiral grain. These timber pieces, which are used as members in timber structures, are cut from logs by sawing in the form of rectangular elongated pieces of wood. The nominal axis of the lumber is intended to coincide with the parallel to grain direction. Due to inherent variability in timber properties, lumbers are graded based on their expected service performance. In grading lumbers, it is tried to evaluate the desired material properties such as bending strength, based on other properties that can be measured in a non-destructive manner, such as stiffness and density, or by visual assessment of the quality of lumber.

1.2.3 Mesoscale and clear wood

The mesoscale of wood spans from a few millimeters to several tens of millimeter. In this scale, a connection between the local mechanical properties and the mesostructure of clear timber can be made. The mesostructure of clear wood is mainly characterized by earlywood-latewood and growth ring arrangements and grain deviations. These can be seen in Figs. 1.2 and 1.3 in transverse and longitudinal sections, respectively. The mesostructure of clear wood in specimens cut in the longitudinal and transverse directions are studied in Sections 3.3 and 5.2.

1.2.4 Orthotropic elasticity and timber

Orthotropic elasticity is usually used to describe timber elastic behavior [28-30]. It is assumed that the three principal elasticity directions coincide with the L, R and T directions of the wood structure. The curvature of the tangential faces is neglected in this assumption. This assumption becomes more acceptable, as the distance from the tree center increases.

$$\begin{bmatrix} \varepsilon_{LL} \\ \varepsilon_{TT} \\ \varepsilon_{RR} \\ 2\varepsilon_{TR} \\ 2\varepsilon_{LR} \\ 2\varepsilon_{LT} \end{bmatrix} = \begin{bmatrix} \frac{1}{E_L} & \frac{-\nu_{LT}}{E_T} & \frac{-\nu_{LR}}{E_R} & 0 & 0 & 0 \\ \frac{-\nu_{LT}}{E_T} & \frac{1}{E_T} & \frac{-\nu_{TR}}{E_R} & 0 & 0 & 0 \\ \frac{-\nu_{LR}}{E_R} & \frac{-\nu_{TR}}{E_R} & \frac{1}{E_R} & 0 & 0 & 0 \\ 0 & 0 & 0 & \frac{1}{G_{TR}} & 0 & 0 \\ 0 & 0 & 0 & 0 & \frac{1}{G_{LR}} & 0 \\ 0 & 0 & 0 & 0 & 0 & \frac{1}{G_{LT}} \end{bmatrix} \begin{bmatrix} \sigma_{LL} \\ \sigma_{TT} \\ \sigma_{RR} \\ \sigma_{TR} \\ \sigma_{LR} \\ \sigma_{LT} \end{bmatrix} \tag{1.1}$$

Nine independent parameters are needed to construct the elasticity matrix of the timber in 3D space: three elastic moduli in L, R and T directions, three shear moduli in LR, LT and TR planes and three Poisson ratios. The constitutive equation for timber, considered as an orthotropic material, is given in Eq. (1.1).

The assumption of plane stress state and transverse isotropy for clear timber [19,20] is considered for the case study performed in Chapter 6. In this case, Eq. (1.1) is simplified to

$$\begin{bmatrix} \varepsilon_{11} \\ \varepsilon_{22} \\ 2\varepsilon_{12} \end{bmatrix} = \begin{bmatrix} \frac{1}{E_{11}} & \frac{-\nu_{12}}{E_{22}} & 0 \\ \frac{-\nu_{12}}{E_{22}} & \frac{1}{E_{22}} & 0 \\ 0 & 0 & \frac{1}{G_{12}} \end{bmatrix} \begin{bmatrix} \sigma_{11} \\ \sigma_{22} \\ \sigma_{12} \end{bmatrix} \tag{1.2}$$

where 1 and 2 correspond to longitudinal and transverse directions. Longitudinal and transverse tensile and longitudinal and shear behavior are often assumed as linear up to failure [13,14,16-21], although some degrees of non-linearity might be present, as was observed in Chapter 4 for transverse tensile behavior. Tensile longitudinal and transverse mechanical behavior of clear timber are studied in Chapters 3 and 4, respectively. In longitudinal and transverse compression, however, there are significant plastic deformation that cannot be neglected [27]. Schematic illustration of compressive stress-strain behavior of clear timber in the longitudinal and transverse directions are shown in Fig. 1.4a and b.

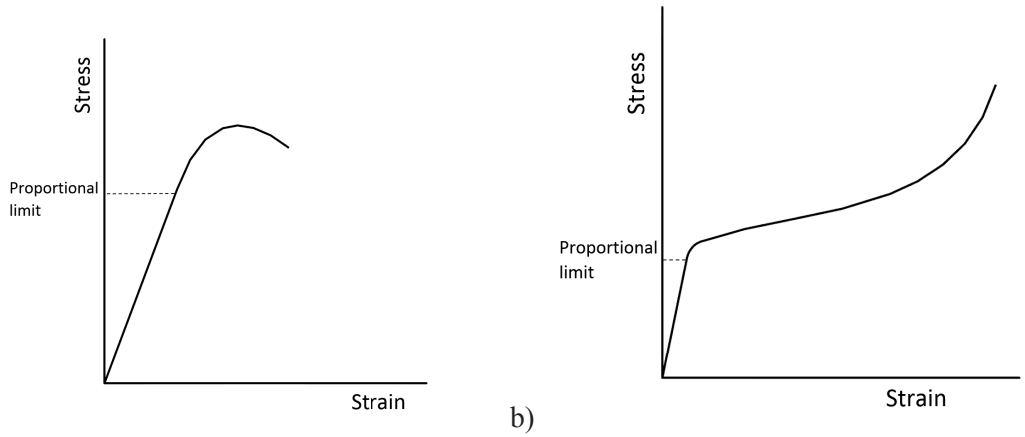

Fig. 1.4: Schematic illustration of stress-strain behavior of clear timber: a) Longitudinal compression b) Transverse compression.

1.3 Uncertainty

Uncertainty is the lack of certainty caused by incomplete and/or unknown information in a situation. In an uncertain situation, one cannot exactly predict an outcome. Mathematical models and experimental measurements can be uncertain in different ways. The following is a list of potential sources of uncertainty that could be present in this project:

- Inherent uncertainty of parameters: This originates from the parameters whose values change randomly in different measured samples such as clear timber mechanical parameters or wind velocity components. The uncertainty in the material properties is also referred to as material randomness.
- Uncertainty in statistics of collected data: This usually results from limited number of tests or observations for a target parameter such as strength parameters.
- Uncertainty due to manufacturing process: The final specimen dimensions might not be exactly the same as expected due to imperfection of the fabrication process which can affect its performance.
- Model uncertainty: This originates from lack of knowledge about the true underlying phenomenon. This also includes the uncertainty from various simplifications/assumptions in the process of modeling, such as assuming an orthotropic behavior for timber.
- Numerical uncertainty: This is due to numerical errors or numerical approximations. Often, due to complexity of models, it is impossible to find the exact solution and resorting to numerical methods, such as Gaussian quadrature for approximation of a definite integral or finite element discretization, as in Chapter 6, for solving a structural problem, becomes necessary. This, however, introduces numerical uncertainty. Considering the current state of computational tools, the numerical uncertainty cannot be eliminated. It can only be minimized or bounded [37].
- Measurement/observation uncertainty: If a measurement is done several times following the exact same setting, no matter how small, there will inevitably be a scatter in the results. For example, the way in which a person fixes a specimen in a testing machine can affect the measured value for the required parameter.
- Testing machine uncertainty: Any testing machine, such as tensile test machines used for tests of Chapter 3 and Chapter 4, has a certain level of accuracy which introduces an uncertainty in the collected data from the test.
- Interpolation/extrapolation uncertainty: The uncertainty introduced when interpolating or extrapolating output data from simulations or experiments for other input settings for which no output data is available.

From another point of view, uncertainty can be classified into two categories [38]. The first is called aleatoric, also known as stochastic/irreducible uncertainty. It is a physical variability in a system or its environment. Parameters that change their values each time the same experiment

is performed, have aleatoric uncertainty. For example, if an arrow is shot several times by a mechanical machine, it will hit the same point on the target due to complex vibrations of the arrow shaft. Another example is the strength of wooden specimens with the same geometry tested in the same conditions. The strength randomly changes from one specimen to the other. Also, there is an aleatoric uncertainty involved in predicting the result of rolling a dice. It is sometimes argued that considering this uncertainty as irreducible is due to lack of sufficient progress in the current science and technology. Probabilistic approaches such as Monte Carlo are used to analyze this kind of uncertainty, as is done in the current study.

Epistemic uncertainty, also known as systematic/reducible uncertainty, is due to lack of knowledge. In other words, it originates from things that we could know to reduce the uncertainty, but in practice we do not. This can be due to lack of sufficient accuracy in measuring a quantity, assumptions involved in the mathematical model and neglecting some effects. Better calibration and improvement of the model can reduce this kind of uncertainty.

Often, in studies on the stochastic structural response assessment of timber or composite structures [5,6,17-21,23-25], as in this thesis, the focus is on the effect of uncertainties in material properties as well as in loading, if present, although other above mentioned uncertainties might exist as well. This is because the level of uncertainty in the properties of these materials is so high that it usually acts as the main factor causing the uncertainty in the structural response. Concerning the randomness in the local elastic moduli investigated in the thesis, the total/ensemble variability is a results of the variability of moduli within each individual specimen, designated as within specimen variability, and the variability of moduli that occurs by changing specimens, referred to as between specimen variability. The latter implies that different specimens can have different average moduli. In the analyses done on the results of performed tests and estimation of the statistics of the properties, both the variability within specimens and between specimen variability were considered. In Sections 3.5.1 and 5.3.1, contributions of within specimen variability and between specimen variability to the total/ensemble variability of the local longitudinal and transverse elastic moduli are discussed.

It is noted that beside safety and uncertainty issues related to randomness of material properties and loading, there are also other safety related issues such susceptibility of timber to fire [39-42] which are not discussed in this thesis.

1.3.1 Statistical distributions

Probability density functions (PDF) such as Weibull and normal are used to represent the uncertainties in the mechanical properties of clear timber. $\mathrm{f}(x)$, defined over real numbers, can be a PDF for the continuous random variable X if: 1) $\mathrm{f}(x) \geq 0$, for all $x \in R$. 2) $\int_{-\infty}^{\infty} \mathrm{f}(x)\,dx = 1.$ 3) $P(a < X < b) = \int_{a}^{b} \mathrm{f}(x)\,dx$.

The PDF of the normal random variable X with mean μ and standard deviation σ is defined as:

$$\mathrm{f}(x)=\frac{1}{\sqrt{2\pi}\sigma}\exp(-\frac{1}{2\sigma^2}(x-\mu)^2),\ -\infty<x<\infty. \tag{1.3}$$

The PDF of the Weibull distribution is defined as

$$\mathrm{f}(x)=\frac{m}{\sigma_0}\left(\frac{x}{\sigma_0}\right)^{m-1}\exp\left[-\left(\frac{x}{\sigma_0}\right)^{m}\right],0\le x<\infty,m>0,\sigma_0>0 \tag{1.4}$$

where σ_0 and m are the scale and shape parameters of the Weibull distribution. The mean and standard deviation for this PDF are as follows:

$$\mu=\sigma_0\,\Gamma\left(1+1/m\right),\ \ \sigma=\sigma_0\left[\Gamma\left(1+2/m\right)-\left(\Gamma\left(1+1/m\right)\right)^2\right]^{0.5} \tag{1.5}$$

The random variable X has a lognormal distribution, if random variable Y with mean μ_Y and standard deviation σ_Y, defined by the equation $Y=\ln(X)$, follows a normal distribution. The PDF of X is:

$$\mathrm{f}(x)=\frac{1}{\sqrt{2\pi}x\sigma_Y}\exp\left[-\frac{1}{2}\left(\frac{\ln(x)-\mu_Y}{\sigma_Y}\right)^2\right],\ 0\le x<\infty \tag{1.6}$$

The mean and standard deviation are as follows:

$$\mu=\exp\left(\mu_y+\frac{{\sigma_y}^2}{2}\right),\ \ \sigma=\left[\left(\exp\left({\sigma_y}^2\right)-1\right)\exp\left(2\mu_y+{\sigma_y}^2\right)\right]^{0.5} \tag{1.7}$$

1.4 Design approaches in timber engineering

Traditionally, the safety of a timber structure or component is assessed via safety factors or partial safety factors. Since fixed values are assigned to load and resistance in these approaches, safety is presented as a deterministic measure. To ensure a target level of safety for the structure, the estimates of load and resistance are considered sufficiently high and sufficiently low, respectively [2]. In probabilistic analyses of timber structures, however, uncertainty of variables are directly taken into account via their respective PDFs. Therefore, a more accurate estimation of the reliability of the structure can be provided.

1.4.1 Allowable stress design (ASD): Safety factor approach

In allowable stress design, ASD, the stresses in the material due to service loads are compared with allowable stresses of the material [43]. The safety of the structures is defined by Eq. (1.8) [2]

$$\sigma_i \leq s_i \tag{1.8}$$

where σ_i is the i^{th} stress component due to service loads, normally obtained via linear stress analysis, and s_i is the corresponding allowable stress component. s_i is defined by dividing the strength parameter of the material s_{ui}, such as ultimate characteristic moment, tension and compression stresses, to a safety factor $\gamma > 1$

$$s_i = s_{ui} / \gamma \tag{1.9}$$

The values for γ is usually chosen with regard to experience, tradition, legal requirements and economic considerations. In this approach, the case of equality in Eq. (1.8) is considered as the failure condition.

1.4.2 Load and resistance factor design (LRFD): Partial safety factor approach

In 1990s, a new design format for timber structures called LRFD was completed by research community and wood industry [43]. In this approach, the effect of factored loads are compared with adjusted nominal capacities (resistance). Uncertainty and failure consequences are explicitly taken into account for developing factors for both resistance and loads which leading to a more differentiated safety analysis. LRFD format for structural members is expressed as [2]

$$\frac{z_d\, r_i}{\gamma_{\text{M}}} = \gamma_G G_i + \gamma_Q Q_i + \ldots \tag{1.10}$$

where r_i is a characteristic resistance of the member, γ_{M} is the partial factor for r_i and z_d is a design variable. G_i and Q_i are the characteristic permanent (dead) load and variable (live) load effects with corresponding partial factors γ_G and γ_Q. Experience, tradition and judgement have largely been involved in determining the partial factors.

Values for safety factors, partial safety factors and characteristic resistances and load effects are normally found in design codes. Characteristic values are normally determined based on the fractile values of the statistical distributions associated with the parameters. For more information on this topic can be found in [43] and in *ASD/LFRD Manual for Engineered Wood Construction* [44].

1.4.3 Reliability-based code calibration

Reliability-based code calibration is an approach for establishing consistent design formats for determining characteristic values of material parameters and partial safety factors. This is to provide consistent levels of safety for different type of structures using structural reliability methods such as FORM. LRFD is normally used as basis for formulating the partial safety factors. In order to determine the partial safety factors, the difference between reliability of a class of structures and a target reliability level should be minimized [45]. The basics of this kind of calibration of partial safety factors has been described in [46].

Concerning timber, Vrouwenvelder and Siems [47] used First-order second moment method to calibrate partial safety factors for building codes of Netherland for different structural members made of timber, steel and concrete. In 2002, Smith and Foliente [48] reported the current international practice for designing mechanical joints based on LRFD and issues for probability based calibration. Svensson and Thelandersson [49], discussed the effect of the change of the type of statistical distribution of random parameters in calibration of reliability based partial safety factors. The duration load factors in LRFD were calibrated using time varying stochastic processes in [50] for wind, snow and imposed loads. Köhler [2] and Köhler et al. [51] developed a probabilistic model code which was adopted by the Joint Committee on Structural Safety. Their approach considers several levels of complexity. The basic level focuses on the common LRFD aspects such as basic material random variables, basic limit state functions and different characteristics of timber. Several refinements have been introduced such as adding new information using Bayesian updating and modeling time dependent damage. Also, a hierarchical spatial variability model was proposed for bending strength.

1.4.4 Stochastic analysis of timber members with knots

Efforts have also been made to develop models to describe behavior of timber members with knots such as lumbers and glulams by considering spatial variability, often lengthwise, of the longitudinal elastic modulus and strength. These work are useful for designing load-bearing timber beams, or possibly columns. Sometimes, the analysis is merely done on the modulus of stiffness in these works. The stochastic input data to these models are usually collected by examining the behavior of smaller parts, with or without knots, of the member. Kline et al. [52] developed a stochastic model for lengthwise variability of elastic modulus of lumber, based on a second order Markov model. Lam and Varoglu [53,54] also conducted experimental and modelling investigations on the spatial variation in the compressive and tensile strengths of lumbers [53-55]. Their model was based on semivariogram and regression analyses and stochastic processes. Isaksson [56] experimentally studied the variability of bending strength within and between timber members. He also developed a model based on stochastic variables such as the distance between weak sections, length of weak sections, strength of weak sections

and strength between weak sections. A calibration based on the Swedish code format has also been performed.

Recently, Fink and Köhler [57], investigated the variability of stiffness properties of timber boards focusing on the effect of knots and knot clusters. They developed a hierarchical model that takes into account both within board variability and between board variability. Köhler et al. [58] developed and calibrated a probabilistic model for longitudinal strength of spruce boards with no longitudinal joints. In this study, a member was considered to be composed of weak sections caused by major knots or knot clusters. The distance between these sections was represented by Poisson stochastic process. More recently, a new approach for modelling tensile stiffness and strength of timber boards and finger joints [59] has been developed based on the dynamic modulus of elasticity and total knot are ratio as influencing random variables.

Fink et al. [60] conducted bending tests on glulam beams and studied the influence of variable material parameters, such as knot ratio and dynamic modulus of elasticity, on the capacity, bending stiffness and failure mechanism in the glulams. The implementation of the results in a numerical model was described.

1.4.5 Direct probabilistic approach and reliability

In the probabilistic analysis of structures or structural components, the final goal is to calculate the probability of survival or reliability, or equivalently the probability of failure. The reliability is defined by the following equation:

$$H = \int_{\mathbf{X}|F(\mathbf{X})\leq 1} p(\mathbf{X})\, d\mathbf{X} \tag{1.11}$$

where $\mathbf{X}$ is a vector which represents the uncertain variables affecting the state of the structure, $F(\mathbf{X})$ is the limit state function or failure criterion (or failure function (FF)) and $p(\mathbf{X})$ is the probability density function (PDF) of the problem being considered. $F(\mathbf{X}) \leq 1$ is the condition of non-failure.

The term ‘direct probabilistic approach’ in the context of this work refers to an approach for estimation of reliability of a chosen structure or component with regard to the uncertainty in material parameters and loading, without using design codes and safety factors for material properties and loading. This does not mean that for the final design of such a structure safety factors are not needed [61]. For potential sources of failure such as an imperfect theory, unknown failure mechanism and human error in fabrication, the safety factors are indispensable. This approach is usually followed in the case of structures/components for which no design code is available, or the code cannot directly be applied due to a change in the involved parameters such as geometry, loading and environmental conditions. An example would be design of adhesively bonded timber joints. Another case is when the effect of a new

phenomenon, which in design codes is not explicitly described, is to be investigated. In the case of clear timber structures, such a phenomenon can be RSV in the mechanical properties. This is because the effect of RSV on the reliability of clear timber has not been previously investigated, although its significant effect has been shown for composite structures, especially when low probabilities of failure are desired.

In this approach, beside the reliability analysis, normally due to lack of an overall (structural/member level) limit state, a structural analysis has to be performed. Usually, due to complexity of geometry or the phenomenon under investigation such as RSV, finite element method is used to obtain the multi-axial stress state within the structure/component. This is especially handy for incorporation of RSV into the analysis. In this case, Monte Carlo approach can conveniently be used for the reliability analysis. Some other reliability methods such as FORM and SORM introduced in the next section, are more convenient when a formula can be established that can directly relate the capacity of the structure/component to load and strength parameters. Three main decisions in this approach are about: (1) the material failure criterion, (2) influencing random factors, (3) reliability estimation method. The methods available in the literature for the evaluation of the reliability are classified into four groups in the following sections.

1.4.5.1 Fast probability integration methods

Fast probability integration methods are based on approximating the failure surface by a predetermined geometric form for which calculation of the reliability integral is practical. In the process of calculation, a most probable point is searched, and the failure surface is approximated by the geometric form. The distance between the origin and this point is called Reliability Index (RI) and expressed in units of standard deviation. The two most famous methods are called first order reliability method (FORM), which is more popular, and second order reliability method (SORM).

In FORM, a linear approximation of the FF is used in the vicinity of design point to estimate RI. Standard normal non-correlated variables are needed in this method; therefore, the vector of random variables **X** of the problem is transformed into the standard non-correlated vector **U**. Then, the reliability index can be obtained by [6]

$$\begin{aligned} &\mathrm{RI} = \min \sqrt{\left(\mathbf{U}.\mathbf{U}^{\mathrm{T}}\right)} \\ &\text{subject to}: \quad \mathrm{F}(\mathbf{U}) = 0 \end{aligned} \tag{1.12}$$

RI represents an Euclidean distance between the origin and the failure function $\mathrm{F}(\mathbf{U})$ in the non-correlated normal space. In case of correlations between the random variables, a Cholesky decomposition of the covariance matrix is used to transform the variables from the real space to the non-correlated standard space [62]. If there are some non-normal variables, Rackwitz–Fiessler technique can be employed [63]. If both correlations and non-normal variables exist at

the same time, Rosenblatt transformation is recommend [64]. Having found the value of RI, it is shown that the reliability can be expressed as $H = \phi(RI)$, where ϕ is the standard normal cumulative distribution function (CDF). Carbillet et al. [25] applied this method to evaluated the reliability of a laminated plate $[0/90]_s$ simply supported at two edges and subjected to the combined action of a uniform pressure and a concentrated force in its centre. They found that RSV has a significant effect on the probability of failure.

SORM is an enhancement of FORM, where the failure function is approximated about the most probable point, using a quadratic Taylor series expansion. Because of inevitable complicated integrations in this method, its applicability in reliability studies is restricted [65].

For some structures/components, such as timber joints with dowel type fasteners, analytical formula or experimental approximate formula for the load bearing capacity as a function of timber and fastener behavior geometrical dimensions can be found [2]. Based on these formula as a member-level limit state, the reliability of such a structure can be estimated based on FORM [2].

1.4.5.2 Monte Carlo method (MC)

Monte Carlo is a very straightforward and accurate method in reliability analysis [46]. This scheme consists of generating random values for stochastic input variables, then substituting them into the failure function and determining if the material fails or not. This procedure is repeated many times, and the reliability H is calculated as the ratio of the number of cases in which failure does not occur to total number of repetitions.

One drawback of the above method is that in cases of high reliability, the total number of simulations increases dramatically [6]. In an effort to overcome this limitation, some more efficient simulation methods have been developed. The importance sampling method appears to be the most promising technique for structural reliability problems [66]. This is a variance reduction technique which uses the idea that some of the input random variables in a simulation have more influence on the parameter being estimated than others. If these important values are emphasized by sampling more frequently, then the variance of the estimate is reduced.

1.4.5.3 Analytical Methods

To introduce more simplicity in reliability analysis, some analytical methods have been proposed in the literature, two of which have received more attention. Philippidis and Lekou [67] developed two analytical approaches, namely Edgeworth expansion method (EDW) and the introduction of Pearson's semi-empirical distribution function (PRS) for UD FRP composites under plane stress loading. In this work, only strengths were considered to be random, each following a Weibull distribution. The purpose of these two analytical approaches was to determine the CDF of the failure function F, based on which the failure probability can be calculated. EDW, which had been previously applied to off-axis composites for the case of

uniaxial tension [68,69], was used to predict the CDF under complex stress state in terms of individual component moments [70]. First, the failure function is expanded in a multivariable Taylor series about mean values of strengths. Then, this function along with central moments of individual strength parameters are used to calculate the central moments of random failure function. EDW uses a series expansion in terms of the standard normal CDF, $\phi(\mathrm{F})$, to approximate an unknown CDF in which the coefficients are functions of central moments of the random variable F. This is given by:

$$\mathrm{P(F)} = \phi(\mathrm{F}) - \frac{1}{3!}\frac{\mu_3}{\mu_2^{3/2}}\phi^3(\mathrm{F}) + \frac{1}{4!}\left(\frac{\mu_4}{\mu_2^2} - 3\right)\phi^4(\mathrm{F}) + \ldots \tag{1.13}$$

where μ_k is the central k-moment of the failure function F and $\phi^\mathrm{n}(\mathrm{F})$ is the nth derivate of the normal CDF $\phi(\mathrm{F})$. Later, this method was enhanced by the same authors considering random elastic properties and random thermal coefficients [5]. For the case of a rotor turbine blade, it was shown that variability of elastic properties affects the failure envelope considerably. In contrast, in the temperature range considered, the effect of thermal properties was negligible.

Alternatively, in PRS method, the unknown CDF of failure function can be fitted by empirical statistical distributions, if the central moments of F are available. In [67], the distribution families presented by Pearson were considered as a solution to the differential Eq. (14)

$$\frac{\mathrm{dp(F)}}{\mathrm{dF}} = \frac{(\mathrm{F} - \lambda)}{\mathrm{b_0} + \mathrm{b_1 F} + \mathrm{b_2 F^2}}\mathrm{p(F)} \tag{1.14}$$

in which λ and $\mathrm{b_i}$ are constant parameters. From Eq. (14), after some mathematical manipulations, these constant parameters can be found in terms of the central moments of the distribution function of F. By using coordinate transformation $\mathrm{k} = \mathrm{F} - \lambda$, Eq. (14) is recast as

$$\frac{\mathrm{dp(F)}}{\mathrm{dk}} = \frac{\mathrm{k}}{\mathrm{B_0} + \mathrm{B_1 k} + \mathrm{B_2 k^2}}\mathrm{p(F)} \tag{1.15}$$

If the roots of the polynomial in the denominator of Eq. (15), $\mathrm{a_1}$ and $\mathrm{a_2}$, are real and of the opposite sign, the distribution in Eq. (15) reduces to Beta distribution, with parameters p and q found by equating the Pearson distribution's moments with that of the failure function:

$$\mathrm{p(z)} = \frac{1}{\mathrm{B(p,q)}}\mathrm{z}^{\mathrm{p}-1}(1-\mathrm{z})^{\mathrm{q}-1}, (\mathrm{p,q} > 0) \tag{1.16}$$

where $\mathrm{z} = (\mathrm{k} - \mathrm{a_1})/(\mathrm{a_2} - \mathrm{a_1})$. In this work, several comparisons between EDW, PRS, MCM and a semi-deterministic failure analyses, were made considering different fiber angles and assumptions for the Tsai-Wu failure criterion. The results obtained with the analytical approaches were in excellent agreement with experimental or Monte Carlo data.

The second major analytical approach was developed by Gurvich and Pipes [71]. They argue that solutions based on other methods such as FORM, SORM, MC etc. are either numerical or approximate ones and, sometimes, those are too time-consuming. Moreover, when there is a high degree of variability in input parameters, careful attention must be exercised regarding the results from those methods. So, they have developed an exact solution for the mean value and variance of the random failure function in terms of statistical characteristics of both stresses and strengths. This approach considers the failure function as a random linear function of products of applied random stresses, instead of the traditional consideration of the FF in the form of a random non-linear function of the stresses and strength parameters. First, a general FF is considered as follows

$$F = \Pi_{ij}\sigma_{ij} + \Pi_{ijkl}\sigma_{ij}\sigma_{kl} + ...;\ \ i,j,k,l = x,y,z \tag{1.17}$$

where Π_{ij}, Π_{ijkl}, … are the strength tensors. The condition of non-failure is $F \le 1$. Now, the following vectors are introduced

$$[s] = [s_1\, s_2 \ldots s_n];\ [\rho] = [\rho_1\, \rho_2 \ldots \rho_n] \tag{1.18}$$

where s_m are components characterizing all required combinations of the stresses, ρ_m are the strength characteristics and n is the number of elements in the matrices. Hence, Eq. (1.17) may be presented as

$$F = \sum_{m=1}^{n} \rho_m s_m \tag{1.19}$$

In a probabilistic framework, s_m, ρ_m and F should be considered as random variables:

$$\tilde{F} = [\tilde{\rho}][\tilde{s}]^T = \sum_{m=1}^{n} \tilde{\rho}_m \tilde{s}_m \tag{1.20}$$

In this formulation, the random matrices $[\tilde{\rho}]$ and $[\tilde{s}]$ may be represented by the mean matrices $[\overline{\rho}]$ and $[\overline{s}]$ and the correlation matrices $[K_s]$, $[K_\rho]$, respectively; all of them considered as initial data. Basic statistical characteristics of $\tilde{F}$ namely mean value, $\overline{F}$, and the standard deviation, σ_F, are obtained as

$$\overline{F} = \sum_{m=1}^{n} \overline{\rho}_m \overline{s}_m;\quad \sigma_F^2 = \sum_{m'=1}^{n}\sum_{m''=1}^{n} \left\{ K_{sm',m''}\overline{\rho}_{m'}\overline{\rho}_{m''} + K_{\rho m',m''}\overline{s}_{m'}\overline{s}_{m''} + K_{sm',m''}K_{\rho m',m''} \right\} \tag{1.21}$$

Here, the correlation between the strength characteristics and stresses has been ignored, but can be taken into account in principle. If the elastic properties are also considered as random variables, as usually is the case for composites and wood, their randomness results in randomness of the stresses even under the application of deterministic external loading. On the other hand, there often exists a correlation between stiffness and strength parameters. Therefore,

in a more accurate analysis, it is necessary to consider the correlation between the strength characteristics and stresses.

The only assumption involved in this approach is connected with the type of distribution for $\tilde{F}$, such as normal, Weibull, gamma distributions etc. In all the other methods cited above, reliability estimation requires an assumption regarding the type of the distributions for strengths and/or stresses, whereas Gurvich's method needs an assumption about the type of the distribution for $\tilde{F}$. In simpler words, Gurvich changes the form of the failure function and states the problem such that, based on the multivariate distribution theory, an exact solution for the mean value and the standard deviation of the random failure function can be found in terms of mean values and correlations of input parameters in the new form.

Gurvich and Pipes illustrated their method in the case of a single composite ply as well as a laminate. For a single ply under in plane loading, the stresses are uniform, similar to stress state at a material point; thus, by assuming a distribution for $\tilde{F}$ the reliability is easily obtained. On the other hand, the reliability of a laminate, in which there are usually different stresses in different plies, can be calculated by multiplication of reliability of all plies, using the concept of first-ply-failure.

Also, a method to extend the concept of reliability to a structural member is to choose a distribution for the random failure function $\tilde{F}$ which already contains an integral for consideration of the spatial variation of stresses. This is usually done with the help of Weibull distribution. The CDF of this distribution is expressed as

$$P(F) = 1 - \exp\left[-\frac{1}{V_0} \int_V \left(F / \sigma_0 \right)^m dV \right] \tag{1.22}$$

where V_0 is a reference volume, σ_0 is the scale parameter and m is the shape parameter. In this way, statistical size effect can be taken into account at the same time. Gurvich and Pipes [72] extended their previous work by introducing a new distribution to incorporate the statistical size effect and spatial variability of stresses, for which the reliability is obtained as:

$$H = \exp\left[-\frac{1}{V_0} \int_V \left(A(x,y,z) \right)^{\beta(x,y,z)} dV \right] \tag{1.23}$$

where parameters A and β are functions of $\overline{F}$ and σ_F . They used Eq. (1.23) to calculate the reliability of a simply-supported beam under distributed random loading. It was shown that when the beam is considered as an assemblage of a number of rectangles, the numerical integration in Eq. (1.24) converges as the size of rectangles becomes smaller:

$$H \approx \exp\left[-\frac{t\Delta x\Delta y}{V_0} \sum_i \sum_j \left(A(x_i, y_j) \right)^{\beta(x_i, y_j)} \right] \tag{1.24}$$

A semi-analyical probabilistic approach in reliability analysis of structural members was proposed by Vallee et al. [73]. In contrast to the two previous analytical methods, which consider a failure criterion with random parameters, they first fitted a quadratic failure criterion, Eq. (1.25), to experimental strength results of composite laminae under combined tensile-shear loading. It means that the failure criterion contains deterministic strength parameters. The failure function is expressed as

$$F = \sqrt{\left(\frac{\sigma_z}{\sigma_{z,u}} \right)^2 + \left(\frac{\tau_{xz}}{\tau_{xz,u}} \right)^2} = 1 \tag{1.25}$$

Then, the failure criterion is considered as a random function with stress components as its random parameters. Next, all the experimental strength data are substituted into the failure function as stress components which lead to a set of numbers scattered around one. Using the concept of brittle failure to apply the method to a structure/component, an adhesively bonded double-lap joint in this case, the following formula was introduced for estimation of probability of survival or reliability:

$$P_s = \prod_{i=1}^{n} \exp\left[-\frac{V_i}{V_0} \left(\frac{F_i}{F_0} \right)^m \right] \tag{1.26}$$

where V_i are small volumes in which the stress can was considered to be uniform and F_i is the value of the failure function in V_i. Instead of the whole volume of the joint, based on experimental observations, three critical paths were chosen to be examined by Eq. (1.26). Next, due to linearity of the problem, there was a direct relationship between external loading and F_i, i.e. $F_i = \alpha_i F_{ext}$ where α_i is different at each volume V_i. They used a finite element model to estimate α_i. Therefore, from Eq. (1.26) a relationship between the external loading and the probability of survival was established.

1.4.5.4 Stochastic finite element method

Recently, as a numerical method, the stochastic finite element modelling has received particular attention in reliability analyses of structures/component [26]. It is noted that the term 'stochastic finite element' has been used in the literature for probabilistic analysis of structures based on finite element models, in which the spatial variability of the mechanical properties may or may not have been taken into account. From a mathematical point of view, SFE method can be seen as a powerful tool for the solution of stochastic partial differential equations. Three different classes of SFE method have been developed in the literature: 1) the perturbation approach [74]

in which the response vector is expanded according to Taylor series, 2) the spectral stochastic finite element method [75] based on representation of each response quantity using a series of random Hermite polynomials and 3) Monte Carlo simulations [76] which is actually a way to extend the previously discussed MC to a structural member with spatially variable stresses.

SFE method has several advantages. First, it is robust meaning that this method can work well in a wide variety of conditions [26]. Next, lots of parameters can be considered as random input variables such as random elastic properties, random geometrical dimensions and random external loading. Moreover, the correlations between parameters can also be taken into account [77]. The other feature of SFE method is that different non-linear constitutive equations can be considered, similar to conventional FEM. The major drawback of this method is that it is computationally expensive.

Lin [78] used SFE method to predict the reliability of angle-ply laminates subject to in-plane edge random loads. This author provides a comparison of different reliability methods and different failure criteria using SFE method to derive the statistics of the First-Ply-Failure load by mean-centered second-order perturbation technique. Recently, Noh [24] proposed a formulation for SFE method based on perturbation techniques to determine the response variability in laminate composite plates considering the randomness of material parameters and different correlation states between them. The results were compared with experimental failure load data of centrally loaded composite plates with different lamination arrangements to study the accuracy of the methods. Recently, Philippidis and Bacharoudis [77] have utilized Monte Carlo-based SFE method to examine the reliability of wind turbine rotor blades. They have taken into account random elastic properties and strengths as well as random external loading.

In timber applications, MC-SFE method has been mainly used, because of its simplicity and robustness. Clouston and Lam [16], considering strengths parameters as random variables, used MC-SFE method to predict the reliability of a center point off-axis bending member made of Douglas-fir laminated veneer. They used Tsai-Wu as failure criteria and Weibull theory in two different ways to take into account the statistical size effect. They also developed their model further [18] into a 2D nonlinear SFE method to simulate the stress strain behavior of strand-based wood composites. The nonlinearity was considered only in compression and characterized within the framework of the theory of orthotropic plasticity, using Tsai-Wu criterion to describe the plastic flow rule. Their modelling results were comparatively in a good agreement with experimental results. They also extended their method into 3D nonlinear stochastic finite element modelling [17].

More recently, the tensile strength of different orientation of wood strands from different growth ring positions was investigated by Jeong and Hindman [79] using MC-SFE method. They distinguished between earlywood and latewood in their model and assigned different random elastic properties and strengths to each of them, with no spatial variability. Predicted

ultimate tensile strengths from SFE method, based on Tsai-Hill failure criterion, were shown to be in good accordance with experimental results with a maximum error of 11.09%. Jeong et al. have also used MC-SFE method to analyze dovetail connections [80].

1.5 Failure criteria

Choosing the failure criterion is a critical step in analyzing the performance of a material under loading. There is a number of failure criteria in the literature to study the performance of clear timber [81]. Most of them have been first developed to analyze the failure of composite materials and then were applied to wood. There are only a few failure functions which are developed especially for wood such as Norris's theory [82] and Hankinson's formula [83]. In the following, the failure criteria are reviewed briefly. It is noted that all failure criteria are based on on-axis stress components.

Hankinson formula

An estimation for the clear timber strength at any grain angle can be obtained based on the strength values of both parallel and perpendicular to grain directions using the following formula, which was introduced by Hankinson in its original form [83]:

$$X_\theta = \frac{XY}{X\sin^n\theta + Y\cos^n\theta} \tag{1.27}$$

where X_θ is the strength at angle θ from the axial direction, X is the strength parallel to grain direction, Y is the strength perpendicular to grain direction and n is an empirically determined constant; in tension $n = 1.5-2$ and in compression $n = 2-2.5$ [27]. The Hankinson formula has been shown to be independent of temperature [84]. This formula is sometimes used along with other failure criteria in wood failure analysis [85,86]

Linear criterion

The linear failure criterion is the simplest among others and is expressed as [87]

$$\frac{\sigma_x}{X} + \frac{\sigma_y}{Y} + \frac{\tau_{xy}}{S} = 1 \tag{1.28}$$

where σ_x, σ_y and τ_{xy} are the in-plane stress components and S is the shear strength. For application of this formula to wood, the difference between magnitude of tensile and compressive strengths must be taken into account. This is also the case for the following failure criteria except for tensorial failure criteria in which this difference is explicitly incorporated. It has been shown that this function is not a good failure predictor for wood [88].

Quadratic Criterion

Quadratic criterion [87] is the simplest quadratic failure criterion and is represented by an ellipsoidal envelope:

$$\left(\frac{\sigma_x}{X}\right)^2+\left(\frac{\sigma_y}{Y}\right)^2+\left(\frac{\tau_{xy}}{S}\right)^2=1 \tag{1.29}$$

This formula is less common compared to the following failure criteria.

Tsai-Hill Criterion

Hill [89] developed a failure criterion for plastic anisotropic materials based on Von Mises distortion energy theory. Later, Azzi and Tsai [90] modified Hill's theory to be used for composites. The criterion referred to as Tsai-Hill is written as

$$\left(\frac{\sigma_x}{X}\right)^2-\frac{\sigma_x\sigma_y}{X^2}+\left(\frac{\sigma_y}{Y}\right)^2+\left(\frac{\tau_{xy}}{S}\right)^2=1 \tag{1.30}$$

Unlike the linear and quadratic failure criteria, this formula includes the interaction between normal stresses. Cabrero et al. [88] have shown that this is a good predictor of wood failure in the cases of combined tensile and compressive stress states.

Norris Criterion

Although originally developed by Norris [82] in 1950, this failure criterion is still being used widely [81]. This criterion, developed specially for wood, is also based on von Mises distortion energy hypothesis:

$$\left(\frac{\sigma_x}{X}\right)^2-\frac{\sigma_x\sigma_y}{XY}+\left(\frac{\sigma_y}{Y}\right)^2+\left(\frac{\tau_{xy}}{S}\right)^2=1,\quad \left(\frac{\sigma_x}{X}\right)^2=1,\qquad \left(\frac{\sigma_y}{Y}\right)^2=1 \tag{1.31}$$

In three dimensional stress states, this criterion is expressed in the following form [21]:

$$\begin{aligned}
&\left(\frac{\sigma_x}{X}\right)^2-\frac{\sigma_x\sigma_y}{XY}+\left(\frac{\sigma_y}{Y}\right)^2+\left(\frac{\tau_{xy}}{S_{xy}}\right)^2=1,\\
&\left(\frac{\sigma_x}{X}\right)^2-\frac{\sigma_x\sigma_z}{XZ}+\left(\frac{\sigma_z}{Z}\right)^2+\left(\frac{\tau_{xz}}{S_{xz}}\right)^2=1,\\
&\left(\frac{\sigma_y}{Y}\right)^2-\frac{\sigma_y\sigma_z}{YZ}+\left(\frac{\sigma_z}{Z}\right)^2+\left(\frac{\tau_{yz}}{S_{yz}}\right)^2=1
\end{aligned} \tag{1.32}$$

Tsai-Wu failure criterion

A failure criterion with a general tensorial form was proposed by Tsai and Wu [81]

$$F_i\sigma_i+F_{ij}\sigma_i\sigma_j=1,\quad i,j=1,2,...,6 \tag{1.33}$$

where F_i and F_{ij} are the strength tensors and σ_i and σ_j are the stress tensors in contracted notation. For the two-dimensional stress state, Eq. (1.33) is expanded as:

$$F_1\sigma_1 + F_2\sigma_2 + F_6\sigma_6 + F_{11}\sigma_1^2 + F_{22}\sigma_2^2 + F_{66}\sigma_6^2 + 2F_{12}\sigma_1\sigma_2 + 2F_{16}\sigma_1\sigma_6 + 2F_{26}\sigma_2\sigma_6 = 1 \quad (1.34)$$

with the condition $F_{11}F_{22} - F_{12}^2 \geq 0$.

The strength tensor components take the following form:

$$F_1 = \frac{1}{X_t} - \frac{1}{X_c},\ F_2 = \frac{1}{Y_t} - \frac{1}{Y_c},\ F_6 = 0,\ F_{11} = \frac{1}{X_t X_c},\ F_{22} = \frac{1}{Y_t Y_c},\ F_{66} = \frac{1}{S^2},\ F_{16} = 0,\ F_{26} = 0 \quad (1.35)$$

where the X_t, X_c, Y_t and Y_c are the tensile and compressive strengths in longitudinal and transverse directions, and S is the shear strength. For the remaining component, F_{12}, there is some controversy in the literature [91], and researchers have presented different expressions for it. Tsai-Wu [92] proposed $F_{12} = -\sqrt{F_{11}F_{22}}/2$. Tsai and Wu argued that Eq. (1.34) in the case of isotropic materials has to reduce to von Mises criterion. Cowin [93] showed that, for bone and wood, the tensor theory is reduced to Hankinson formula and proposed the expression $F_{12} = \sqrt{F_{11}F_{22}} - 1/(2S^2)$. Hoffman [94] suggested $C = -F_{11}/2$ which is based on theories presented by von Mises and Hill, but assuming a brittle failure. Van der put [95] also proposed $F_{12} = 0$, arguing that this can better represent the behavior of timber.

In previous models, the interaction term F_{12} can be experimentally obtained based on the results of on-axis uniaxial tests. The more direct approach is to use on-axis multiaxial tests or off-axis uniaxial tests. For example, if multiaxial hydrostatic tension P is applied to the specimen, using Eq. (1.34), F_{12} is obtained as [81]

$$F_{12} = \frac{1}{2P^2}\left[1 - P(F_1 + F_2) - P^2(F_{11} + F_{22})\right] \quad (1.36)$$

Similarly, in the case of uniaxial off-axis test, after calculating on-axis stress components as a function of the off-axis stress σ_θ, substituting them into Eq. (1.34) and doing some mathematical manipulation, F_{12} is obtained as

$$F_{12} = \frac{1}{2\sigma_\theta^2}\left[\left(\frac{1}{\sin^2\theta\cos^2\theta}\right) - \left(\frac{F_1}{\sin^2\theta} + \frac{F_2}{\cos^2\theta}\right)\sigma_\theta - \left(F_{66} + \frac{F_{11}}{\tan^2\theta} + F_{22}\tan^2\theta\right)\sigma_\theta^2\right] \quad (1.37)$$

This method is easier in practice than performing multiaxial tests; therefore, it is important to consider which angle θ is most suitable. Clearly, it should be large enough to produce acceptable on-axis stress in transverse direction. Clouston et al. [96] showed that the most suitable angle is 15°.

1.6 Thesis justification

The literature lacks sufficient information on the experimental and theoretical aspects of the RSV of clear timber properties and its effect on the response of clear timber components, such as bonded joints, under external loading. More specifically, there are only a limited number of studies on the characterization of the RSV of the mechanical properties of clear timber [97-99], and the RSV is usually not studied at the mesoscale. There is no size effect model at this scale for clear timber. Also, to the best of the authors' knowledge, no previous study has taken the RSV of clear timber properties, as multi-dimensional fields, into account for assessing the random response of clear timber components.

This thesis is focused on the variability of the mechanical properties of clear timber, with emphasis on the mesoscale variations, and its effect on the properties of clear specimens of different sizes and on the stochastic response of clear timber components such as adhesively bonded timber joint. The emphasis on the mesoscale is because in the finite element analyses of those timber structures/components in which failure occurs in the clear wood, the failure initiation is normally equivalent to the first element failure. These elements are often at scale of millimeters. Therefore, for an accurate prediction of the failure initiation, the local behavior of clear timber becomes of critical importance. At this scale, both elastic moduli and strength parameters spatially change their values as the spatial position changes (Chapters 3 and 5). A change in local values of the elastic moduli at critical areas of a structural component with high stress gradients, assuming fixed geometry and boundary conditions, will change the stress field at those areas. Consequently, when a failure function is used for failure prediction, these changes in the stress components and strengths parameters will affect the prediction. This is why taking into account the variability of the mechanical properties is important in analysis of clear timber structures.

Experiments are needed to characterize the size effects and RSV for the longitudinal and transverse tensile strengths of clear timber at mesoscale. Also, there are no information in the literature on the correlation between elastic and strengths parameters at mesoscale for clear timber which can be important for stochastic simulations. In parallel, models are also needed for describing these phenomenons as well as further predictions.

Based on these arguments the thesis objectives were defined and are presented in the next section. As mentioned earlier, this thesis focuses on clear timber. However, it is also regarded as a fundamental step toward a wider framework capable of assessing performance of timber structures with knots. In [100], an approach has been proposed for estimating the elastic deflection of beams with knots based on the test results of clear timber specimens. In this approach, the distribution of knots in a timber beam are modelled, as spatially distributed imperfections, by a random field. Other approaches, such as direct modeling of knots in the finite element model might be applicable as well [29].

1.7 Objectives

The purpose of the present study is to experimentally investigate the size effects and RSV of the mechanical properties of clear timber, and to establish models for the size effect on the strength and the assessment of the stochastic response of structures made of clear timber. In this regard, the first objective is to develop a size effect model for clear timber strength. The second and third objectives are to experimentally characterize the size effect, RSV and meso-correlation between local modulus and strength for longitudinal and transverse directions. The final objective is to establish an SFE framework that uses the data on the size effects, RSV and correlations to model the stochastic response of clear timber components such as bonded timber joints. These objectives are listed below:

1. The experimental characterization of the RSV of the longitudinal mechanical properties of clear timber and the evaluation of the size effects and correlation between properties at the mesoscale.
2. The experimental characterization of the RSV of the transverse mechanical properties of clear timber and the evaluation of the size effects and correlation between properties at the mesoscale.
3. The establishment of a strength size effect model taking into account the RSV of clear timber strength.
4. The development of an efficient SFE framework for clear timber components and its application to an adhesively-bonded timber joint.

1.8 Methods of investigation

Both experimental and numerical methods have been used to achieve the objectives. Methods 1 to 4 correspond to objectives 1 to 4 of the previous section:

1. A significant number of quasi-static tensile tests (165 tests with proper failures) were carried out on clear specimens of different sizes, cut in the longitudinal direction of timber boards and conditioned to 12% moisture content. Local deformations were measured via video extensometry.
2. A large number of quasi-static tensile tests (226 tests) were performed on clear specimens of different sizes, cut in the transverse direction of timber boards and conditioned to 12% moisture content. Again, local deformations in each specimen were measured via video extensometry.
3. The theory of random fields based on the spectral representation scheme was used to model the RSV of the strength field in MATLAB. The weakest link theory and the Monte Carlo method were used to obtain the size effect on the strength.

4. An SFE framework was established using MATLAB and ABAQUS. The RSV of the mechanical properties, taking into account their correlations, was modeled in MATLAB based on the spectral representation scheme and transferred to finite elements via the ABAQUS user-defined element (UEL) subroutine. The Monte Carlo simulation method was used to assess the stochastic structural response. To show the capability of the framework in modeling clear timber components, an adhesively-bonded clear timber joint was modeled based on an experimental data from the literature for the same joint. Due to lack of experimental data for the spatial variability of the mechanical properties, an average value considered for correlation lengths of all the involved elastic and strength parameters. By using an appropriate value for this average correlation length, the applicability of the model to clear timber components was validated. However, experimental input data are necessary to validate the efficiency of the model in predicting the load bearing capacity of clear timber components.

1.9 Thesis organization

The thesis is organized into seven chapters. The first chapter is the thesis introduction. Five next chapters are the main body of the thesis. Chapter 2 describes the developed size effect model for clear timber strength. Chapters 3 to 5 present the performed experiments and the results on RSV, size effect and correlations for mechanical properties of clear timber in longitudinal and transverse directions. Chapter 6 describes the procedures of the developed SFE framework for evaluation of stochastic response of clear timber components and the case study performed on an adhesively bonded timber joint. To evaluate the stochastic response, the model of the joint is built in ABAQUS which uses the experimental data on RSV and correlations between elastic and strength parameters, as well as the developed size effect model. The size effect model adjusts the strength parameters between the tested specimen size and the size of the area around the integration point in the finite elements of the joint model. The thesis organization is illustrated in Fig. 1.5. It can be considered as a developed tool for design of clear timber component, although the size effect model of Chapter 2 or the experimental results can be used on their own as well. However, the information specified by dashed lines in Fig. 1.5, are missing for validation of the model. For a general clear timber component, these include input experimental data on RSV and correlations for the material properties for shear and compression as well as experimental data on the component capacity. Nevertheless, the applicability of the tool developed for estimation of the stochastic response of clear timber components was shown in Chapter 6 by modeling the tensile failure behavior of bonded joints, using experimental data from the literature and finding an average appropriate value for the correlation length. Finally, Chapter 7 concludes the thesis.

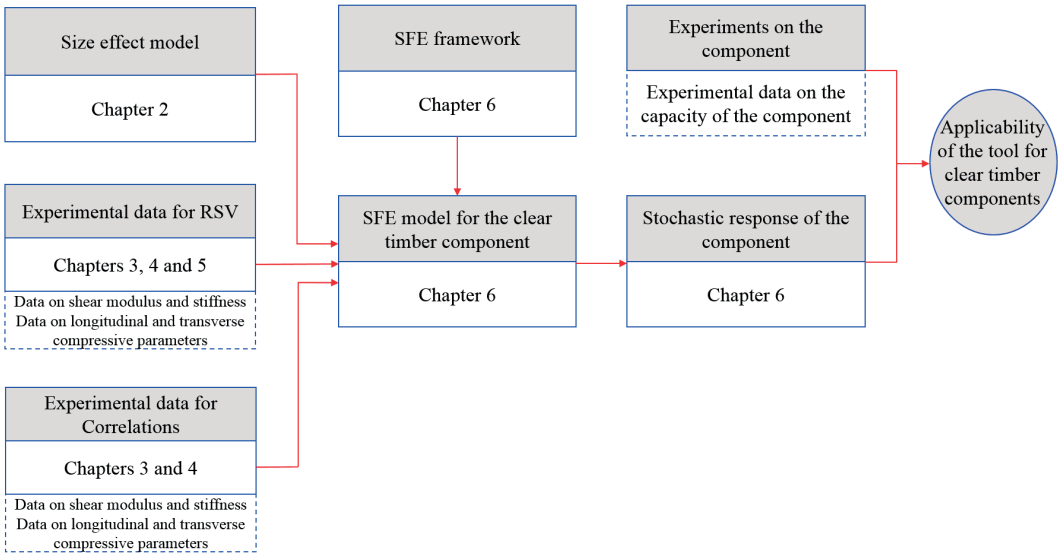

Fig. 1.5: Schematic overview of the thesis.

The overview of each chapter is given in the following.

Chapter 1 – Introduction: The natural randomness in the timber properties and its significance in the analysis of timber structures/components is discussed and the relevant literature is reviewed. The wood structure, different types of uncertainty and timber design approaches are explained. The knowledge gap, based on which the research objectives are defined, is discussed. The experimental and theoretical investigation methods adopted to achieve the objectives are explained. A summary of the thesis content is provided in this chapter. Discussions for thesis justification and its limitations are also carried out.

Chapter 2 – Size effect model: A model is proposed to express the size effect on clear timber strength that takes into account the spatial variability in the strength field to fulfill objective 3. The theory of random fields was used to model the random 3D spatial variability of the strength field. Using the spectral representation scheme, realizations, which are samples of a random field, of the strength field in each specimen were generated. The stochastic response was obtained via the Monte Carlo method along with the weakest link theory. This procedure was repeated for specimens with different volumes to estimate the effect of size on strength. In determination of model unknown parameters, the experimental data from the literature on the longitudinal strengths of two sets of specimens with different volumes, for each one of spruce and Japanese larch wood, were used. These data were sufficient to obtain the two unknown parameters of the model for each species. This way, the correlation lengths for longitudinal strength of the woods were obtained. This calibration (finding appropriate parameters) was possible due to the improvement of the proposed model compared to the classical Weibull model, and it was shown that Weibull model can never be calibrated for none of the woods

considered. An analytical expression to approximate the numerical results of the 3D random field modeling was also introduced.

Chapter 3 – Longitudinal mechanical properties of clear timber: RSV and size effects: Specimens of different lengths were prepared and their quasi-static behavior was experimentally investigated under tensile loading, concerning objective 1. In addition to the global displacement monitoring, the local deformations along the length of each specimen were measured. The effect of the mesostructure of the clear timber on the local elastic modulus was examined. The spatial variability of the elastic modulus was experimentally characterized. Also, statistics concerning the elastic modulus, strength and strain to failure as well as correlations between elastic modulus, strength and density were derived. Moreover, the size effect on these properties due to the length change was studied.

Chapter 4 – Transverse mechanical properties of clear timber: Uncertainty and size effects: Quasi-static experiments were performed on specimens with different lengths in the transverse direction, concerning objective 2. In addition to the global displacement monitoring, the local deformations along the length of each specimen were measured. The mechanical behavior of specimens of different lengths cut in a regular and random manner from different boards was studied. The statistics concerning the elastic modulus, strength and strain to failure as well as the effect of size on these properties were examined. The accuracy of the CWSEL for modeling the transverse tensile strength of small clear specimens was also evaluated, and the correlations between the mechanical properties and between the mechanical properties and material density were investigated. Specimens were also grouped based on failure type, and an analysis of variance (ANOVA) was used to find statistically significant differences between the mean strengths of these groups.

Chapter 5 – Transverse mechanical properties of clear timber: Spatial variability: The experimental data from the transverse tensile tests were further used for characterization of the RSV, concerning objective 2. The spatial variability in the transverse elastic modulus, transverse strength and transverse strain to failure in both longitudinal and transverse directions was characterized. Also, the effect of the mesostructure of the clear timber on the local elastic modulus was studied. Finally, the effect of some defects on the timber properties were examined.

Chapter 6 – SFE modeling framework for clear timber structures: A 2D stochastic finite element framework was developed for the stochastic structural response assessment of timber structural members made of clear timber concerning objective 4. The realizations of material properties, considering their correlations, were generated in MATLAB based on the spectral representation scheme, and the size effect on the strength was also taken into account using the model of Chapter 2. These realizations were transferred to actual finite elements in the commercial finite element software ABAQUS by writing a UEL subroutine. As a real

application, the behavior of an adhesively-bonded double-lap beech joint was simulated under tensile loading and the stochastic response was obtained using the Monte Carlo method, based on the experimental data from the literature on the statistics of beech mechanical properties. The size effect model developed in Chapter 2 was used for adjustment of strength parameters from small clear specimens. The experimental data from the literature on the joint capacity were used to find an appropriate average correlation length for beech properties. This was done so that result of the model joint, with its other existing constraints such as pre-determined statistics for all the mechanical properties, be as close as possible to the experimental results. This correlation length was also used in the size effect adjustment.

Chapter 7 – Conclusions and future work: The thesis conclusions drawn from experimental and theoretical/numerical results are summarized. This chapter also highlights the original contributions of this work to the research field. Finally, recommendations concerning future efforts for the continuation of the current work are given.

1.10 Thesis limitations/assumptions

The limitations/assumptions of the thesis are as follows:

- The developed models and performed experiments are for the case of short-term quasi static behavior.
- All experiments are performed at a moisture content of 12% and laboratory temperature of 22±3 °C.
- The main focus of the thesis is the variability of the mechanical properties and its effect on the stochastic response of clear timber components. Other kind of variabilities such as variability of the external loading and variability of the structure dimensions are not covered.
- Clear timber was considered for all the investigations.
- Only tensile longitudinal and transverse properties were experimentally characterized.
- Linear elastic, small deformation assumption, which leads to brittle failure of the material, was used in the models.
- Chapter 2: Although the size effect model predicts the effect of size on the strength for volumes outside the range of the available experimental data as well, which has a physical justification as explained in Chapter 2, more experimental data would be desirable in these range. Therefore, it can be stated that the model is more descriptive outside this range, meaning that although the size effect is predicted based on sound physical concepts, it is not experimentally validated. In Chapter 4, however, the left asymptotic behavior was experimentally validated. It was assumed that the correlation length is the same in longitudinal and transverse directions to reduce the number of

unknowns. The correlation length is most likely to be different in different orthotropic material directions. Nevertheless, since the cross-sectional dimensions of the tested specimens were rather small compared to the longitudinal dimension, the estimated correlation lengths are much closer to the true longitudinal correlation length.

- Chapter 3: The experimental investigation of the size effect was performed for modulus of elasticity, strength and strain to failure. However, the RSV was only characterized for the longitudinal elastic modulus. Also, the transverse variation of the longitudinal properties in the study of size effect and RSV have been implicitly taken into account, so the provided statistics represent the total variability of the longitudinal properties.
- Chapters 4-5: The lumbers used for fabricating specimens in these chapters were cut in the so-called radial plane, but the specimens were not positioned exactly in the radial plane that crosses the pith. The experimental investigation of the size effect was performed for modulus of elasticity, strength and strain to failure. However, the RSV was mainly characterized for the transverse elastic modulus, although the RSV for transverse strength and strain were also investigated with the available data.
- Chapter 6: The main novelty of this chapter was the establishment of the new SFE framework that, with appropriate input data on RSV, can potentially be applied to different clear timber components under various loading conditions, taking into account the orthotropic behavior of clear timber. The developed SFE framework was applied to an adhesively bonded timber joint. For the simulation, due to lack of experimental data for the shear properties as well as the joint capacity, the experimental data from literature were used. An average correlation length for strength and elastic parameters was considered for the simulations. This average value was obtained with regard to experimental data on joint capacity. Complete experimental data on the correlation length and simulations of different components are needed for validation of the model. Therefore, the model is, at its current state, is more descriptive than predictive. The aim of this simulation was first to show the capabilities of the developed SFE framework in modelling real structures via a demonstrative example, and second, was to show that with appropriate value for the correlation length, the predicted results can be in a fairly well agreement with the experimental results for the joint capacity.

1.11 List of Publications

The results of this research have been included in five journal papers that correspond to Chapters 2 to 6 of the thesis. Three papers have been submitted, one of which is accepted, and the last two of the five papers are in progress. The papers are as follows:

Paper 1: Moshtaghin, A.F., Franke, S., Keller, T., Vassilopoulos, A.P., 2016. Random field-based modeling of size effect on the longitudinal tensile strength of clear timber. Structural Safety 58, 60-68.

Paper 2: Moshtaghin, A.F., Franke, S., Keller, T., Vassilopoulos, A.P., February 2015. Experimental characterization of longitudinal mechanical properties of clear timber: Random spatial variability and size effects. Submitted to Construction and Building materials.

Paper 3: Moshtaghin, A.F., Franke, S., Keller, T., Vassilopoulos, A.P., December 2015. Transverse mechanical properties of clear timber: Uncertainty and size effects. Submitted to Wood Science and Technology.

Paper 4: Moshtaghin, A.F., Franke, S., Keller, T., Vassilopoulos, A.P., 2016. An experimental study on the spatial variability in transverse mechanical properties of clear timber. In progress.

Paper 5: Moshtaghin, A.F., Franke, S., Keller, T., Vassilopoulos, A.P., 2016. ABAQUS-based non-intrusive stochastic finite element framework: Application to adhesively-bonded timber joints. In progress.

1.12 References

[1] Food and Agriculture Organization (FAO), 2014. Forest Products Annual Market Review.

[2] Köhler, J., 2007. Reliability of timber structures, PhD thesis, ETH Zurich.

[3] Sriramula, S., Chryssanthopoulos, M.K., 2013. An experimental characterisation of spatial variability in GFRP composite panels. Structural Safety 42, 1-11.

[4] Choi, S.K., Canfield, R.A., Grandhi, R.V., 2007. Reliability-based structural design, Springer-Verlag, London.

[5] Lekou, D.J., Philippidis, T.P., 2008. Mechanical property variability in FRP laminates and its effect on failure prediction. Composites Part B: Engineering 39, 1247-56.

[6] Chiachio, M., Chiachio, J., Rus, G., 2012. Reliability in composites - A selective review and survey of current development. Composites Part B: Engineering 43,902-913.

[7] Dill-Langer, G., Hidalgo, R.C., Kun, F., Moreno, Y., Aicher, S., Herrmann, H.J., 2003. Size dependency of tension strength in natural fiber composites. Physica A: Statistical Mechanics and its Applications 325, 547-560.

[8] Zhu, J., Kudo, A., Takeda, T., Tokumoto, M., 2001. Methods to estimate the length effect on tensile strength parallel to the grain in Japanese larch. Journal of Wood Science 47, 269-274.

[9] Barrett, J.D., 1974. Effect of size on tension perpendicular-to-grain strength of Douglas-fir. Wood and Fiber 6, 126-143.

[10] Barrett, J.D., Foschi, R.O., Fox, S.P., 1975. Perpendicular-to-grain strength of Douglas-Fir. Canadian Journal of Civil Engineering 2, 50-57.

[11] Fox, S.P., 1974. Strength and stiffness of laminated Douglas-fir blocks in perpendicular-to-glueline tension. Wood and Fiber 6, 156-163.

[12] Norlin, L.P., Lam, F., 1998. Fatigue behaviour and size effects perpendicular to the grain of laminated Douglas fir veneer. Materials and structures 32, 298-303.

[13] Pedersen, M.U., Clorius, C.O., Damkilde, L., Hoffmeyer P., 2003. A simple size effect model for tension perpendicular to the grain. Wood Science and Technology 37, 125-140.

[14] Astrup, T., Clorius, C.O., Damkilde, L., Hoffmeyer P., 2007. Size effect of glulam beams in tension perpendicular to grain. Wood Science and Technology 41, 361-372.

[15] Weibull, W., 1939. A statistical theory of strength of materials. In: Proceedings of the Royal Swedish Institute. Research No. 151, Stockholm, Sweden.

[16] Clouston, P., Lam, F., Barrett, J.D., 1998. Incorporating size effects in the Tsai-Wu strength theory for Douglas-fir laminated veneer. Wood Science and Technology 32, 215-226.

[17] Clouston, P.L., Lam, F., 2002. A stochastic plasticity approach to strength modeling of strand-based wood composites. Composites Science and Technology 62, 1381-1395.

[18] Clouston, P.L., Lam, F., 2001. Computational modeling of strand-based wood composites. Journal of Engineering Mechanics 127, 844-851.

[19] Tannert, T., Vallée, T., Hehl, S., 2012. Probabilistic strength prediction of adhesively bonded timber joints. Wood Science and Technology 46, 503-513.

[20] Tannert, T., Vallée, T., Hehl, S., 2012. Experimental and numerical investigations on adhesively bonded hardwood joints. International Journal of Adhesion and Adhesives 37, 65-69.

[21] Tannert, T., Lam, F., Vallée, T., 2010. Strength prediction for rounded dovetail connections considering size effects. Journal of Engineering Mechanics 136, 358-366.

[22] Rollet, Y., Bonnet, M., Carrere, N., Leroya, F-H., Maire J-F., 2009. Improving the reliability of material databases using multiscale approaches. Composite Science Technology 69, 73-80.

[23] Shaw, A.J., Sriramula, S, Gosling, P.D., Chryssanthopoulos, M.K., 2010. A critical reliability evaluation of fibre reinforced composite materials based on probabilistic micro and macro-mechanical analysis. Composites Part B Engineering 41, 446-53.

[24] Noh, H-C., 2011. Stochastic finite element analysis of composites plates considering spatial randomness of material properties and their correlations. Steel and Composite Structures 11, 115-30.

[25] Carbillet, S., Richard, F., Boubakar, e.L., 2009. Reliability indicator for layered composites with strongly non-linear behaviour. Composites Science and Technology 69, 81-87.

[26] Stefanou, G., 2009. The stochastic finite element method: Past, present and future. Computer Methods in Applied Mechanics and Engineering 198, 1031-51.

[27] Dinwoodie, J.M., 2000. Timber: Its nature and behaviour. Taylor & Francis Group.

[28] Hassani, M.M., Wittel, F.K., Hering, S., Herrmann, H.J., 2015. Rheological model for wood. Computer Methods in Applied Mechanics and Engineering 283: 1032-1060.

[29] Jenkel, C., Kaliske, M., 2014. Finite element analysis of timber containing branches - An approach to model the grain course and the influence on the structural behaviour. Engineering Structures 75, 237-247.

[30] Hofstetter, K., Hellmich, C., Eberhardsteiner, J., 2007. Micromechanical modelling of solid-type and plate-type deformation patterns within softwood materials. A review and an improved approach. Holzforschung 61, 343-351.

[31] Hoadley, R.B., 2000. Understanding wood. The Taunton Press.

[32] Haygreen J.G., Bowyer J.L., 1996. Forest products and wood Science, an introduction. Third edition. Iowa State University Press/AMES.

[33] Fink, G., Köhler, J., Frangi, A., 2012. Experimental analysis of the deformation and failure behaviour of significant knot clusters. World Conference on Timber Engineering.

[34] Fink, G., Köhler, J., 2014. Model for the prediction of the tensile strength and tensile stiffness of knot clusters within structural timber. European Journal of Wood and Wood Products 72, 331-341.

[35] Niemz, P., 2004. Physik des Holzes. Lecture Notes (in German). ETH Zürich, Switzerland.

[36] Jenkel, C., Leichsenring, F., Graf, W., Kaliske, M., 2015. Stochastic modelling of uncertainty in timber engineering. Engineering Structures 99, 296-310.

[37] Freitas, C. J., 2002. The issue of numerical uncertainty. Applied Mathematical Modelling 26, 237-248.

[38] Kiureghian, A.D., Ditlevsen, O., 2009. Aleatory or epistemic? Does it matter? Structural Safety 31, 105-112.

[39] Schmid, J., Klippel, M., Just, A., Frangi, A., 2014. Review and analysis of fire resistance tests of timber members in bending, tension and compression with respect to the Reduced Cross-Section Method. Fire Safety Journal 68, 81-99.

[40] Knobloch, M., Pauli, J., Somaini, D., Frangi, A., 2014. Cross-sectional capacity and flexural buckling resistance under fire conditions: An experimental study. Stahlbau 83, 657-667.

[41] Klippel, M., Frangi, A., Hugi, E., 2014. Experimental analysis of the fire behavior of finger-jointed timber members. Journal of Structural Engineering (United States) 140, 04013063-1 - 04013063-12.

[42] Frangi, A., Fontana, M., Hugi, E., Jübstl, R., 2009. Experimental analysis of cross-laminated timber panels in fire. Fire Safety Journal 44, 1078-1087.

[43] Breyer, D.E., Cobeen, K.E., Fridley, K.J., Pollock, D.G., 2015. Design of Wood Structures-ASD/LRFD. Seventh edition, McGraw-Hill.

[44] American wood council, 2012. ASD/LFRD Manual for Engineered Wood Construction.

[45] Sørensen, J.D., Kroon, I.B., Faber, M.H., 1994. Optimal reliability-based code calibration. Structural Safety 15, 197-208.

[46] Ditlevsen, O., Madsen, H.O., 1996. Structural reliability methods. Wiley.

[47] Vrouwenvelder, A.C.W.M., Siemes, A.J.M., 1987. Probabilistic calibration procedure for derivation of partial safety factors for the Netherlands building codes. Heron 32, 9-29.

[48] Smith T., Foliente, G.C., 2002. Load and resistance factor design of timber joints: International practice and future direction. Journal of structural engineering 128, 48-59.

[49] Svensson, S., Thelandersson, S., 2003. Aspects on reliability calibration of safety factors for timber structures. Holz als Roh - und Werkstoff 61, 336-341.

[50] Sørensen, J.D., Svensson, S., Dela Stang, B. 2005. Reliability-based calibration of load duration factors for timber structures. Structural Safety 27, 153-169.

[51] Köhler, J., Sørensen, J.D., Faber, M.H., 2007. Probabilistic modeling of timber structures. Structural Safety 29 255-267.

[52] Kline, D., Woeste, F., Bendtsen, B., 1986. Stochastic model for modulus of elasticity of lumber. Wood and Fiber Science 18, 228-238.

[53] Lam, F., Varoglu, E., 1991. Variation of tensile strength along the length of lumber - Part 1: Experimental. Wood Science and Technology 25, 351-359.

[54] Lam, F., Varoglu E., 1991. Variation of tensile strength along the length of lumber - Part 2: Model development and verification. Wood Science and Technology 25, 449-458.

[55] Lam, F., Barrett, J.D., 1992. Modeling lumber strength spatial variation using trend removal and kriging analyses. Wood Science and Technology 26, 369-381.

[56] Isaksson, T., 1999. Modelling the variability of bending strength in structural timber - length and load configuration effects. PhD thesis, Lund University.

[57] Fink, G., Köhler J., 2011. Multiscale variability of stiffness properties of timber boards. Applications of statistics and probability in civil engineering -Proceedings of the 11th International Conference on Applications of Statistics and Probability in Civil Engineering.

[58] Köhler, J., Brandner, R., Thiel, A.B., Schickhofer, G., 2013. Probabilistic characterisation of the length effect for parallel to the grain tensile strength of Central European spruce. Engineering Structures 56, 691-697.

[59] Fink, G., Köhler, J., 2015. Probabilistic modelling of the tensile related material properties of timber boards and finger joint connections. European Journal of Wood and Wood Products 73, 335-346.

[60] Fink, G., Frangi, A., Köhler, J., 2015. Probabilistic approach for modelling the load-bearing capacity of glued laminated timber. Engineering Structures 100, 751-762.

[61] Doorn, N., Hansson, S.O., 2011. Should probabilistic design replace safety factors? Philosophy and Technology 24, 151-168.

[62] Shinozuka, M., 1983. Basic analysis of structural safety. Journal of Structural Engineering 109, 721-40.

[63] Fiessler, B., Rackwitz, R., Neumann H., 1979. Quadratic limit states in structural reliability. Journal of Engineering Mechanics 105, 661-76.

[64] Rosenblatt, M., 1952. Remarks on a multivariate transformation. Annals of Mathematical Statistics 23, 470-2.

[65] Ucci, A., 1992. Probability techniques for reliability analysis of composite materials. Master's thesis, State University, New York (Buffalo).

[66] Harbitz, A., 1986. An efficient sampling method for probability of failure calculation. Structural Safety 3, 109–15.

[67] Philippidis T.P., Lekou, D.J., 1998. Probabilistic failure prediction for FRP composites. Composites Science and Technology 58, 1973-82.

[68] Wetherhold, R., 1981. Reliability calculations for strength of a fibrous composite under multiaxial loading. Journal of Composite Materials 15, 240-248.

[69] Cramér, H., 1971. Mathematical methods of statistics. USA: Princeton University Press.

[70] Hahn, G., Shapiro, S., 1994. Statistical models in engineering. John Wiley & Sons.

[71] Gurvich M.R., Pipes, R.B., 1998. Reliability of composites in a random stress state. Composites Science and Technology 58, 871-81.

[72] Gurvich M.R., 1999. Strength size effect for anisotropic brittle materials under a random stress state. Composites Science and Technology 59, 1701-11.

[73] Vallée, T., Correia, J.R., Keller, T., 2006. Probabilistic strength prediction for double lap joints composed of pultruded GFRP profiles - Part II: Strength prediction. Composites Science and Technology 66, 1915-30.

[74] Kleiber, M., Hien, T.D., 1992. The stochastic finite element method: basic perturbation technique and computer implementation. John Wiley & Sons.

[75] Ghanem, R., Spanos, P., 1991. Stochastic finite elements: a spectral approach. Springer.

[76] Spanos, P., Kontsos, A., 2008. A multiscale Monte Carlo finite element method for determining properties of polymer nanocomposites. Probabilistic Engineering Mechanics 23, 456-70.

[77] Bacharoudis, K.C., Philippidis, T.P., 2013. A probabilistic approach for strength and stability evaluation of wind turbine rotor blades in ultimate loading. Structural Safety 40, 31-8.

[78] Lin, S., 2000. Reliability predictions of laminated composite plates with random system parameters. Probabilistic Engineering Mechanics 15, 327-38.

[79] Jeong, G.Y., Hindman, D.P., 2009. Ultimate tensile strength of loblolly pine strands using stochastic finite element method. Journal of Materials Science 44, 3824-32.

[80] Jeong G.Y., Park, M.J., Park, J.S., Hwang, K.H., 2012. Predicting load-carrying capacity of dovetail connections using the stochastic finite element method. Wood and Fiber Science 44, 430-9.

[81] Kasal, B., Leichti, R.J., 2005. State of the art in multiaxial phenomenological failure criteria for wood members. Progress in Structural Engineering and Materials 7, 3-13.

[82] Norris, G.B., 1950. Strength of orthotropic materials subjected to combined stress. Report no. 1816. US Department of Agriculture, Forest Research Laboratory, Madison.

[83] Hankinson, R.L., 1921. Investigation of crushing strength of spruce at varying angles of spruce at varying angles of grain. Air Service Information Circular 3(259). Material Section Paper No. 130.

[84] Suzuki, S., Tamai A., Hirai N., 1982. Effect of temperature on orthotropic properties of wood. Part III: Anisotropy in the LR-plane. Mokuzai Gakkaishi 8, 401-406.

[85] Liu, J.Y., 1984. Evaluation of the tensor polynomial strength theory for wood. Journal of Composite Materials 18, 216-226.

[86] Woodward, C., Minor, J., 1988. Failure theories for Douglas-fir in tension. Journal of Structural Engineering 114, 2808-2813.

[87] Aicher, S., Klock, W., 2001. Linear versus quadratic failure criteria for in-plane loaded wood based panels. Otto-Graff-Journal 12, 187-199.

[88] Cabrero, J.M., Blanco, C., Gebremedhin, K.G., Martin-Meizoso A., 2012. Assessment of phenomenological failure criteria for wood. European Journal of Wood and Wood Products70, 871-882.

[89] Hill, R., 1950. The mathematical theory of plasticity. Oxford, Clarendon Press.

[90] Azzi, V.D., Tsai, S.W., 1965. Anisotropic strength of composites. Experimental Mechanics 5, 283-288.

[91] Theocaris, P.S., Philippidis, T.P., 1991. On the validity of the tensor polynomial failure theory with stress interaction terms omitted. Composites Science and Technology 40, 181-191.

[92] Tsai, S.W., Wu, E.M., 1971. A general theory of strength for anisotropic materials. Journal of Composite Materials 5, 58-80.

[93] Cowin, S.C., 1979. On the strength anisotropy of bone and wood. Journal of Applied Mechanics 46, 832–838.

[94] Hoffman, O., 1967. The brittle strength of orthotropic materials. Journal of Composite Materials 1, 200-6.

[95] Van der Put, T.A.C.M., 2005. The tensor polynomial failure criterion for wood. Delft Wood Science Foundation, Delft.

[96] Clouston, P., Lam, F., Barrett, J.D., 1998. Interaction term of Tsai-Wu theory for laminated veneer. Journal of Materials in Civil Engineering 10, 112-6.

[97] Brandner, R., Schickhofer, G., 2014. Spatial correlation of tensile perpendicular to grain properties in Norway spruce timber. Wood Science and Technology 48, 337-352.

[98] Xavier J., Avril S., Pierron F., Morais J., 2009. Variation of transverse and shear stiffness properties of wood in a tree. Composites: Part A 40, 1953-1960.

[99] Pereira, J., Xavier J., Morais J., Lousada J., 2014. Assessing wood quality by spatial variation of elastic properties within the stem: Case study of Pinus pinaster in the transverse plane. Canadian Journal of Forest Research 44, 107-117.

[100] Casciati, S., Domaneschi, M., 2007. Random imperfection fields to model the size effect in laboratory wood specimens. Structural Safety 29, 308-321.

2 Random field-based size effect model for longitudinal strength of clear timber

2.1 Introduction

From a structural point of view, wood/timber can be considered as a natural unidirectional fiber composite with highly anisotropic properties. For specific species, geographical location, and local growth conditions, the material properties depend on factors such as age, structural imperfections, location of timber within the tree, and load history and are therefore inherently highly variable. One of the consequences of this variability is the phenomenon known as statistical size effect. When the failure mode is brittle, the mean strength of a specimen with a larger volume is lower than that of a smaller one, which is also the case for any other level of cumulative probability, and this difference increases with the level of variability in material properties. This is normally attributed to the higher probability of critical defects occurring in a larger volume.

The classical Weibull size effect law (CWSEL) [1] is the most common model used in the literature [2] for the description of statistical size effects on timber strength in its brittle failure modes. According to this model, a structural member fails when the stress level reaches the strength at a single material point.

The size effect on timber strength can be treated as a volume effect, for example see [3-6] where such an assumption was adopted for the failure analysis of adhesively-bonded, welded and dovetail timber joints and [7-9] in which the elastoplastic behavior of strand-based wood composites and laminated veneer was studied. The Weibull law was applied only in tensile mode, while plastic behavior was considered only in compressive mode. Alternatively, the size effect can be split into length and cross-sectional effects - see e.g. [10,11] - on the strength prediction of clear timber under bending and [12] in the case of structural lumber.

Nevertheless, research efforts for the quantification of size effect on the strength of clear wood, by conducting pure tensile tests on specimens with different volumes, are very limited in the literature. Dill-Langer et al. [13] conducted longitudinal tensile experiments on specimens made of spruce wood. Two groups of specimens with different volumes were tested and a fiber bundle model was introduced in order to simulate the macroscopic behavior in terms of microscopic damage. Zhu et al. [14] introduced a length-effect parameter to quantify the size effect due to the length change on the longitudinal tensile strength of Japanese larch wood.

In current practice using the CWSEL, a Weibull distribution is fitted to data obtained from experiments on specimens with standardized dimensions. Then, the CWSEL is used to predict the strength of pieces of timber either with higher volumes [2,10,11], like timber beams, or lower volumes [4,7], which are usually small elements considered in finite element analyses of timber structures. However, using experimental data from the literature [13,14], it is shown in the current study that this procedure can result in relative errors in the prediction of the size effect on timber strength as high as 400%. This is attributed to the fact that the spatial correlation in the strength field is neglected in the CWSEL. It is noted that the inaccuracy of the CWSEL, when small volumes of materials are concerned, is already known; however, the issue has been overlooked in the case of timber. Nevertheless, it is important, particularly in the FE content, to extend size effect predictions to small volumes.

As an alternative to the CWSEL, timber strength can be modeled as a random field, considering, in addition to strength variation between different specimens as in conventional statistical analyses, the spatial variation within each specimen in a random manner. There are several methods to generate realizations of a random field in each specimen. The two more commonly used methods are the spectral representation method [15] and the The Karhunen–Loève (K–L) expansion [16]. A comparison between the two methods showed that the spectral representation method is faster and more efficient [17]. Among other methods, turning bands method [18], the autoregressive moving average–autoregressive models [19], the optimal linear estimation [20] and the expansion optimal linear estimation method [21] can be mentioned. A realization is a randomly generated sample of a random field and describes the spatial variability of the field for that sample in the physical domain considered, e.g. the volume of a specimen. Realizations of the strength field for specimens with different volumes can be used for investigating the size effect. Recently, Arwade et al. [22,23] used the random field approach to characterize the lengthwise spatial variability in the elastic modulus and compressive strength of parallel strand lumbers as 1D random fields. However, there is no study in the literature that has been devoted to the size effect on the longitudinal tensile strength of clear timber, and the spatial correlation in the strength field, i.e. the way in which the strength value at one point influences the strength at the surrounding points, has usually been neglected.

Studying the size effect on the longitudinal tensile strength of clear timber using random fields, is a problem of finding the extreme value statistics. This is because the failure mode is brittle, and to investigate the size effect, the distributions of minima of strength fields for specimens of different volumes has to be obtained. The extreme value problem was studied thoroughly by Gumbel in 1958 [24]. Concerning random fields, lots of research on this problem has been conducted in different scientific domains, e.g., by mathematicians [25], and in hydrology [26], climate [27], and cosmology [28]. Useful information on this topic can be found in [29]. Analytical solutions are only available for a few cases [30], and therefore, numerical methods such as simulations [31] or asymptotic approximation methods [30] are usually employed.

This study presents a model for the size effect on timber strength that takes into account the spatial variability in the strength field. The theory of random fields was used to model the random 3D spatial variability of the longitudinal strength. Using the spectral representation scheme, realizations of strength field in each specimen were generated considering the Weibull distribution and squared exponential function for statistical variability and spatial variability, respectively. The stochastic response was obtained via the Monte Carlo method along with the weakest link theory. This procedure was repeated for specimens with different volumes to estimate the effect of size on strength. The current results were compared to experimental data from the literature. An analytical expression able to efficiently approximate the numerical results of the random field modeling has also been introduced in this Chapter.

2.2 Classical Weibull size effect law and its limitations

2.2.1 Weibull size effect theory

The CWSEL has been widely used to model the size effect on timber strength [2,4-12]. According to this model, the material is considered as a structure made up of linked elements, which fails with the first element failure. The mean strength of a specimen under uniaxial loading, $\bar{\sigma}(V)$, is related to its volume V as [32]:

$$\bar{\sigma}(V) = \sigma_0 \Gamma(1+1/m)\left(\frac{V_0}{V}\right)^{1/m} \tag{2.1}$$

where σ_0 and m are the scale and shape parameters of the Weibull distribution, Γ is the Gamma function, and V_0 is a reference volume. Eq. (2.1) can be plotted as a straight line in a log-log scale. The procedure to obtain this formula is explained in [32].

It can be shown that, at any given failure probability level, the strengths of two pieces, σ_1 and σ_2, with volumes V_1 and V_2 are related:

$$\frac{\sigma_1}{\sigma_2} = \left(\frac{V_2}{V_1}\right)^{1/m} \tag{2.2}$$

based on the assumption of independent identically distributed random variables [33]. The analytical procedure to obtain Eq. (2.2) is explained in [34]. For a numerical representation of the method, the larger volume V_2 is divided into n segments with volumes equal to V_1 and a random strength value from the Weibull distribution, corresponding to volume V_1, is assigned to each segment. The minimum value of the segment strengths is considered as the strength of

V_2 based on the weakest link theory. This simulation is repeated as many times as necessary to collect sufficient data points for estimating the statistics of the strength distribution of V_2. When V_2 / V_1 is not an integer, interpolation can be used. Finally, having obtained the strength distributions for both volumes, it is easy to show that their relationship follows Eq. (2.2). However, due to this independent spatial assignment of the strength to smaller segments in the larger volume, The CWSEL tends to overestimate the effect of size on strength [33]. In reality, there is always a spatial correlation in the strength field that can be considered by using the random field approach. Moreover, Eq. (2.2) implies that the CWSEL can be scaled arbitrarily; i.e., its form does not change even for very small volumes of materials. Therefore, for very small volumes ($V \to 0$) the scale parameter, or equivalently the mean value of the strength distribution, approaches infinity. However, this is not the case in reality, and there is an upper limit for strength as volume decreases.

2.2.2 Modeling size effect on longitudinal tensile strength of clear timber with CWSEL

In most works related to the size effect on the longitudinal tensile strength of clear wood, tensile tests parallel to the grain are only performed on specimens with a constant volume. This is because testing a set of specimens with a constant volume suffices to determine the unknown parameter of the CWSEL. Thus, by fitting the Weibull distribution to the experimental data, the shape parameter is estimated, and the CWSEL is then used in the related application, such as estimation of a wooden joint capacity [4]. To the authors' knowledge, there are only two works [13, 14] in which the effect of volume change on the longitudinal tensile strength of clear timber has been investigated experimentally. The specimen dimensions in these works and the corresponding Weibull parameters are given in Table 2.1. The dimensions correspond to the middle part of specimens with a constant cross-sectional area. In [13], longitudinal tensile tests were conducted on two sets of clear specimens made of spruce wood. The dimensions of the larger specimen are approximately three times those of the smaller specimen. In [14], however, only the length of the specimen has been changed. Nevertheless, in each of these works, the Weibull shape parameters obtained from fitting the experimental results of the smaller and larger specimens exhibit some differences. To examine the size effect within the Weibull theory framework, it is necessary to have a constant shape parameter; therefore, an average value was used in this study for examining the accuracy of the CWSEL; i.e., 9.3 and 4.0 for the experimental results from [13] and [14] respectively. The error introduced in the calculation of mean values due to this averaging, compared to mean values from experimental data, is less than 0.5% in both cases.

Table 2.1: Experimental results for longitudinal tensile strength of clear timber.

Researchers	Type of wood	Specimen dimensions (mm^3)	Weibull scale parameter (MPa)	Weibull shape parameter	Mean value (MPa)
Dill-Langer et al. [13]	spruce	2×6×35	146.2	8.3	138.7±19.8
		6×20×110	134.0	10.3	127.1±14.9
Zhu et al. [14]	Japanese larch	5×25×30	122.9	3.77	111.4±32.9
		5×25×120	114.0	4.22	103.3±27.7

When specimen volumes and Weibull shape parameters for spruce are substituted into Eq. (2.2), an increase of 45% in the mean value strength, from larger specimens to smaller ones, is predicted. However, experimental results show only a 9.1% increase in strength. Therefore, the absolute error in the Weibull prediction for strength change is $|45-9.1|=35.9\%$. In the case of Japanese larch, an increase of 41.4% in the mean strength is predicted by the CWSEL. However, there is only a 7.8% increase in the strength according to experiments. In this case, the absolute error introduced in the prediction of strength change due to size effect is $|41.4-7.8|=33.6\%$.

To highlight the inaccuracy of the classical law, the relative error is also calculated. This value shows the error in prediction of strength change compared to the absolute value of the change obtained from experimental results. The relative errors, in the case of spruce and Japanese larch, are $|45-9.1|/9.1\times100=394\%$ and $|41.4-7.8|/7.8\times100=431\%$, respectively. In both cases, the CWSEL overestimates the change in strength by a factor of 5, approximately.

The above calculations show that the CWSEL can severely overestimate the effect of size on timber strength.

2.3 Strength of timber as random field

Random variability and spatial variability in material properties usually exist in parallel. For example, in a set of specimens prepared for standard mechanical tests, the properties randomly change from one to another. Also, these specimens have already been cut from spatially different places in a timber board or composite panel that comprises spatial variability. The combination of random and spatial variability is referred to as random spatial variability. Taking this variability into account can result in more accurate and realistic numerical models, leading to more reliable and optimized timber-based designs. However, the spatial variability in the properties of clear timber has frequently been neglected in the literature [3-12]. Although knots are frequently present in timber structures, in some applications such as timber joints, the failure

usually occurs in the clear wood that is being considered in this thesis. Moreover, the current study can form a basis for developing models for structures containing knots.

The stochastic/random field approach can be used to model the random spatial variation of the strength [35]. Unlike composite laminas and laminates, which can usually be safely considered as 2D structures such as plates due to their low thickness, timber structures are normally modeled as beam, columns etc., which have 3D spatial variation along their lengths as well as their cross sections. Hence, a 3D random field should be used for the appropriate modeling of the strength field in timber.

To model timber strength as a random field, statistical variability and spatial variability have to be analytically formulated. Statistical variability is described by the marginal distribution of the random field. Marginal distribution is the statistical distribution of samples of the random field simulated in a small volume of material in which spatial variability can be neglected. In other words, the simulated field has the same value throughout a specific sample, but this can change from one sample to another. Also, spatial variability is normally characterized using an appropriate autocorrelation function that specifies the degree of correlation in strength values at a specific material point and its surrounding points. The term auto indicates the correlation between values of the same parameter. This autocorrelation function contributes to the generation of realizations of the random field, as shown in the next section.

The autocorrelation function of the random field $Y(\mathbf{x})$ is defined by the following equation [34]:

$$R_{YY} = \int_{-\infty}^{+\infty}\int_{-\infty}^{+\infty} y_1 y_2 f_{YY}(y_1, y_2) dy_1 dy_2 \tag{2.3}$$

where random variables y_1 and y_2 represent $Y(\mathbf{x})$ at the positions $\mathbf{x}_1$ and $\mathbf{x}_2$, and $f_{YY}(y_1, y_2)$ is the joint probability density function (PDF) of the random variables y_1 and y_2. The marginal PDF is not always available [21], and only the marginal PDF is usually at hand:

$$f_Y(y_1) = \int_{-\infty}^{+\infty} f_{YY}(y_1, y_2) dy_2 \tag{2.4}$$

which is independent of $\mathbf{x}$ for stationary random fields, as is the case in the current study. In practice, different autocorrelation functions have been developed that can be used for different random fields [29]. Concerning material parameters, exponential and squared exponential autocorrelation functions have proved to be most successful [35,36-39]. Some applications for material characterization include unidirectional composites [35], strand chopped mats [40], concrete [41] and glass fibers [33]. The squared exponential function was selected in the present study, as it has been used more often for fibrous composites [35,36,39,40] and is expressed as:

$$R = \sigma^2 \, \mathrm{e}^{-(\xi_1^2+\xi_2^2+\xi_3^2)/d^2} \tag{2.5}$$

where σ is the standard deviation of the strength field, d is a correlation length and ξ_1, ξ_2 and ξ_3 are separation distance components along x_1, x_2 and x_3 directions respectively. Correlation length specifies the level of correlation in space; the shorter the correlation length, the faster the correlation decreases. The assumption of having the same value for correlation length in the longitudinal and transverse directions is commonly found in the literature [35,36,39,40] for composites. This assumption would be more justifiable for timber structures where the cross-sectional dimensions of structural members are normally smaller than the longitudinal ones and also the ones used in this study. Nevertheless, due to the orthotropic behavior of timber, it is most likely that the correlation length would be different in the transverse direction, which is commonly considered to be the isotropic plane.

2.4 Random field modeling procedure

In order to model timber strength as a random field it is necessary to generate spatial variation of strength in a specified domain, and to obtain the desired response based on this spatial variation.

2.4.1 Generating realizations of strength as a 3D random field

Within the framework of the spectral representation scheme, simulation of a non-Gaussian random field is based on simulating an underlying Gaussian one. After this underlying Gaussian random field has been determined, the translation technique can be applied to generate realizations of the target non-Gaussian field. The translation technique is a memory-less non-linear transformation of a Gaussian field into a non-Gaussian field [42].

The method for simulating a Gaussian random process was first presented by Shinozuka and Jan [43] and later extended to multidimensional random fields [15]. In this method, the Gaussian random field $f_G(\mathbf{x})$ is expanded as a sum of cosine functions having random phase angles and deterministic amplitudes. The amplitudes depend on the power spectral density function of the random field, which in 3D space is defined as:

$$S_G(\boldsymbol{\kappa}) = \frac{1}{(2\pi)^3} \int_{-\infty}^{\infty} \int_{-\infty}^{\infty} \int_{-\infty}^{\infty} R_G(\boldsymbol{\xi}) \, \mathrm{e}^{-i(\kappa_1\xi_1+\kappa_2\xi_2+\kappa_3\xi_3)} d\xi_1 d\xi_2 d\xi_3 \tag{2.6}$$

where R_G is the autocorrelation function and κ_1, κ_2 and κ_3 are the corresponding wave numbers. The formula to simulate the Gaussian random field is [15]

$$f_G(x_1,x_2,x_3)=\sum_{n_1=0}^{N_1-1}\sum_{n_2=0}^{N_2-1}\sum_{n_3=0}^{N_3-1}\Big[A_{n_1n_2n_3}\Big[\cos(\kappa_{1n_1}x_1+\kappa_{2n_2}x_2+\kappa_{3n_3}x_3+\phi^1_{n_1n_2n_3}) \\ +\cos(\kappa_{1n_1}x_1+\kappa_{2n_2}x_2-\kappa_{3n_3}x_3+\phi^2_{n_1n_2n_3}) \\ +\cos(\kappa_{1n_1}x_1-\kappa_{2n_2}x_2+\kappa_{3n_3}x_3+\phi^3_{n_1n_2n_3}) \\ +\cos(\kappa_{1n_1}x_1-\kappa_{2n_2}x_2-\kappa_{3n_3}x_3+\phi^4_{n_1n_2n_3})\Big]\Big] \tag{2.7}$$

where:

$$A_{n_1n_2n_3}=2\sqrt{S_G(\kappa_{1n_1},\kappa_{2n_2},\kappa_{3n_3})\Delta\kappa_1\Delta\kappa_2\Delta\kappa_3} \tag{2.8}$$

$$\kappa_{1n_1}=n_1\Delta\kappa_1,\quad \kappa_{2n_2}=n_2\Delta\kappa_2,\quad \kappa_{3n_3}=n_3\Delta\kappa_3 \tag{2.9}$$

$$\Delta\kappa_1=\frac{\kappa_{1u}}{N_1},\quad \Delta\kappa_2=\frac{\kappa_{2u}}{N_2},\quad \Delta\kappa_3=\frac{\kappa_{3u}}{N_3} \tag{2.10}$$

$$A_{n_1n_20}=A_{n_10n_3}=A_{0n_2n_3}=0 \quad \text{for:} \\ n_1=0,1,...,N_1-1;\quad n_2=0,1,...,N_2-1;\quad n_3=0,1,...,N_3-1 \tag{2.11}$$

In Eq. (2.7), $\phi^i_{n_1n_2n_3}\,(i=1,2,3,4)$ are random phase angles and $\kappa_{iu}\,(i=1,2,3)$ are upper cut-off wave numbers. κ_{iu} are selected as being sufficiently large to cover the whole wave range of interest. Also, a random number generator is used to produce the independent random phase angles in each sample function that are uniformly distributed in the range $[0,2\pi]$. Moreover, the fast Fourier transform technique can be applied when calculating the series in Eq. (2.7) to reduce the computation time of sample function generation. This is a major advantage especially when dealing with 3D random fields. As pointed out in [17], the computational efficiency of this method is far better than the other popular method known as the Karhunen-Loeve expansion.

Recently, a simple and efficient scheme has been introduced by Shields et al. [42] for the simulation of general non-Gaussian one-dimensional random processes based on simulating an underlying Gaussian process. In the present study, an extension to 3D random fields has been introduced. This scheme is based on the translation technique for estimating the non-Gaussian random field:

$$f_{nG}(x_1,x_2,x_3)=F^{-1}_{nG}\{F_G[f_G(x_1,x_2,x_3)]\} \tag{2.12}$$

where F_{nG}^{-1} is the inverse of non-Gaussian cumulative distribution function (CDF) and F_G denotes the CDF of the underlying Gaussian random field. If the autocorrelation function of the underlying Gaussian random field is known, this transformation can always be applied. However, the autocorrelation function of the non-Gaussian field is normally available, see (Eq. (2.5)), instead of the autocorrelation function of the Gaussian field. S_{nG} can therefore be obtained by substituting R_{nG} estimated by Eq. (2.5) into Eq. (2.6):

$$S_{nG} = \sigma^2 \frac{d^3}{8\pi^{1.5}} e^{-\frac{d^2}{4}\left(\kappa_1^2+\kappa_2^2+\kappa_3^2\right)} \tag{2.13}$$

This integration was done in MATLAB. An autocorrelation function for the underlying Gaussian field is estimated in an iterative manner, using the non-Gaussian marginal distribution, and the R_{nG} and S_{nG} as input data. When R_G has been estimated, a Gaussian sample function can be generated using Eq. (2.7). Finally, the transformation in Eq. (2.12) is applied to obtain the target non-Gaussian sample function, which expresses the spatial variation of the strength field in each specimen.

Each Gaussian realization is generated at one step using Eq. (2.7), with no iteration. This equation includes a converted form of correlation function but also lots of randomly generated numbers, based on the 'uniform' statistical distribution between 0 and 2π . The final summation of series gives a function of only space coordinates. Now the insertion of the coordinates of each point in the space will give the value of the parameter at that point in that realization. The random difference between realizations comes from the randomly generated numbers for each realization.

This single sudden step will generate a realization with an underlying Gaussian distribution and with the desired spatial correlation structure. After that, the translation to the Non-Gaussian realization is done using Eq. (2.12), which distorts the spatial correlation structure. An iterative procedure is needed to maintain the original spatial correlation structure according to the correlation function of Eq. (2.5), as explained above.

2.4.2 Random response assessment

In this study, the Monte Carlo method was used to estimate the statistics of the stochastic response of the tensile strength of wooden specimens with different volumes. Following the above-mentioned method, realizations of the strength random field were generated in each specimen. The spatial variation of the random parameter in the generated realizations were continuous and smooth, indicating that a sufficient number of terms were considered in calculating the series in Eq. (2.7). The strength of a specimen under a uniform uniaxial stress state can be determined as the minimum value of the strength field in the corresponding

realization, as the failure mode is brittle for timber in parallel to the grain direction. Therefore, the smoothness of the spatial distribution is important for accurate estimation of the minimum value of the field in each specimen. By generating a statistically significant number of realizations and selecting the minimum strength value in each of them, a good estimation of the statistical distribution for the strength of a specimen with a specific volume can be obtained. In the current study, a sample size of 4000 realizations has been considered for each specific volume and material property, which suffices to achieve a high level of accuracy [44]. This process is repeated for specimens with different volumes and the statistical distributions for their strengths are obtained. By comparing strength statistics, such as mean values, for specimens with different volumes, the effect of size on timber strength can be determined.

2.5 Estimating random field parameters for spruce and Japanese larch

The experimental data given in Table 2.1 were used for estimating the correlation length of the autocorrelation function and the marginal distribution parameters of strength as a random field for spruce and Japanese larch wood.

The two-parameter Weibull distribution has been considered to represent statistical variability. For the shape parameter, as discussed in Section 2.2.2, the mean value obtained from experimental results is used. The remaining two unknowns are the scale parameter of the marginal distribution and the correlation length. Scale parameters of two different volumes for each type of wood are shown in Table 2.1. Therefore, it is possible to obtain the two unknown values for each wood. By extensive numerical experimentation, assuming different values for the correlation length and scale parameter of the marginal distribution, i.e. trial and error approach, appropriate values were estimated and are given in Table 2.2. It can be seen that the value of the scale parameter for each wood, which has a direct relationship to the mean value, is higher than the corresponding values in Table 2.1. This is because the marginal mean value gives the higher bound for the strength as the volume approaches zero. In the next section, it is shown that using the values given in Table 2.2 a good agreement with the experimental results can be achieved.

Table 2.2: Parameters of marginal Weibull distribution and correlation length of strength field for spruce and Japanese larch.

Type of wood	Marginal shape parameter	Marginal scale parameter (MPa)	Correlation length (mm)
spruce	9.3	155.5	62.0
Japanese larch	4.0	130.9	225.0

A value of 62mm for the correlation length means that when the distance between two points inside the material is 62mm, the correlation between field values at these points is reduced by a factor of exp(-1) according to Eq. (2.5) compared to the case of two coincident points. It is noted that the field value at any specific point inside the material can be considered as a random variable, because when the coordinates of a point are substituted into Eq. (2.7), only statistical variability remains.

The approach used to estimate the correlation length can be considered as a reversed approach, compared to the direct approach of measuring the strength at enough number of points within a sample of the material. If the correlation length is known from a direct approach, it can be used to produce realizations of the actual strength field in specimens of different sizes and investigate the size effect. These results, are unique, provided that enough number of simulations have been performed. Therefore, the reverse procedure could also be followed; i.e., having the size effect results, a unique correlation length could be found that would reproduce those results. The addition of more specimen sets of different volumes can improve the estimation of the correlation length.

2.6 Random field modeling results and discussion

The random field modeling of longitudinal tensile strength was performed for the two volumes of spruce wood with the dimensions given in Table 2.1. Three indicative realizations, i.e. randomly generated spatial distribution of the strength, for both volumes are shown in Figs. 2.1 and 2.2. As can be seen, the spatial variability of strength generally exhibits a more complicated pattern for the larger volume (Fig. 2.2). This is because the correlation length is a material parameter that expresses the degree to which the value of the field at one specific point influences field values in the surrounding points as a function of spatial distance. Generally, the more macroscopically homogeneous a material is, the higher the value of the correlation length of its mechanical properties such as strength.

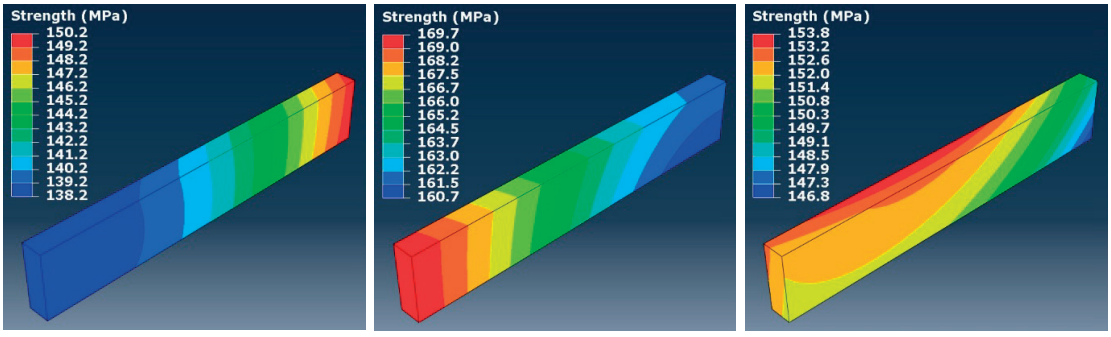

Fig. 2.1: Three indicative, randomly generated realizations for longitudinal tensile strength as random field in spruce specimen of volume 2×6×35 mm^3.

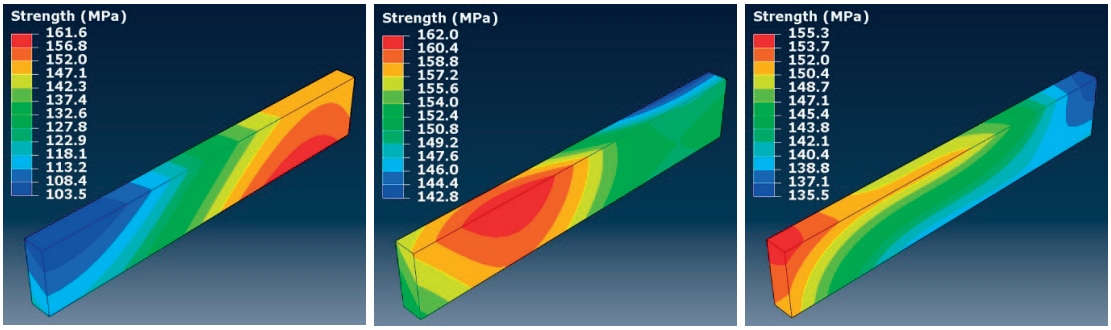

Fig. 2.2: Three indicative, randomly generated realizations for longitudinal tensile strength as random field in spruce specimen of volume 6×20×110 mm^3.

As in a larger volume greater distances between material points are anticipated, the possibility of more spatial variation increases. Naturally, the possibility of the occurrence of a minimum strength with a lower value also increases in each specimen, as evidenced by the numerical values of the strength field given in Figs. 2.1 and 2.2. Strength field within each specimen has a minimum value, and for a larger specimen it is more probable that its minimum value be lower than the minimum value in a smaller specimen. The above constitutes the basis for the random field modeling of the size effect on strength.

Histograms of strength results from numerical simulations and fitted PDFs along with corresponding CDFs for spruce specimens with dimensions 2×6×35 mm^3 and 6×20×110 mm^3 are shown in Figs. 2.3 and 2.4, respectively. The three most common statistical distributions used for material properties, i.e. normal, lognormal and Weibull, have been fitted to the simulation results to ascertain which one is the most representative. PDFs and CDFs of experimental results based on the Weibull distribution are also given and labeled as 'Experiment'.

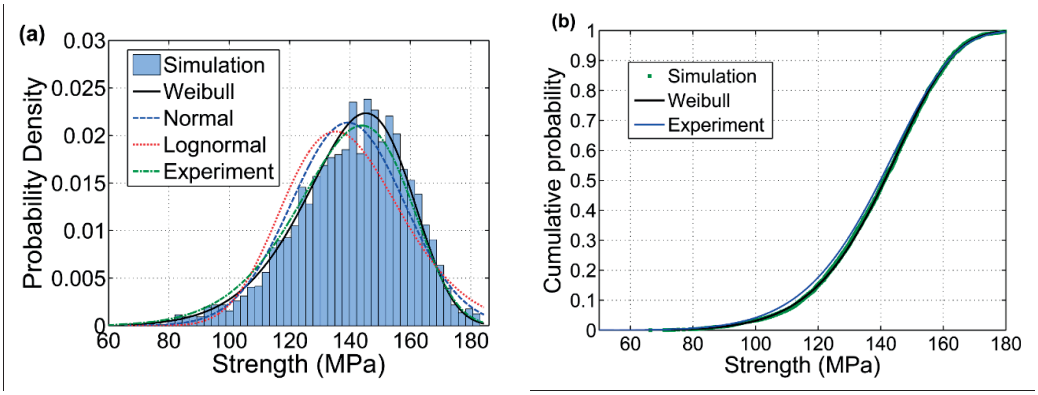

Fig. 2.3: a) Probability density and b) cumulative distribution functions for strength of spruce specimen with volume 2×6×35 mm^3.

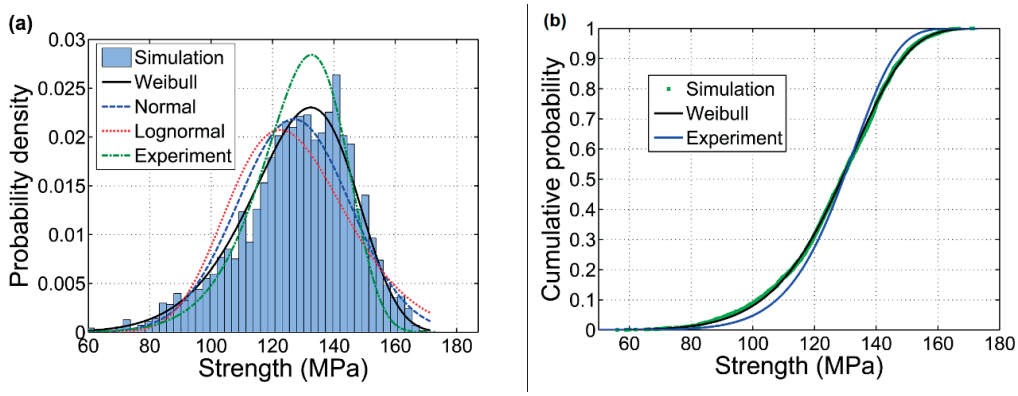

Fig. 2.4: a) Probability density and b) cumulative distribution functions for strength of spruce specimen with volume 6×20×110 mm3.

It can be seen in Figs. 2.3a and 2.4a that the Weibull PDF is the best descriptor for the simulation results. The fitted Weibull distributions to the simulation results are also closer to the experimental distributions in both cases. Weibull parameters as well as the results of goodness of fit tests, Anderson-Darling (AD) and Kolmogorov-Smirnov (KS), at a significance level of 0.05 are provided in Table 2.3. Regarding the results of the statistical tests, a value of zero denotes that sampled data are taken from the corresponding distribution, while a value of one denotes that the presumed distribution is not accepted. It is observed that both AD and KS tests support Weibull distribution for the longitudinal tensile strength while rejecting normal and lognormal distributions. Therefore, the strength results obtained from selecting the minimum strength value from each realization follow a Weibull distribution. Values provided for the shape parameter of Weibull distributions in Table 2.3 exhibit a slight change compared to that of the marginal distribution; however, as mentioned earlier, its effect on the mean value of the distribution is negligible. The Weibull parameters based on simulation results in Table 2.3 are slightly different from parameters of Weibull distributions fitted to the experimental data in Table 2.1. These difference, which are not very significant, are common in stochastic studies [6,9,35,45]. The experimental parameters are always more trustable when a sufficiently large number of tests have been performed.

Table 2.3: Results for statistical parameters of simulations and goodness of fit tests for longitudinal tensile strength of spruce.

Dimensions of spruce specimen (mm^3)	Weibull parameters		Weibull		Normal		Lognormal	
	Scale factor	Shape factor	AD	KS	AD	KS	AD	KS
2×6×35	147.2	8.9	0	0	1	1	1	1
6×20×110	134.4	8.5	0	0	1	1	1	1

The random field modeling of longitudinal strength was also performed for Japanese larch wood. Simulation results and fitted PDFs along with corresponding CDFs are shown in Figs. 2.5 and 2.6, respectively. Similarly to the previous case, the Weibull PDF is the best descriptor for the simulation results.

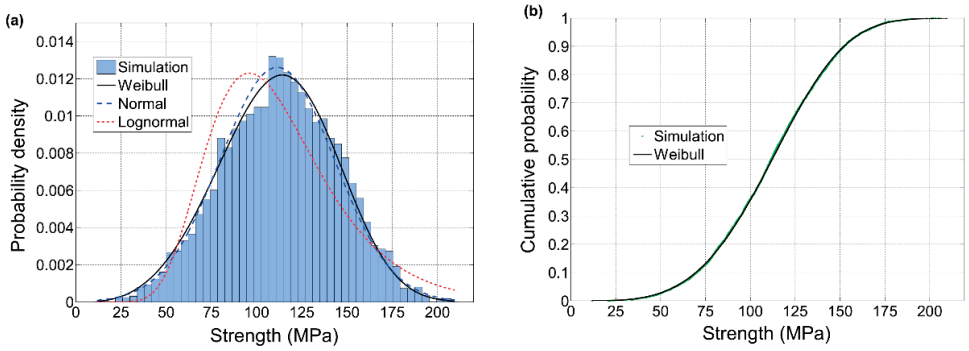

Fig. 2.5: a) Probability density and b) cumulative distribution functions for strength of Japanese larch specimen with volume 5×25×30 mm^3.

Weibull parameters as well as results of goodness of fit tests are given in Table 2.4. Both AD and KS tests support the Weibull distribution for the longitudinal tensile strength while rejecting lognormal distribution. However, a normal distribution was only rejected by the AD test. The effect of a small variation in values for the Weibull shape parameter, given in Table 2.4, on the mean values is again negligible.

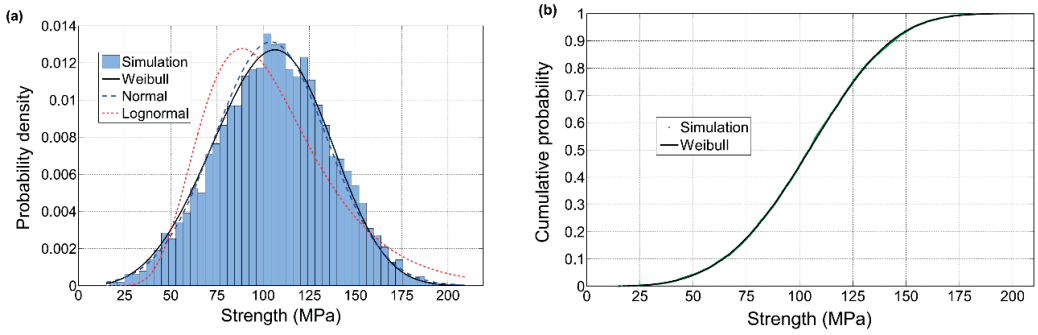

Fig. 2.6: a) Probability density and b) cumulative distribution functions for strength of Japanese larch specimen with volume 5×25×120 mm^3.

Table 2.4: Results for statistical parameters of simulations and goodness of fit tests for longitudinal tensile strength of Japanese larch.

Dimensions of spruce specimen (mm^3)	Weibull parameters		Weibull		Normal		Lognormal	
	Scale factor	Shape factor	AD	KS	AD	KS	AD	KS
5×25×30	123.2	3.9	0	0	1	0	1	1
5×25×120	115.1	3.8	0	0	1	0	1	1

Based on the parameters in Tables 2.3 and 2.4, the prediction accuracy of the random field modeling can be evaluated by computing the ratio between the mean values of strength for shorter and longer specimens. The mean values are summarized in Table 2.5. This ratio is 1.098 for spruce and 1.072 for Japanese larch; i.e., a 9.8% and 7.2% increase in the strength for smaller specimens compared to the larger ones, respectively. From the experimental data, the corresponding values are 9.1% and 7.8%. The relative errors of random field predictions compared to experiments, for both cases, are computed as $|9.8-9.1|/9.1\times100=7.7\%$ and $|7.2-7.8|/7.8\times100=7.7\%$. It can be seen that the error has been reduced from 394% and 431% to 7.7% for both woods by using the random field approach instead of the CWSEL.

Table 2.5: Mean values for longitudinal tensile strength of spruce and Japanese larch based on simulations.

Type of wood	Specimen dimensions (mm^3)	Mean value strength (MPa)
Spruce	2×6×35	139.3±18.7
	6×20×110	126.9±17.8
Japanese larch	5×25×30	111.5±32.0
	5×25×120	104.0±30.6

2.6.1 Size effect in wider volume ranges of clear timber and analytical approximation

The developed model can be used for investigating the size effect on strength in a wider volume range of clear timber. First, Japanese larch is considered because the size effect is examined as specimen length changes; therefore, owing to the change in only one dimension, it is easier to demonstrate the asymptotic behaviors of the size effect. Fig. 2.7 displays simulation results using red dots for the mean value of strength of a specimen with cross-sectional dimensions $5\times25\,mm^2$ versus its length on a logarithmic scale. It can be seen that there are two asymptotes. In the left asymptote where specimen length decreases to zero, the curve gradually approaches a constant value. Based on visual observations of this curve, the length limit below which the strength can be considered to be independent of specimen length is approximately 0.1 of the

correlation length, d. The upper bound mean value for the strength of the Japanese larch specimen is 114.9 MPa, which is lower than the mean value of the marginal distribution, 118.6 MPa, calculated based on the data in Table 2.2 and shown as a solid horizontal line in Fig. 2.7. This difference highlights the fact that the strength field was modeled as a 3D random field, and therefore, strength can change spatially across the cross section, even when the length approaches zero, leading to a decrease in the mean value of strength. As the length of the specimen increases, strength variation gradually approaches a line with a constant slope similar to that of the CWSEL. This indicates that for a very long specimen, the effect of the spatial correlation between adjacent material points becomes insignificant. Therefore, the prediction by the current model approaches that of the CWSEL in which spatial correlation is neglected. The length of specimen above which the CWSEL can be used accurately is approximately 10 times the correlation length by visual observation of the curve in Fig. 2.7.

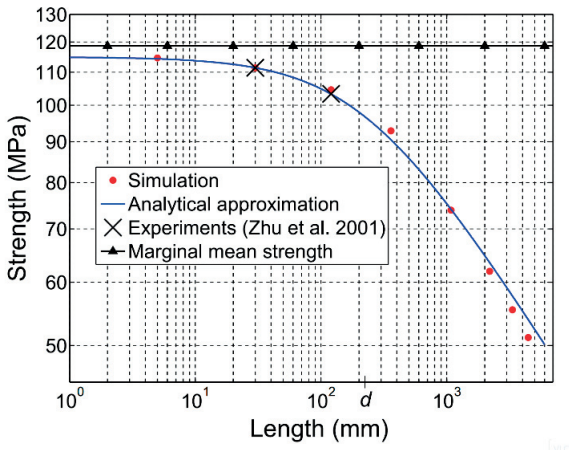

Fig. 2.7: Mean value strength versus length of Japanese larch specimen. *d* on horizontal axis indicates correlation length of Japanese larch wood.

An analytical formula is proposed in the following that approximates the numerical results reasonably well and facilitates the application of the proposed size effect model for clear timber. This formula mainly modifies the part of Eq. (2.1) related to the volume of the material:

$$\bar{\sigma}(L_1, L_2, L_3) = \sigma_{0m}\Gamma(1+1/m)\left[\left(\frac{d}{d+L_1}\right)\left(\frac{d}{d+L_2}\right)\left(\frac{d}{d+L_3}\right)\right]^{1/m} \tag{2.14}$$

where L_1, L_2 and L_3 are dimensions along x_1, x_2 and x_3 directions, respectively, for a specimen with uniform uniaxial stress state, and d is the correlation length already introduced in Eq. (2.5).

Eq. (2.14) is proposed based on the following arguments: 1) The general form of the classical formula in Eq. (2.1) has been used as a basis for this equation and the shape parameter of the Weibull distribution has been used in the same manner. 2) Contrary to the CWSEL, the effect of volume change on the strength has been broken into three components corresponding to three coordinate axes, because the level of spatial variability in each direction depends on the corresponding specimen dimension. 3) The reference volume in Eq. (2.14) has been considered as being a very small volume of the material in which spatial variability can be neglected. Thus, when specimen dimensions approach zero, the expression powered by $1/m$ approaches one, similar to the classical formula. Naturally, what remains should represent the mean value of the marginal distribution. Therefore, σ_0 in Eq. (2.1) has been changed to σ_{0m} in Eq. (2.14). 4) The correlation length of the strength field has been incorporated in the classical formula, in such a way that the asymptotic behaviors of the size effect predicted by the numerical simulations hold.

Eq. (2.14) cannot be arbitrarily scaled because the correlation length, d, as a material parameter, introduces a length scale into the size effect law in a natural way. This equation has also been plotted in Fig. 2.7. The two above-mentioned asymptotic behaviors observed in the numerical results are also satisfied by this equation. In other words, the mean value of strength approaches a constant value as specimen dimensions become small compared to the correlation length. On the other hand, the CWSEL can be applied when specimen dimensions are much larger than the correlation length. Finally, it is noted that Eq. (2.14) also predicts a lower left asymptotic value of strength than the marginal strength for the Japanese larch specimen with cross-sectional dimensions $5\times 25\,\mathrm{mm}^2$ because when the length of the specimen approaches zero, only L_3 is removed in Eq. (2.14). Therefore, the expression powered by $1/m$ will still have a value lower than 1.

The left asymptotic behavior is justified according to the theory of random fields in which an underlying statistical distribution for the physical parameter, modelled as a random field, is considered. The right asymptotic behavior from numerical results, which is a line with a slope close to $-1/m$ (m is the Weibull shape factor from experiments) is justified according to the CWSEL. As the specimen length increases to one or more orders of magnitude larger than the correlation length, the effect of the spatial correlation on the strength of the specimen becomes negligible. Therefore, the numerical results approach to the CWSEL. Nevertheless, experimental data are desired for validation of these asymptotic behaviors. Moreover, in this model wood is considered as a continuum material. Therefore application of this model for lengths less than 1 mm is not recommended, since new effects might become important as the specimen length approaches the size of microstructural characteristics of clear wood. Concerning the right asymptote, as long as clear specimens are obtainable, the model is applicable. However the application of the model for lengths more than 1 or 2 meters is not

practically justifiable, since knots usually have some effects on the capacity of timber components/structures in these ranges.

Also, in the case studies performed the same correlation length was considered in longitudinal and transverse directions, in order to reduce the number of unknown for description of RSV to two parameters mentioned in Section 2.5. This is justifiable since the cross sectional dimensions of the specimens were smaller than the longitudinal dimension. The presented numerical model and formula (2.14) are equally applicable to cases with different correlation lengths in different directions, if sufficient experimental data are available.

In order to examine if there are other sets of marginal shape factor and correlation length that could lead to the same size effect on the longitudinal strength as the size effect in experimental data, the following analysis was performed on the result already presented in Fig. 2.7 for larch, using Eq. (2.14). First, considering the original value of 118.66 MPa for the marginal shape factor, the effect of increasing and decreasing the correlation length on the size effect curve is shown in Fig. 2.8. It is seen that none of the experimental data points can be obtained in this way.

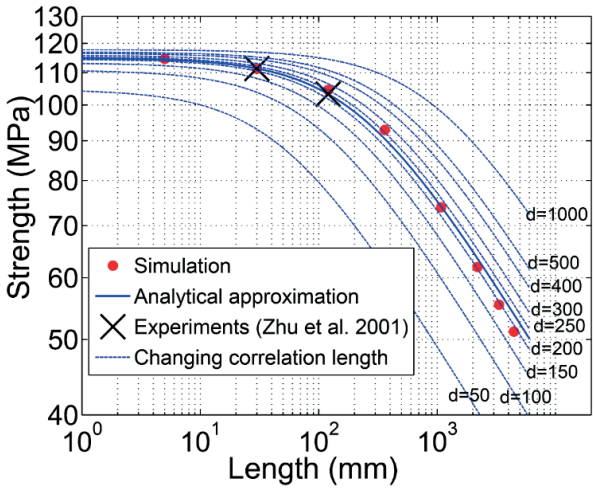

Fig. 2.8: The effect of changing the correlation length on the size effect curve for a marginal shape factor of 118.66 MPa.

As a noticeable reduction in the value of the shape factor, a value of 90.0 MPa for the marginal shape factor is considered. The effect of increasing and decreasing the correlation length on the size effect curve is shown in Fig. 2.9. Again none of the experimental points can be obtained.

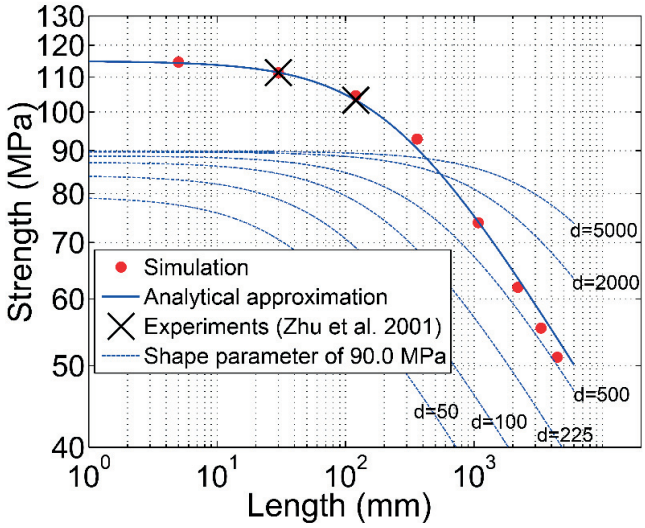

Fig. 2.9: The effect of changing the correlation length on the size effect curve for a marginal shape factor of 90.0 MPa.

Also, as a noticeable increase in the value of the shape factor, a value of 150.0 MPa is considered. The effect of increasing and decreasing the correlation length on the size effect curve is shown in Fig. 2.10. In this case, only one of the experimental points can be obtained by an individual size effect curve. Therefore, based on the trends of the size effect model in Figs. 2.8-2.10, there are no other set of values for the marginal shape factor and the correlation length for the model so that it crosses both experimental data points.

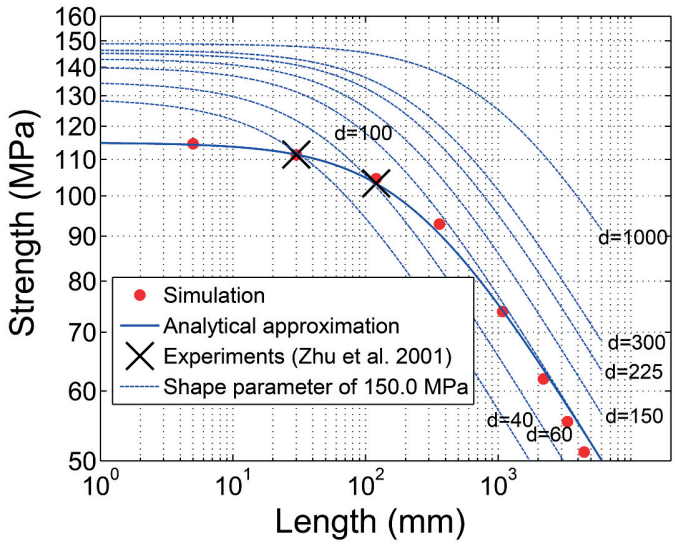

Fig. 2.10: The effect of changing the correlation length on the size effect curve for a marginal shape factor of 150.0 MPa.

A similar analysis can be performed for spruce wood. However, because all the specimen dimensions vary in this case, it is not possible to plot strength variations as a function of L_1, L_2 and L_3. In Table 2.6, the mean value strengths of specimens with various volumes obtained from numerical simulations have been compared to those predicted by Eq. (2.14). The results of the analytical formula are well corroborated by the numerical simulations except for larger volumes where the error increases up to 11.2%, see Table 2.6. When all the specimen dimensions become very small, the predicted mean strength value approaches the marginal mean value. For large specimen dimensions, the prediction by the current model approaches that of the CWSEL.

Table 2.6: Comparison of numerical results for mean value of strength (MPa) of spruce wood with predicted values of analytical approximation.

Dimensions (mm)	Numerical simulation	Analytical approximation	Error (%)
2×2×2	146.5	146.0	0.34
2×6×35	139.3	138.7	0.43
6×20×110	127.0	126.9	0.079
9.6×28.8×163.2	121.6	121.3	0.25
19.2×57.6×326.4	107.2	109.6	2.2
57.6×172.8×979.2	83.8	87.9	4.9
172.8×518.4×2937.6	61.3	66.2	8.0
1036.8×1036.8×2937.6	47.1	52.4	11.2

2.7 Conclusions

In this chapter, a random field-based size effect model has been proposed for the longitudinal tensile strength of timber. The statistical and spatial variability of the strength as a 3D random field were taken into account by its marginal distribution and autocorrelation function. Realizations of the strength field were generated in specimens with different volumes using the spectral representation scheme, and the strength results were obtained based on the Monte Carlo method along with the weakest link concept. The main conclusions are as follows:

- The application of the CWSEL to the experimental data in the literature showed a very high level of error. On the other hand, the current model was in a good agreement with the experimental data.
- The current model predicts an upper bound for the strength as specimen dimensions approach zero. On the other hand, when the dimensions are sufficiently large compared

to the correlation length of the strength field, the result obtained by the current model approaches that of the CWSEL.

- It was shown that the limits for the left and right asymptotic behaviors of the model are approximately 0.1 and 10 times the correlation length because, in the denominator of Eq. (2.14), if L is much smaller than d, L can be disregarded and vice versa. This range covers most real applications, which emphasizes the practical aspect of the current study.
- Values of 62 mm and 225 mm for the correlation lengths of the strength fields of spruce and Japanese larch were obtained. These values can be used in the stochastic simulation of timber structures under different loading conditions such as bending. Also, this indicates that the correlation length of the strength field in timber can vary significantly between different species.
- Finally, an analytical formula was proposed that closely approximates numerical results and facilitates the application of the current model. This formula, unlike its classical counterpart, is not arbitrarily scalable and includes the correlation length as a length scale.

The proposed model is in good agreement with experimental data, and it seems more appropriate than the CWSEL, particularly in the FE context, to extend the size effect predictions to small volumes. This can improve the current design of timber structures, such as timber joints, in which the size effect on the strength of clear wood is important. In this regard, conducting additional tests are suggested with different species. This work can also constitute a preliminary step toward developing models that take knots into account.

2.8 References

[1] Weibull, W., 1939. A statistical theory of strength of materials. In: Proceedings of the Royal Swedish Institute. Research No. 151, Stockholm, Sweden.

[2] Arwade, S.R., Clouston, P.L., Krupka, M.T., 2011. Length effects in tensile strength in the orthogonal directions of structural composite lumber. Journal of Testing and Evaluation 39, 1-7.

[3] Vallée, T., Tannert, T., Ganne-Chedville, C., 2012. Capacity prediction of welded timber joints. Wood Science and Technology 46, 333-347.

[4] Tannert, T., Vallée, T., Hehl, S., 2012. Probabilistic strength prediction of adhesively bonded timber joints. Wood Science and Technology 46, 503-513.

[5] Tannert, T., Vallée, T., Hehl, S., 2012. Experimental and numerical investigations on adhesively bonded hardwood joints. International Journal of Adhesion and Adhesives 37, 65-69.

[6] Tannert, T., Lam, F., Vallée, T., 2011. Structural performance of rounded dovetail connections: Experimental and numerical investigations. European Journal of Wood and Wood Products 69, 471-482.
[7] Clouston, P.L., Lam, F., 2002. A stochastic plasticity approach to strength modeling of strand-based wood composites. Composites Science and Technology 62, 1381-1395.
[8] Clouston, P.L., Lam, F., 2001. Computational modeling of strand-based wood composites. Journal of Engineering Mechanics 127, 844-851.
[9] Clouston, P., Lam, F., Barrett, J.D., 1998. Incorporating size effects in the Tsai-Wu strength theory for Douglas-fir laminated veneer. Wood Science and Technology 32, 215-226.
[10] Madsen, B., 1990. Size effects in defect-free Douglas fir. Canadian Journal of Civil Engineering 17, 238-242.
[11] Madsen, B., Tomoi, M., 1991. Size effects occurring in defect-free spruce-pine-fir bending specimens. Canadian journal of civil engineering 18, 637-643.
[12] Madsen, B., 1990. Length effects in 38 mm spruce-pine-fir dimension lumber. Canadian Journal of Civil Engineering 17, 226-237.
[13] Dill-Langer, G., Hidalgo, R.C., Kun, F., Moreno, Y., Aicher, S., Herrmann, H.J., 2003. Size dependency of tension strength in natural fiber composites. Physica A: Statistical Mechanics and its Applications 325, 547-560.
[14] Zhu, J., Kudo, A., Takeda, T., Tokumoto, M., 2001. Methods to estimate the length effect on tensile strength parallel to the grain in Japanese larch. Journal of Wood Science 47, 269-274.
[15] Shinozuka, M., Deodatis, G., 1996. Simulation of multi-dimensional Gaussian stochastic fields by spectral representation. Applied Mechanics Reviews 49, 29-53.
[16] Grigoriu, M., 2006. Evaluation of Karhunen-Loève, spectral, and sampling representations for stochastic processes. Journal of Engineering Mechanics 132, 179-189.
[17] Stefanou, G., Papadrakakis, M., 2007. Assessment of spectral representation and Karhunen-Loève expansion methods for the simulation of Gaussian stochastic fields. Computer Methods in Applied Mechanics and Engineering 196, 2465-2477.
[18] Fenton, G.A., 1994. Error evaluation of three random-field generators. Journal of Engineering Mechanics 120, 2478-2497.
[19] Deodatis, G., Shinozuka, M., 1988. Auto-regressive model for non-stationary stochastic processes, Journal of Engineering Mechanics 114, 1995–2012.
[20] Li, C.C., Kiureghian, A.D., 1993. Optimal discretization of random fields. Journal of Engineering Mechanics 119, 1136-1154.
[21] Sudret, B., der Kiureghian, A., 2000. Stochastic finite element methods and reliability: a state-of-the-art report. Rep. No. UCB/SEMM-2000/08, University of California at Berkeley, USA.
[22] Arwade, S.R., Clouston, P.L., Winans, R., 2009. Measurement and stochastic computational modeling of the elastic properties of parallel strand lumber. Journal of Engineering Mechanics 135, 897-905.

[23] Arwade, S.R., Winans, R., Clouston, P.L., 2010. Variability of the compressive strength of parallel strand lumber. Journal of Engineering Mechanics 136, 405-412.
[24] Gumbel, E.J., 1958. Statistics of Extremes. Columbia University Press, New York (reprinted in 2004 by Dover, New York).
[25] Adler, R.J., Taylor, J.E., 2007. Random fields and Geometry, Springer Monographs in Mathematics, Springer, New York.
[26] Katz R.W., Parlange M.B., Naveau P., 2002. Statistics of extremes in hydrology. Advances in Water Resources 25, 1287-1304.
[27] Beniston, M., Stephenson, D.B., Christensen, O.B., Ferro, C.A.T., Frei, C., Goyette, S., Halsnaes, K., Holt, T., Jylhä, K., Koffi, B., Palutikof, J., Schöll, R., Semmler, T., Woth, K., 2007. Future extreme events in European climate: an exploration of regional climate model projections. Climate Change 81, 71-95.
[28] Colombi, S., Davis, O., Devriendt, J., Prunet, S., Silk, J. Extreme value statistics of smooth Gaussian random fields. Monthly Notices of the Royal Astronomical Society 414, 2436-2445.
[29] Vanmarcke, E., 2010. Random fields: analysis and synthesis. World Scientific.
[30] Yakir, B., 2013. Extremes in Random Fields: A Theory and Its Applications. John Wiley & Sons, Inc.
[31] Yeh, C.H., Rahman, M., 1998. Stochastic finite element methods for the seismic response of soils. International Journal for Numerical and Analytical Methods in Geomechanics 22, 819-850.
[32] Bažant, Z.P., 1999. Size effect on structural strength: A review. Archive of Applied Mechanics 69, 703-725.
[33] Vořechovský, M., Chudoba, R., 2006. Stochastic modeling of multi-filament yarns: II. Random properties over the length and size effect. International Journal of Solids and Structures 43, 435-458.
[34] Choi, S.K., Canfield, R.A., Grandhi, R.V., 2007. Reliability-based structural design, Springer-Verlag, London.

[35] Wu, W.F., Cheng, H.C., Kang, C.K., 2000. Random field formulation of composite laminates. Composite Structures 49, 87-93.
[36] Stefanou, G., Papadrakakis, M., 2004. Stochastic finite element analysis of shells with combined random material and geometric properties. Computer Methods in Applied Mechanics and Engineering 193, 139-160.
[37] Ngah, M.F., Young, A., 2007. Application of the spectral stochastic finite element method for performance prediction of composite structures. Composite Structures 78, 447-456.
[38] Chen, N.Z., Guedes Soares, C., 2008. Spectral stochastic finite element analysis for laminated composite plates. Computer Methods in Applied Mechanics and Engineering 197, 4830-4839.

[39] Sasikumar, P., Suresh, R., Gupta, S., 2013. Stochastic finite element analysis of layered composite beams with spatially varying non-Gaussian inhomogeneities. Acta Mechanica, 1-20.
[40] Sriramula, S., Chryssanthopoulos, M.K., 2013. An experimental characterisation of spatial variability in GFRP composite panels. Structural Safety 42, 1-11.
[41] Vořechovský, M., 2007. Interplay of size effects in concrete specimens under tension studied via computational stochastic fracture mechanics. International Journal of Solids and Structures 44, 2715-2731.
[42] Shields, M.D., Deodatis, G., Bocchini, P., 2011. A simple and efficient methodology to approximate a general non-Gaussian stationary stochastic process by a translation process. Probabilistic Engineering Mechanics 26, 511-519.
[43] Shinozuka, M., Jan, C.M., 1972. Digital simulation of random processes and its applications. Journal of Sound and Vibration 25, 111-128.
[44] Stefanou, G., 2009. The stochastic finite element method: Past, present and future. Computer Methods in Applied Mechanics and Engineering 198, 1031-1051.
[45] Clouston, P., Lam, F., Barrett, J.D., 1998. Interaction term of Tsai-Wu theory for laminated veneer. Journal of Materials in Civil Engineering 10, 112-116.

3 Characterization of longitudinal mechanical properties of clear timber: RSV and size effects

3.1 Introduction

As a natural unidirectional fiber composite, wood/timber has highly anisotropic properties [1]. Different factors such as age, location of timber within the tree, structural imperfections, load history such as wind and snow etc. can affect the material properties of timber taken from the same species, and grown in the same geographical location and local growth conditions. Consequently, there is a considerable variability in mechanical properties. This variability, also observed in other materials such as composites, is both random and spatial and is usually referred to as "random spatial variability" [2-3].

The effect of the high scatter of timber elastic properties [4] on the response of timber structures has received less attention in the literature than the effect of the scatter of strength. In the few works that take the statistical variability of the elastic modulus into account, when assessing the structural response, the local point-by-point variability, i.e. the spatial variability, is commonly neglected [5,6]. This local variability of the elastic modulus can affect the local stress state of the material, which can be critical in estimating the failure probability under external loading. Recently Arwade et al. [7] have experimentally characterized the longitudinal spatial variability in the elasticity of parallel strand lumber using bending tests. They incorporated the experimental results in a stochastic model with orthotropic elasticity.

The mean strength of timber decreases as its volume increases due to the size effect on the strength. A small number of works have used pure tensile tests, on specimens of different sizes, to investigate the size effect on the strength of clear timber. In [8], a length effect parameter was introduced by Zhu et al. to quantify the size effect, due to the length change, on the longitudinal tensile strength of Japanese larch wood. Dill-Langer et al. [9] conducted longitudinal tensile experiments on two groups of specimens composed of spruce wood, and observed that the volume of the material significantly affects the strength.

The classical Weibull size effect law (CWSEL) [10] is commonly used in the literature for modeling this effect [5,6,9]. Some researchers have considered this effect as a volume effect. For example, this assumption was applied in [11-14] for the failure analysis of adhesively-bonded, welded and dovetail timber joints and in [5,6,15] for the study of the elastoplastic

behavior of strand-based wood composites and laminated veneer. Others, however, have split this effect into length and cross-sectional effects, see e.g. [16,17] on the bending strength of clear timber and [18] for the case of structural lumber. Nevertheless, in a recent study [19], it was highlighted that "Although no conclusive evidence has yet arisen concerning the accuracy of probabilistic strength theories to describe the size in the strength of timber, the existence of significant size effects is largely accepted within the scientific community."

The spatial variability is most likely to influence the response of structures made of clear timber, but this has not been studied before. This work is an attempt to investigate the random spatial variability of the timber elastic modulus. Also, it is partly aimed at experimentally characterizing the size effect on the strength of clear timber using specimens of different lengths, which can be used for developing more accurate models for the size effect on timber strength.

Four groups of specimens of different lengths were prepared and their quasi-static behavior was experimentally investigated under tensile loading. In addition to the global displacement monitoring, the local deformations along the length of each specimen were measured. The effect of the mesostructure of the clear timber on the local elastic modulus was examined. The spatial variability of the elastic modulus was experimentally characterized. Also, Statistics concerning the elastic modulus, strength and strain to failure as well as correlations between elastic modulus, strength and density were derived. Moreover, the size effect on these properties due to the length change was studied.

3.2 Experimental investigation

3.2.1 Material

Norway spruce wood was used for the specimens' preparation in this study. Although the boards contained a certain number of knots, the specimens were cut sufficiently far from these defects. All specimens were conditioned to 12% moisture content according to the ASTM standard D143-14 in a conditioning chamber and were tested at the laboratory temperature of 22±3 °C. The average density of the wooden specimens after conditioning was 443.3 kg/m3.

3.2.2 Specimen description

Specimens of different lengths were fabricated for the purpose of this study. In order to exclude variations in the properties in the cross-sectional plane, the nominal cross section of the specimens had to be as small as possible and yet it had to be possible to fabricate them well using a CNC machine. Due to these requirements, a new specimen geometry for longitudinal tensile tests on timber was designed. This geometry is shown in Fig. 3.1. The gradual change

in the dimensions of the cross-sectional area, from the gripping part to the middle part, via two connected curves, provides an appropriate smooth stress distribution. Moreover, this specimen is easy to fabricate since it has an extruded geometry.

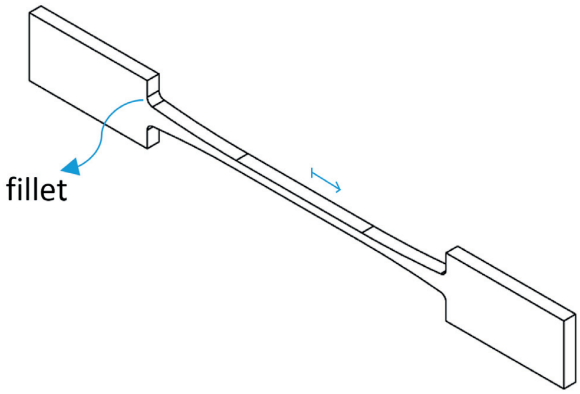

Fig. 3.1: Specimen geometry designed for tensile tests. The straight arrow shows the longitudinal timber direction.

The specimen's geometrical configuration is shown in Fig. 3.2a. The cross section of the middle part is a square of 2×2 mm^2. In Fig. 3.2a, L denotes the length of the middle zone of the specimen with the values of 2, 8, 32 and 128 mm. Sample specimens are shown in Fig. 3.2b. Specimen edges were carefully treated with very soft sandpaper, P240, to remove the cutting residual.

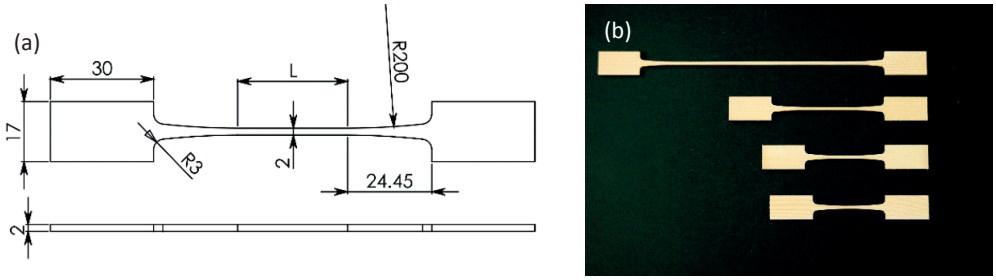

Fig. 3.2: a) Dimensions of specimen used for longitudinal tensile test, in millimeters b) Fabricated specimens of different lengths.

The following system is used to refer to the specimens in this study: LT-abc-4-de where 'LT' refers to longitudinal tensile, 'abc' is the specimen length in mm, 4 is the cross-sectional area in mm^2 and 'de' is the specimen number within a group of specimens with the same geometry. In the next sections, it is seen that the strengths of the four specimen sets with different lengths, although cut from different boards, show approximately the same level of scatter. This

demonstrates that a sufficient number of specimens in each group have been considered to capture the randomness of the properties of the material used.

3.2.3 Experimental set-up and instrumentation

All experiments were carried out on a 25-kN MTS Landmark servo-hydraulic testing machine with a built-in load cell calibrated to 20% of the full capacity. Quasi-static tensile tests were performed under displacement-control mode. Different stroke rates for different lengths were selected on the basis of the pre-testing of additional specimens so that the final failure occurred within 180 ± 60 s during the whole testing program. A constant stroke rate among different groups was not used because the specimen sizes were different. Due to the scatter in the strength and stiffness, the failure time varied for specimens with the same geometry.

A video extensometry system composed of a 10-bit Sony XCLU1000 CCD connected to a Fujinon HF35SA-1 lens, with a focal length of 35-mm and an aperture, f 1.4-22, able to provide an accuracy of ±0.005 mm, was used during the tests to measure the axial deformation. Prior to the tests, small black target dots of 1.3-mm in diameter were applied on the specimens' surfaces as shown in Fig. 3.3 for a specimen of 32 mm-length. The distance between each two consecutive dots was 4 mm for all groups of specimens, except for specimens with a nominal length of 2 mm, where the distance between the two dots was 2 mm. The axial coordinates of the dots were recorded at a frequency of 5 Hz by the camera throughout loading. Using these data, the strain between each two consecutive dots was calculated. The axial stresses were also calculated using the load level and the initial cross-sectional area.

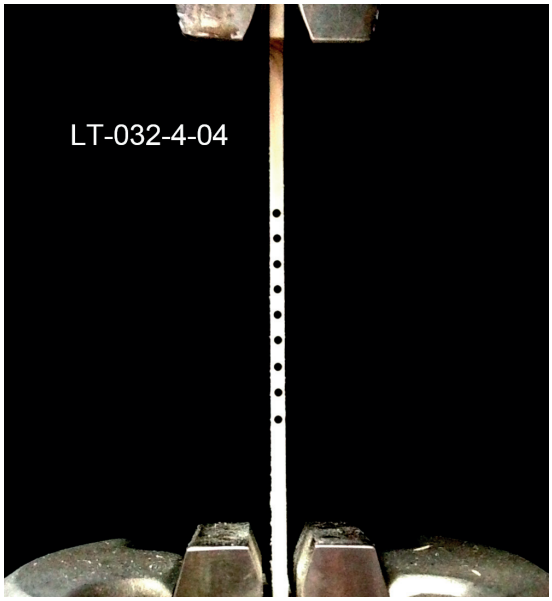

Fig. 3.3: Specimen of 32-mm nominal length with applied dots inside machine grips.

3.3 Timber mesostructure and local mechanical properties

The mesostructure of clear spruce wood is mainly characterized by the earlywood-latewood patterns which affect the local mechanical properties. This is the origin of random spatial variability in the properties. Some of these mesostructural features observed in the specimens are shown in Fig. 3.4. The darker parts of the growth rings are latewood that has higher mechanical properties, referred to as strips of latewood. Although all the specimens were cut in the nominal longitudinal direction of the board, the fiber direction along the specimen length is often not parallel to the specimen axial direction. Figure 3.4a illustrates the fiber misalignment with respect to the nominal longitudinal direction of the board. This misalignment can reduce the local longitudinal elastic modulus. Another consequence is that at some points along the length of a specimen a new strip of latewood or an existing strip may cross the specimen border. This is the main cause of sudden changes in the local elastic modulus. Figure 3.4b exhibits another feature that can affect the local elastic modulus. The distance between two consecutive strips of latewood, or growth ring thickness, is smaller in Fig. 3.4b than that in Fig. 3.4a. The decrease in thickness increases the local density which, in turn, can increase the local elastic modulus, and vice versa. In the current study, it may also lead to an increase in the number of latewood strips in the same cross section. Finally, Fig. 3.4c shows the fiber waviness that tends to reduce the value of the local elastic modulus.

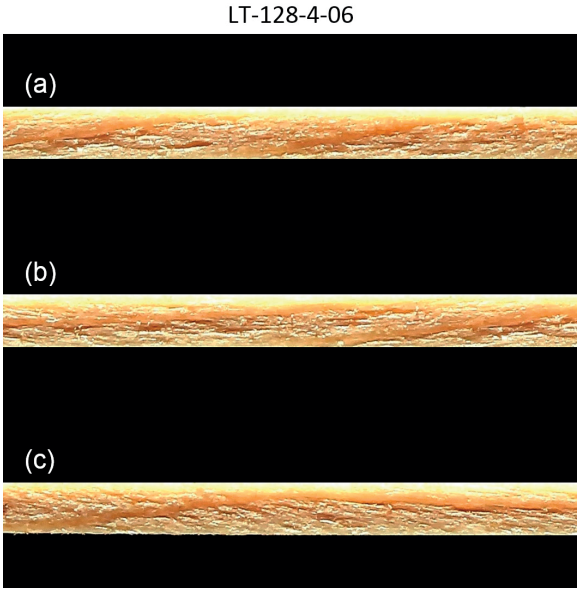

Fig. 3.4: Mesostructural features of spruce wood: a) fiber misalignment b) uneven growth ring thickness c) fiber waviness.

Typical examples of the correlation between the local elastic modulus and the local mesostructure of spruce wood are given in Fig. 3.5, considering two specimens of 128-mm

length. In specimen LT-128-4-06, it can be seen that, initially, there is an obvious fiber misalignment that gradually diminishes so that the fiber becomes parallel to the nominal axis of the specimen. Subsequently, the fiber starts to deviate from the nominal axis again. Correspondingly, the local elastic modulus generally first increases and then decreases. In specimen LT-128-4-07, there is an obvious fiber waviness over the first few millimeters of the length, which is why the local elastic modulus suddenly increases from 8.0 GPa to 13.0 GPa.

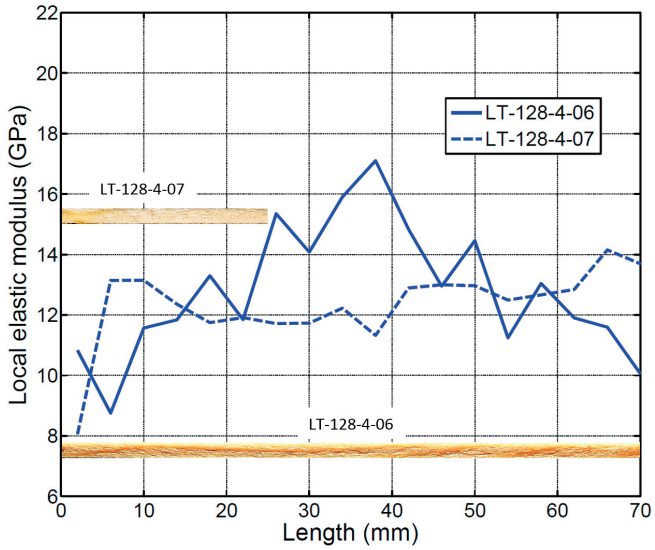

Fig. 3.5: Correspondence between mesostructure of spruce and variability of local elastic modulus.

The spatial variability of the elastic modulus along the length is examined here for specimens of 128-mm length. This involves 40 sets of 32 data points, each set being collected from a single specimen. The values of the local elastic modulus are shown in Fig. 3.6. The three solid horizontal lines show the range of values 11.0±1.4GPa (mean±SD). Also, the spatial variability of three indicative specimens are highlighted via the thicker lines. It can be seen that the variability in some specimens is lower along their lengths and the local elastic modulus oscillates around the effective elastic modulus of the specimen; see for example the dashed and dotted lines corresponding to specimens LT-128-4-05 and LT-128-4-09. On the other hand, some specimens exhibit more significant changes in their local modulus, e.g. from 15 GPa to 7 GPa, approximately, shown by the thick solid line corresponding to specimen LT-128-4-04. Also, Fig. 3.6 shows that the measured value of the local elastic modulus was 21.1 GPa at one point in specimen LT-128-4-20. This was because in that region of the specimen, two strips of latewood happened to be almost parallel to the nominal axis of the specimen. The corresponding segment of the specimen is shown by a yellow circle in Fig. 3.7. The local modulus of the

segment on the right has a lower value of 18.6 GPa, which is because some of the latewood crosses the specimen border in this segment.

In some parts of some specimens, as in specimen LT-128-4-05, consecutive decrease and increase occurred in the value of the local elastic modulus. However, in some other parts, as in the same specimen between 74 mm and 98 mm, there was no consecutive decrease and increase.

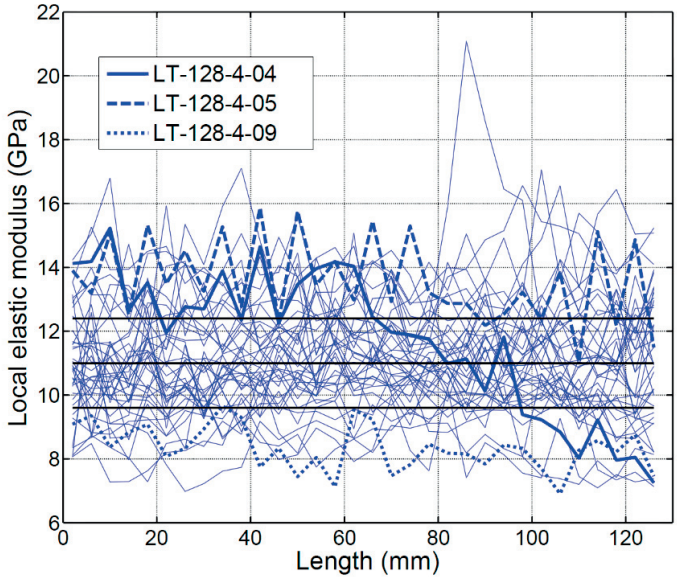

Fig. 3.6: Variation of local elastic modulus along length of 128-mm specimens.

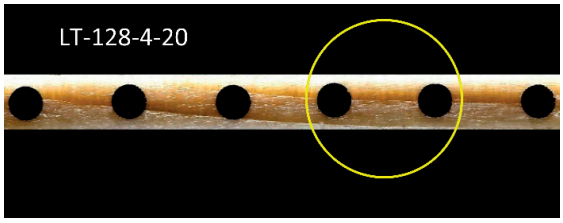

Fig. 3.7: Segment with highest measured local elastic modulus (indicated by a circle).

Specimen failures can be roughly categorized into two different forms, schematically shown in Fig. 3.8a and b. The first form is a failure that exhibits a sharp angle between each face of the fracture zone and the nominal axis of the specimen. In the second form, however, the angle is more open, and the fracture faces are frequently more uneven than in the first case. Generally, the specimens with a failure form of the first category had higher strength values. For example, eight out of 10 specimens, of 128-mm length, with the highest strength values fell into the first category. On the other hand, seven out of 10 specimens with the lowest strength values fell into the second category. Examples of these two forms are shown in Fig. 3.8c and d. There was

always some degree of misalignment in the specimens, and the fracture path did not cross the latewood in most cases. As a result, in cases with less misalignment, the fracture surface was larger, which naturally required higher forces for fracture initiation. The observation that higher and lower strengths were not always associated with first and second failure forms, respectively, is attributed to the fact that microdefects may also influence specimen strength.

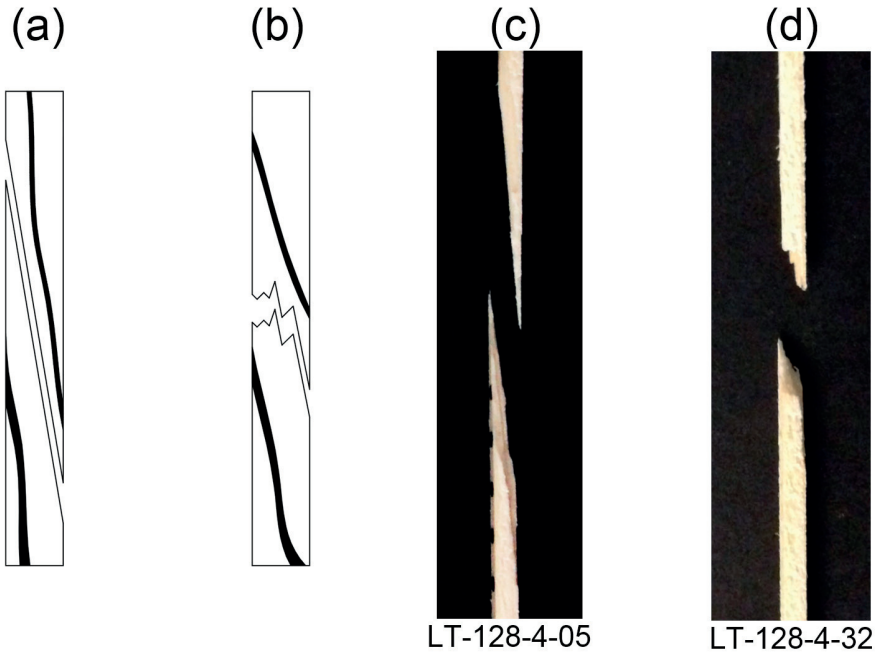

Fig. 3.8: a and b) Schematic illustration of two failure modes; c and d) Typical specimen failures.

3.4 Mechanical behavior of specimens

Typical tensile stress-strain curves are shown in Fig. 3.9. These curves have been obtained directly using the axial displacements of the two end dots. Therefore, the slope of each curve indicates the elasticity of the whole nominal length of the corresponding specimen, referred to as the effective elastic modulus in the current study. The term 'effective' is used to distinguish it from local elastic modulus. It is seen that the mechanical behavior is linear up to failure. The high scatter in the strength and the effective elastic modulus of the specimens can be clearly seen in this figure. The elasticity of a specimen segment between two consecutive dots is the local elastic modulus which is attributed to the center of the segment.

Each specimen can be considered as a set of series of springs, with each segment, between two consecutive dots, corresponding to a spring. The measured values for the local elastic moduli were used to calculate the value of the effective elastic modulus of the specimen, based on the concept of the series of springs, using the following formula:

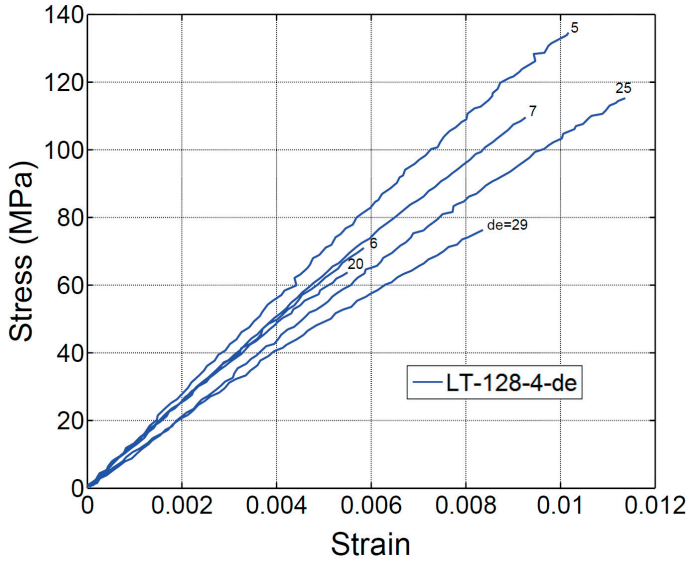

Fig. 3.9: Typical longitudinal tensile stress-strain curves of spruce wood.

$$\frac{n}{E_{eff}} = \frac{1}{E_1} + \frac{1}{E_2} + \ldots + \frac{1}{E_n} \tag{3.1}$$

in which E_{eff} is the effective elastic modulus of the specimen and $E_i (i = 1, 2, ..., n)$ are the local elastic moduli. The value of E_{eff}, computed using Eq. (3.1), was compared to that obtained by using the end-dot displacements. The difference was less than 0.1% in all specimens, which confirmed the accurate measurement of the local elastic moduli, since any significant error in the measured values for the local moduli would result in a significant error in the value for the effective elastic modulus, calculated based on the concept of series of springs. Also, it can be mathematically proven that E_{eff} from Eq. (3.1) is always smaller than the arithmetic average of E_i's ($\sum_{i=1}^{n} E_i / n$).

The mechanical properties of each specimen including the effective elastic modulus, the strength and the strain to failure, as well as their density, are given in Table 3.1. The density was obtained by dividing the weight of each specimen by its volume, after conditioning as mentioned earlier. Certain sections of the table contain dashes because some specimens did not fail in the middle part with constant cross section, or, in some cases, there were problems in recording the deformation during the tensile experiments.

Table 3.1: Effective elastic modulus, strength, strain to failure and density for all tested specimens.

Specimen length (mm)	Specimen code	Effective elastic modulus (GPa)	Strength (MPa)	Strain to failure (%)	Density (kg/m^3)
2mm	LT-002-4-01	9.93	136.7	1.38	449.9
	LT-002-4-02	14.96	118.0	0.79	446.1
	LT-002-4-03	10.67	122.9	1.15	427.3
	LT-002-4-04	6.25	89.4	1.43	417.8
	LT-002-4-05	8.77	95.6	1.09	436.3
	LT-002-4-06	-	83.2	-	419.9
	LT-002-4-07	7.77	96.5	1.24	421.6
	LT-002-4-08	11.40	114.8	1.01	421.7
	LT-002-4-09	10.55	124.1	1.18	446.0
	LT-002-4-10	8.07	103.8	1.29	442.5
	LT-002-4-11	7.19	87.7	1.22	421.7
	LT-002-4-12	8.56	109.0	1.27	436.7
	LT-002-4-13	-	84.4	-	422.0
	LT-002-4-14	12.56	126.4	1.01	485.9
	LT-002-4-15	12.40	122.5	0.99	437.1
	LT-002-4-16	10.62	124.4	1.17	424.6
	LT-002-4-17	9.82	103.0	1.05	443.6
	LT-002-4-18	12.02	131.1	1.09	470.5
	LT-002-4-19	11.42	121.9	1.07	457.9
	LT-002-4-20	9.74	118.8	1.22	453.7
	LT-002-4-21	12.13	118.5	0.98	439.3
	LT-002-4-22	10.86	93.5	0.86	437.1
	LT-002-4-23	11.07	105.8	0.96	437.8
	LT-002-4-24	8.85	104.9	1.19	440.9
	LT-002-4-25	8.69	109.1	1.26	446.6
	LT-002-4-26	6.62	108.1	1.63	450.9
	LT-002-4-27	10.99	117.8	1.07	446.9
	LT-002-4-28	14.05	132.0	0.94	475.9
	LT-002-4-29	11.53	139.1	1.21	443.3

	LT-002-4-30	11.48	117.7	1.03	453.3
	LT-002-4-31	7.46	101.5	1.36	430.1
	LT-002-4-32	10.35	117.7	1.14	443.1
	LT-002-4-33	11.45	129.9	1.13	462.5
	LT-002-4-34	8.70	111.4	1.28	429.8
	LT-002-4-35	12.79	143.4	1.12	469.4
	LT-002-4-36	10.29	87.5	0.85	451.9
	LT-008-4-37	10.37	124.5	1.20	424.1
8mm	LT-008-4-01	11.10	110.1	0.99	429.0
	LT-008-4-02	8.17	105.0	1.29	423.8
	LT-008-4-03	11.91	103.6	0.87	455.8
	LT-008-4-04	9.19	110.6	1.20	439.2
	LT-008-4-05	9.53	115.0	1.21	455.7
	LT-008-4-06	12.23	135.0	1.10	459.4
	LT-008-4-07	9.28	91.9	0.99	411.8
	LT-008-4-08	12.13	124.2	1.02	482.1
	LT-008-4-09	9.07	100.2	1.11	438.5
	LT-008-4-10	9.77	106.9	1.09	428.1
	LT-008-4-11	9.89	103.8	1.05	433.0
	LT-008-4-12	12.39	138.3	1.12	455.8
	LT-008-4-13	8.94	118.3	1.32	426.1
	LT-008-4-14	12.06	112.4	0.93	463.8
	LT-008-4-15	11.80	128.7	1.09	443.2
	LT-008-4-16	12.08	120.3	1.00	461.5
	LT-008-4-17	14.71	138.4	0.94	462.2
	LT-008-4-18	8.86	115.4	1.30	453.6
	LT-008-4-19	8.75	99.3	1.14	436.9
	LT-008-4-20	8.76	98.6	1.13	448.1
	LT-008-4-21	9.74	101.2	1.04	463.0
	LT-008-4-22	8.13	113.4	1.39	445.6
	LT-008-4-23	7.81	85.2	1.09	431.8
	LT-008-4-24	6.94	91.2	1.31	447.1
	LT-008-4-25	10.38	120.8	1.16	440.3

	LT-008-4-26	7.11	101.0	1.42	417.8
	LT-008-4-27	11.43	144.5	1.26	453.6
	LT-008-4-28	8.97	86.5	0.96	434.8
	LT-008-4-29	8.36	103.8	1.24	439.0
	LT-008-4-30	7.51	83.1	1.11	421.9
	LT-008-4-31	8.84	123.4	1.40	445.5
	LT-008-4-32	10.36	115.5	1.11	470.6
	LT-008-4-33	10.20	123.5	1.21	463.8
	LT-008-4-34	9.38	92.7	0.99	435.3
	LT-008-4-35	9.51	87.3	0.92	433.2
	LT-008-4-36	13.21	137.6	1.04	461.5
	LT-008-4-37	9.82	119.3	1.21	453.8
	LT-008-4-38	8.80	106.6	1.21	450.6
	LT-008-4-39	10.65	117.2	1.10	434.4
	LT-008-4-40	13.03	147.3	1.13	478.1
	LT-008-4-41	13.39	131.5	0.98	458.4
	LT-008-4-42	11.57	120.6	1.04	452.8
	LT-008-4-43	16.16	126.2	0.78	489.5
	LT-008-4-44	11.82	125.7	1.06	470.1
	LT-008-4-45	8.26	105.7	1.28	417.9
	LT-032-4-01	6.34	83.4	1.32	428.1
	LT-032-4-02	8.22	82.4	1.00	468.0
	LT-032-4-03	9.95	116.2	1.17	448.0
	LT-032-4-04	12.47	134.5	1.08	448.0
	LT-032-4-05	13.32	-	-	445.4
	LT-032-4-06	7.16	97.4	1.36	424.3
	LT-032-4-07	11.59	108.4	0.94	444.0
	LT-032-4-08	8.38	102.4	1.22	439.7
	LT-032-4-09	11.90	111.6	0.94	450.0
	LT-032-4-10	10.44	98.4	0.94	446.2
	LT-032-4-11	11.02	124.3	1.13	453.8
	LT-032-4-12	11.37	116.8	1.03	431.0
	LT-032-4-13	12.45	128.0	1.03	461.5

32mm	LT-032-4-14	7.98	74.7	0.94	435.0
	LT-032-4-15	12.63	150.0	1.19	488.2
	LT-032-4-16	-	-	-	-
	LT-032-4-17	7.81	85.9	1.10	467.4
	LT-032-4-18	-	-	-	-
	LT-032-4-19	9.98	103.1	1.03	446.1
	LT-032-4-20	13.79	-	-	474.5
	LT-032-4-21	10.81	102.4	0.95	439.7
	LT-032-4-22	11.55	-	-	448.1
	LT-032-4-23	10.78	129.6	1.20	453.8
	LT-032-4-24	13.29	146.4	1.10	460.0
	LT-032-4-25	12.64	125.7	0.99	449.6
	LT-032-4-26	8.84	87.7	0.99	436.7
	LT-032-4-27	12.52	137.4	1.10	452.7
	LT-032-4-28	12.80	126.3	0.99	463.5
	LT-032-4-29	11.79	110.0	0.93	453.9
	LT-032-4-30	-	-	-	-
	LT-032-4-31	-	-	-	-
	LT-032-4-32	10.07	113.4	1.13	456.0
	LT-032-4-33	8.16	100.0	1.23	424.3
	LT-032-4-34	11.65	106.8	0.92	476.1
	LT-032-4-35	9.55	94.4	0.99	452.7
	LT-032-4-36	-	-	-	-
	LT-032-4-37	9.46	110.8	1.17	429.8
	LT-032-4-38	9.63	124.0	1.29	439.7
	LT-032-4-39	10.36	120.8	1.17	437.8
	LT-032-4-40	11.37	119.3	1.05	453.2
	LT-128-4-01	-	105	-	441.4
	LT-128-4-02	-	87.6	-	458.4
	LT-128-4-03	-	-	-	462.7
	LT-128-4-04	11.26	97.2	0.86	460.6
	LT-128-4-05	13.48	136.0	1.01	457.4
	LT-128-4-06	12.25	72.9	0.60	449.6

128mm	LT-128-4-07	11.88	110.7	0.93	440.8
	LT-128-4-08	12.22	136.3	1.12	469.6
	LT-128-4-09	8.31	90.9	1.09	439.1
	LT-128-4-10	12.16	113.5	0.93	460.7
	LT-128-4-11	12.93	101.6	0.79	424.6
	LT-128-4-12	10.94	108.7	0.99	445.0
	LT-128-4-13	10.24	104.7	1.02	456.2
	LT-128-4-14	13.78	110.8	0.80	453.7
	LT-128-4-15	11.96	121.0	1.01	465.0
	LT-128-4-16	8.62	101.1	1.17	409.2
	LT-128-4-17	11.28	104.8	0.93	465.1
	LT-128-4-18	9.03	87.0	0.96	404.3
	LT-128-4-19	10.38	113.4	1.09	462.6
	LT-128-4-20	11.59	65.2	0.56	460.6
	LT-128-4-21	10.97	100.2	0.91	428.9
	LT-128-4-22	10.62	97.9	0.92	455.0
	LT-128-4-23	10.29	105.8	1.03	436.0
	LT-128-4-24	10.45	118.4	1.13	460.7
	LT-128-4-25	10.41	117.2	1.13	435.5
	LT-128-4-26	12.01	120.4	1.00	455.3
	LT-128-4-27	10.06	110.9	1.10	429.4
	LT-128-4-28	9.92	88.6	0.89	435.0
	LT-128-4-29	9.16	77.7	0.85	419.5
	LT-128-4-30	11.57	-	-	446.0
	LT-128-4-31	11.91	110.6	0.93	442.3
	LT-128-4-32	8.11	73.8	0.91	415.3
	LT-128-4-33	12.41	113.2	0.91	446.8
	LT-128-4-34	9.63	91.1	0.95	421.1
	LT-128-4-35	10.79	105.6	0.98	454.3
	LT-128-4-36	12.69	-	-	444.7
	LT-128-4-37	10.40	105.1	1.01	441.4
	LT-128-4-38	13.41	117.8	0.88	467.9
	LT-128-4-39	9.88	99.8	1.01	424.0

	LT-128-4-40	11.07	101.3	0.92	436.7
	LT-128-4-41	12.29	123.2	1.00	473.0
	LT-128-4-42	11.06	112.4	1.02	454.2
	LT-128-4-43	9.87	93.7	0.95	451.9

As a typical laboratory testing program, several factors could affect the measured values and introduce uncertainty with different levels of relative importance. These includes the person conducting the tests that fixes the specimen in the testing machine, slight change in the environmental conditions during the tests, the accuracy of the read value from the machine, accuracy of the measured specimen dimensions, the accuracy of the video-extensometer and the accuracy of the enriching process of putting black target dots at their places on the specimens. Nevertheless, it is believed that the error/uncertainty that these factors introduce in the measured values are quite small compared to the random uncertainty in the measured values for the mechanical properties at mesoscale. The random uncertainty in the local elastic moduli at mesoscale is particularly high compared to that of timber pieces with the larger dimensions, such as dimensions of structural lumbers, because at mesoscale the effect of local fiber misalignment and waviness are not averaged over a larger volume.

3.5 Statistics concerning elastic modulus, strength and strain to failure

3.5.1 Statistics concerning elastic modulus

The statistics concerning the effective elastic modulus for the four groups of specimens are shown in Table 3.2. It can be seen that the mean value does not change significantly with increasing length and is in agreement with the reported value of 11.0 GPa in the literature [1] for the longitudinal elastic modulus of spruce wood. The mean values and the corresponding standard deviations are plotted in Fig. 3.10. The mean effective elastic moduli of specimens of longer lengths have slightly higher values. The difference between the mean values of the shortest and longest specimens is 6.4%. The standard deviation (SD) significantly decreases from the shortest to the longest specimens. The coefficient of variation (COV) is almost the same for 2-mm and 8-mm specimens. With increasing length, the COV starts to diminish, decreasing from a value of 19.6% for 2mm specimens to 12.7% for 128-mm specimens. Fig. 3.11 shows the COV of the effective elastic modulus vs. the specimen length in a logarithmic scale. It can be seen that the COV approaches a constant value for very small lengths, which can be considered as an upper bound for the COV of the longitudinal tensile modulus in the length range examined. This is attributed to the spatial correlation in the elastic modulus field. In other words, from a length of 2mm to 8mm, the spatial correlation remains at a high level,

with the modulus statistics remaining the same. The reduction of the variability in the effective elastic modulus with increasing length can be explained by considering each larger specimen as a series of smaller specimens. Naturally, the variability in the effective elastic modulus is reduced for the longer specimen, because the elasticity of each smaller specimen contributes to the elasticity of the larger specimen.

The COV variation presented in Fig. 3.11 is mainly intended for the range presented in the figure. Extrapolations are possible as long as new influencing factors do not emerge. For the range under 1 mm the microstructural effects might become important. On the right side, the extrapolation can be justifiable as long as there are no new influencing factors such as knots. Practically, however, the application is limited to lengths of not more than a few hundred millimeters, since defects such as knots are commonly influential for higher lengths. Theoretically, the COV for specimens of infinite length (sufficiently long) would approach zero, since the effective elastic modulus of any of such specimens would include the effect of sufficient variations of the local elastic modulus along its length, so that all specimens would have the same effective elastic modulus.

The presence of scatter in the mechanical properties of timber leads to uncertainty regarding the response of timber structures. For probabilistic modeling of timber structures, it is necessary to know the statistical distribution governing the mechanical properties. The three most commonly used statistical distributions for mechanical properties, i.e. normal, lognormal and Weibull, were fitted to the experimental data for the four groups of specimens. The results of the goodness-of-fit tests, Anderson-Darling (AD) and Kolmogorov-Smirnov (KS), at a significance level of 0.05 are given in Table 3.3. A ‘zero’ denotes that sampled data are taken from the corresponding distribution, while ‘one’ rejects the presumed distribution.

Table 3.2: Statistics of effective elastic modulus for four groups of specimens.

Length (mm)	Mean (GPa)	SD (GPa)	COV (%)
2	10.3	2.02	19.6
8	10.3	2.03	19.8
32	10.6	1.91	18.0
128	11.0	1.40	12.7

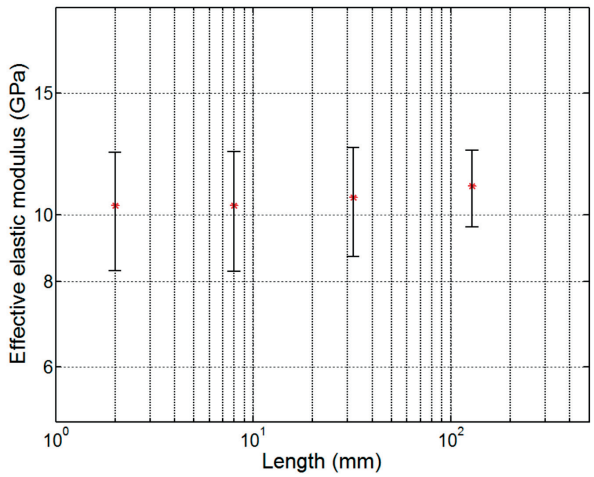

Fig. 3.10: Mean value of effective elastic modulus for specimens of different lengths. Error bars indicate standard deviation for each length.

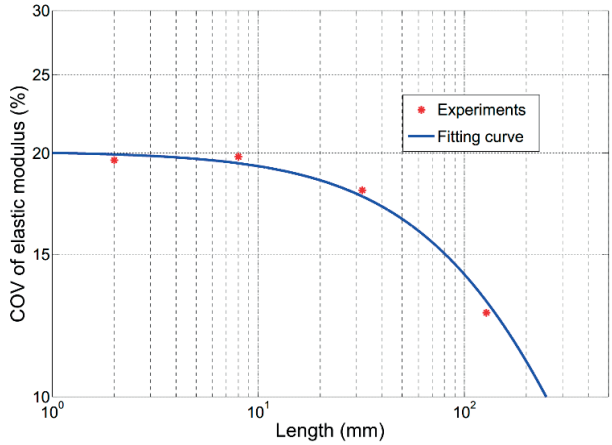

Fig. 3.11: COV of effective elastic modulus as function of specimen length.

It can be seen that the tests support these statistical distributions for all four groups of specimens, except for the AD test in the case of the Weibull distribution. Therefore, both normal and lognormal distributions can represent the statistical variability of the elastic modulus in stochastic simulations of timber structures. From a computational point of view, using the normal distribution is preferable as it is simpler to implement. However, the normal distribution, when used in stochastic simulations, can be problematic by generating negative values for the elastic modulus which is a by definition a positive quantity. For example, Stefanou and Papadrakakis [16] have shown that adopting normal distribution might in some cases lead to erroneous results due to the possible negative values for the elastic modulus in Monte Carlo simulations. Nevertheless, they tried to solve the issue through discarding the negative values. Lognormal and Weibull distributions do not cause such a problem due to being defined over

the positive part of the real numbers set. They are, however, computationally more demanding, especially for generating realizations of non-Gaussian random fields, as shown in Chapter 2.

Table 3.3: Results of goodness-of-fit tests for effective elastic modulus of spruce.

Specimen length (mm)	Normal		Lognormal		Weibull	
	AD	KS	AD	KS	AD	KS
2	0	0	0	0	0	0
8	0	0	0	0	1	0
32	0	0	0	0	0	0
128	0	0	0	0	0	0

The mean value, SD and COV of the collected data points for the local elastic modulus (corresponding to a total of 1280 segments with 4-mm length) are compared to those of the effective modulus of the 128-mm specimens in Table 3.4. The mean value of the local moduli, 11.2 GPa, is slightly higher than the mean value of the effective moduli, 11.0 GPa. This is because the effective modulus of each specimen is calculated using the values of the local modulus based on the concept of series of springs, shown in Eq. (3.1). The COV of the local modulus, 16.4%, is also higher than that of the effective modulus, 12.7%, due to the averaging that occurs during calculation of the effective modulus, which tends to reduce the scatter.

Table 3.4: Statistics of local and effective elastic moduli of 128-mm specimens.

	Number of data points	Mean (GPa)	SD (GPa)	COV (%)
Local modulus	1280	11.2	1.84	16.4
Effective modulus	40	11.0	1.40	12.7

Further, from Fig. 3.11, a COV of 19.8% for the elastic modulus of the specimens of 4-mm lengths can be obtained using the fitted curve. This value is larger than the COV of the local moduli, 16.4% (see Table 3.4) obtained from 4-mm segments. This difference in the COV is attributed to the fact that the data in Fig. 3.11 are obtained from independent specimens; however, the COV for the 4-mm segments of 128-mm specimens is obtained based on the data points that are not totally independent. There is a spatial correlation within each set of 32 values for the local elastic modulus obtained from a single specimen. This spatial correlation leads to a reduction of scatter when the 40 sets of 32 data points are considered collectively.

Two types of variability contribute to the ensemble COV of 16.4% for the mentioned 1280 data points, taken from the 4-mm segments of the 128-mm specimens. The first, designated within-specimen variability, is the COV of the 32 data points for the local elastic moduli in a single specimen of 128-mm length. The mean value of these 40 COVs, corresponding to 40 specimens of 128-mm length, is equal to 9.7%, which represents the average variability of the local elastic modulus in each specimen. The second, designated between-specimen variability, is the COV of the 40 values for the effective elastic moduli of the 40 specimen of 128-mm lengths. The value of the between-specimen variability is 12.7%, as given in Table 3.2. Therefore, the contribution of the between-specimen variability to ensemble variability is more than that of the within-specimen variability for the considered specimen length.

3.5.2 Statistics concerning longitudinal tensile strength

The statistical characteristics for the longitudinal tensile strength of spruce wood are given in Table 3.5 for the four groups of specimens. It can be seen that, as the length increases from 2mm to 8mm, the change in the mean value of the strength is negligible. As the length increases further, the mean strength starts decreasing. This decrease is more significant between the 32-mm and 128-mm specimens. The COV of the strength does not change significantly as the specimen length increases. In Table 3.5, from a length of 2 mm to a length of 32 mm, the COV increases a little and then decreases a little for 128-mm specimens. Therefore, an average value of 15.1% is considered as representing the scatter in the longitudinal tensile strength of spruce wood, which is independent of specimen length. Such a difference in the COVs for specimens of different sizes was observed in a previous study [9] for two different volumes of spruce wood.

Table 3.5: Statistics of longitudinal tensile strength of spruce wood for specimens of different lengths.

Specimen length (mm)	Mean (MPa)	SD (MPa)	COV (%)
2	112.9	15.9	14.1
8	113.0	16.3	14.5
32	111.6	18.6	16.7
128	103.8	15.7	15.1

In Figs. 3.12 and 3.13, the mean values and COVs for the strengths of the four specimen groups have been plotted against their lengths in the logarithmic scales, respectively. The solid blue line is a fitting curve based on the size effect model of Chapter 2, Eq. (2.14). Comparing this curve with that in Fig. 3.11, it can be seen that the COV of the stiffness and the mean value of the strength vary in more or less the same way as the length increases. This might suggest that both of these properties may be modeled using the same theory, such as the theory of stochastic

processes [20]. The difference is that as the size increases the previously mentioned averaging for the elastic modulus tends to decrease its COV, while its mean value remains almost unchanged, whereas the weakest link concept, which governs the fracture of brittle materials, tends to decrease the mean value of the strength, while the COV remains almost unchanged.

The fitting of the size effect model leads to values of 128.6 mm and 121.4 MPa for the longitudinal correlation length and the marginal Weibull shape factor. The marginal mean value was obtained to be 114.2 MPa.

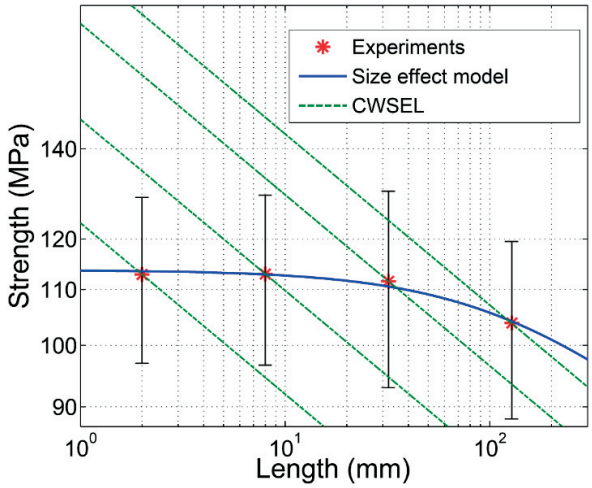

Fig. 3.12: Mean value for longitudinal tensile strength vs. specimen length for spruce wood. Error bars indicate standard deviation for each length.

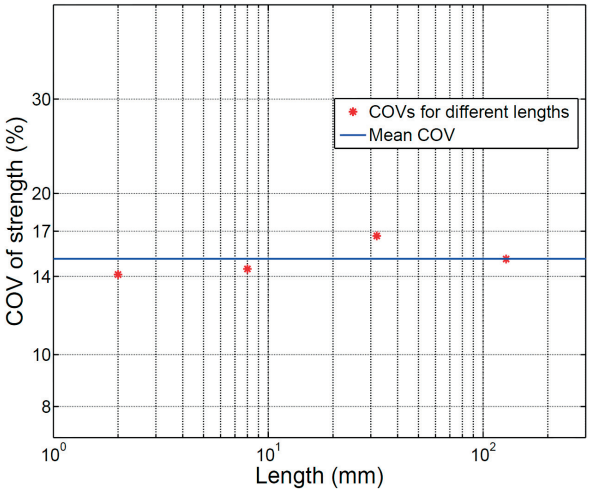

Fig. 3.13: COV of strength for specimens of different lengths.

In the reliability analysis of timber structures, based on ultimate limit states, accurate representation of the variability in strength via a statistical distribution is critical. Commonly used statistical distributions for mechanical properties in the literature, i.e. Weibull, normal and lognormal, were fitted to the experimental data for the longitudinal strength. The results of AD and KS tests are given in Table 3.6. Both tests support Weibull and normal distributions, but the AD test rejects lognormal distribution for 128-mm specimens. However, it is generally accepted that the Weibull distribution is the best one for representing variability in the strength of brittle materials where it also has a physical meaning.

Table 3.6: Results of goodness-of-fit tests for longitudinal tensile strength of spruce.

Specimen length (mm)	Weibull		Normal		Lognormal	
	AD	KS	AD	KS	AD	KS
2	0	0	0	0	0	0
8	0	0	0	0	0	0
32	0	0	0	0	0	0
128	0	0	0	0	1	0

3.5.2.1 Comparison of experimental results with CWSEL prediction

According to the CWSEL for the failure of brittle materials, which is still widely used [5, 6, 9-15, 19, 21], as the volume of the material decreases, the mean strength increases following a straight line with a constant slope in logarithmic scales. Therefore, when the volume approaches zero, an unbounded value is predicted for the strength. However, the experimental results in the current study show that as the volume decreases, the mean value approaches a constant value of 113.0 MPa, which is the upper bound value for the mean strength of spruce wood used in this study.

In order to quantitatively examine the error involved in the prediction of the CWSEL, the following formula was used [12]:

$$\frac{\bar{\sigma}_1}{\bar{\sigma}_2} = \left(\frac{V_2}{V_1} \right)^{1/m} \tag{2}$$

where m is the shape factor of the Weibull distribution. This formula is a straight line with a slop of -1/m in logarithmic scales. The average value of 15.1% for the COV of the strength leads to a value of 7.85 for the Weibull shape factor. A shape factor of 8.3 was reported in [9] for specimens of nominal dimensions 2×6×35 mm^3. As shown in Fig. 3.12, depending on the one data point that is chosen to fully determine the CWSEL line, this line can change its

position. For example, considering the nominal volume of a specimen of 128-mm length as reference volume, the predicted mean values are 11.0%, 30.8% and 56.2% higher for specimens of 32-mm, 8-mm and 2-mm lengths, respectively, than the experimental results. These calculations show that the CWSEL overestimates the effect of size on strength, although the statistical variability of the strength within each group of specimens can be described well via the Weibull distribution with the same shape factor.

3.5.3 Statistics concerning strain to failure

The statistical variability in the strain to failure for the four groups of specimens is examined here. Table 3.7 shows the statistics for the mean value, SD and COV of the tensile strain to failure of spruce wood in the longitudinal direction. The mean value is slightly reduced as the length increases, from 1.14% for 2-mm length to 0.96% for 128-mm length. This reduction is attributed to the fact that longer specimens have a lower mean strength while exhibiting a similar mean effective elastic modulus. The reduction of the SD is more significant with increasing length leading to a reduction in the COV of the strain to failure, except between 32-mm and 128-mm lengths. This may be because the statistics for both elastic modulus and strength affect the statistics for the strain to failure, leading to a trend change in the COV of the strain to failure.

Table 3.7: Statistics of strain to failure for spruce specimens under longitudinal tensile loading.

Specimen length (mm)	Mean (%)	SD (%)	COV (%)
2	1.14	0.17	15.2
8	1.12	0.14	12.9
32	1.08	0.12	11.4
128	0.96	0.13	13.3

Some stochastic problems are better formulated in terms of strain to failure rather than strength [22]. In these cases, the type of distribution representing the statistical variability of the strain to failure is important. Table 3.8 shows results of the goodness-of-fit tests for the strain to failure. The AD and KS tests support the normal and lognormal distributions as being representative of the statistical variability of the strain to failure. The Weibull distribution is rejected by the AD test for 32-mm specimens.

Table 3.8: Results of goodness-of-fit tests for strain to failure of spruce.

Specimen length (mm)	Lognormal		Normal		Weibull	
	AD	KS	AD	KS	AD	KS
2	0	0	0	0	0	0
8	0	0	0	0	0	0
32	0	0	0	0	1	0
128	0	0	0	0	0	0

3.6 Correlations

Figure 3.14 shows the tensile strength of each specimen vs. the corresponding local elastic modulus measured at the failure zone. In this figure, the data from each of the four specimen groups are indicated by a different symbol. Also, the centroid of each group is indicated via a larger symbol of the same type, and the average regression line (solid line) is shown. No significant difference between the scatter in the results of the four groups can be observed, except for 128-mm specimens, which have a lower mean value for the strength. The linear correlation coefficient was found to be 0.686. This is an important parameter for modeling the variability of the mechanical properties in timber structures. For example, when in a finite element model, a value is randomly assigned to the elastic modulus, the variability of the distribution, based on which a value is randomly assigned to the strength at that material point, is reduced. This reduction of variability depends on the level of the correlation; e.g., when the correlation coefficient is 1, there remains no variability for the second parameter.

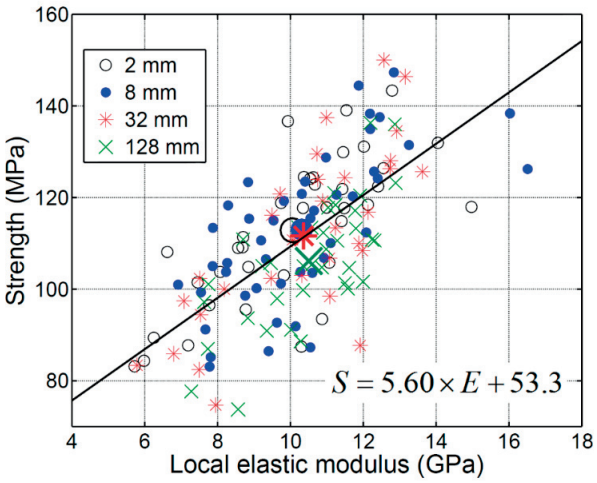

Fig. 3.14: Correlation between local elastic modulus and tensile strength in parallel-to-grain direction.

Figures 3.15 and 3.16 show the effective elastic moduli and the strengths versus the densities, respectively, for the four specimen groups based on which correlation coefficients of 0.696 and 0.580 were obtained. The larger symbols indicate the centroids of the specimen groups, while the average regression line is also given. The mean values of the densities for specimens of different lengths are approximately the same. The mean value, SD and COV of the density of the spruce are 443.3 kg/m3, 39.0 kg/m3 and 8.8%, respectively. The correlations between the density and the mechanical properties are used in seismic and acoustic applications where dynamic forces are present.

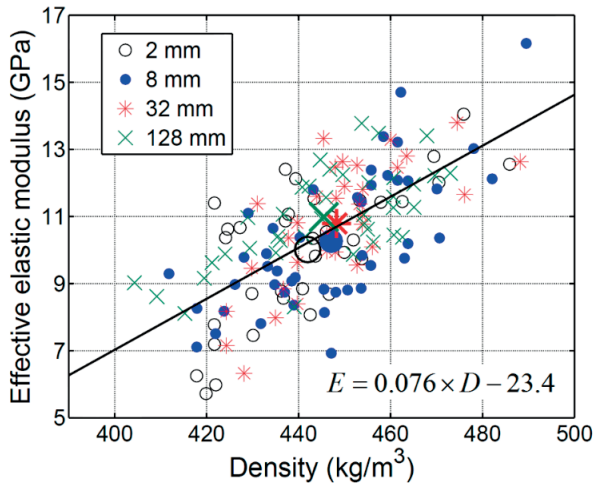

Fig. 3.15: Correlation between density and effective elastic modulus.

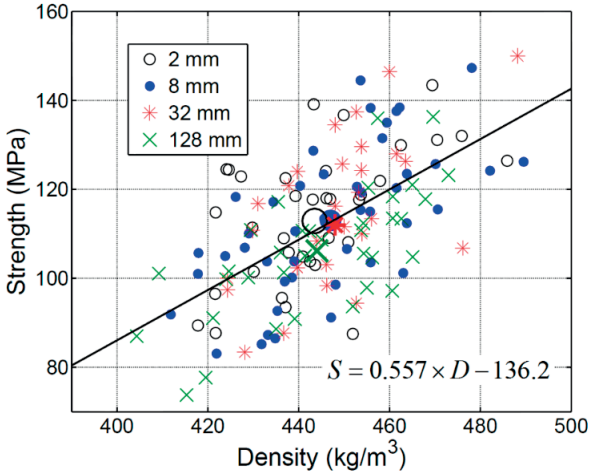

Fig. 3.16: Correlation between density and strength.

3.7 Conclusions

In this chapter, an experimental campaign consisting of the longitudinal tensile tests on the four groups of specimens composed of spruce wood was conducted. The total number of specimens was 165. The nominal length of specimens varied from 2 mm to 128 mm in order to investigate the effect of length on the elasticity and strength. The cross-sectional area was the same for all specimens and sufficiently small as to exclude the effect of the variability of properties in the transverse plane and to find the upper bound values for the investigated properties. The following main conclusions were drawn:

- The new specimens with the extruded geometry proposed for tensile tests on timber are simple and efficient because they are easy to fabricate, and the failure in almost all specimens occurred in the middle part with a constant cross-sectional area.
- The main reason for the spatial variability of the local elastic modulus is irregular changes in the mesostructure of the wood including fiber misalignment, fiber waviness and growth ring thickness.
- Specimens with higher strength levels tend to fail in such a way that the fracture surfaces form a sharper angle to the axial direction than those of specimens with lower strength levels, which is attributed to the latewood pattern around the failure zone. The failure was brittle for all specimens.
- Considerable spatial variability in the local elastic modulus was observed along specimen lengths. The contribution of the between-specimen variability to the ensemble variability is greater than that of the within-specimen variability for the examined specimen length.
- The COV of the effective elastic modulus in the parallel-to-grain direction has an upper bound of ca. 20% when the length is very small due to spatial correlation in the elastic modulus field and decreases to 12.7% for a length of 128 mm. The mean value does not change significantly.
- An upper bound value of 113.0 MPa was obtained for the mean value of the longitudinal tensile strength when the length is very small. The existence of the upper bound is again due to the spatial correlation of the strength field. The mean value decreased to 103.8 MPa for a length of 128 mm. The change in the COV of the tensile strength with specimen length was negligible, with an average value of 15.1%. The variation of the mean strength with specimen size cannot be appropriately modeled by the CWSEL.

With recent progress in computational power, more advanced stochastic analyses of timber structures are feasible. As has been shown, the mechanical properties of timber are spatially variable in a random manner. The random field approach can take the random spatial variability of material properties into account. Therefore, using this approach leads to more realistic models of timber structures.

The case of short term static loading of clear timber was studied in this chapter. In practical applications, the loading duration also affects the response of timber pieces/structures. Beside the initial instantaneous elastic deformation, the creep deformation occurs over time. The duration of load also affects the strength/capacity of timber pieces/structures. For example, the maximum bending strength decreases nearly linearly in logarithm scales with period of loading [1].

3.8 References

[1] Dinwoodie, J.M., 2000. Timber: Its nature and behaviour. Taylor & Francis Group.
[2] Vořechovský, M., 2007. Interplay of size effects in concrete specimens under tension studied via computational stochastic fracture mechanics. International Journal of Solids and Structures 44, 2715-2731.
[3] Sriramula, S., Chryssanthopoulos, M.K., 2013. An experimental characterisation of spatial variability in GFRP composite panels. Structural Safety 42, 1-11.
[4] Forest Product Laboratory, 1999. Wood handbook: Wood as an engineering material, USDA, Madison, Wis.
[5] Clouston, P.L., Lam, F., 2002. A stochastic plasticity approach to strength modeling of strand-based wood composites. Composites Science and Technology 62, 1381-1395.
[6] Clouston, P.L., Lam, F., 2001. Computational modeling of strand-based wood composites. Journal of Engineering Mechanics 127, 844-851.
[7] Arwade, S.R., Clouston, P.L., Winans, R., 2009. Measurement and stochastic computational modeling of the elastic properties of parallel strand lumber. Journal of Engineering Mechanics 135, 897-905.
[8] Zhu, J., Kudo, A., Takeda, T., Tokumoto, M., 2001. Methods to estimate the length effect on tensile strength parallel to the grain in Japanese larch. Journal of Wood Science 47, 269-274.
[9] Dill-Langer, G., Hidalgo, R.C., Kun, F., Moreno, Y., Aicher, S., Herrmann, H.J., 2003. Size dependency of tension strength in natural fiber composites. Physica A: Statistical Mechanics and its Applications 325, 547-560.
[10] Weibull, W., 1939. A statistical theory of strength of materials. In: Proceedings of the Royal Swedish Institute. Research No. 151, Stockholm, Sweden.
[11] Vallée, T., Tannert, T., Ganne-Chedville, C., 2012. Capacity prediction of welded timber joints. Wood Science and Technology 46, 333-347.
[12] Tannert, T., Vallée, T., Hehl, S., 2012. Probabilistic strength prediction of adhesively bonded timber joints. Wood Science and Technology 46, 503-513.
[13] Tannert, T., Vallée, T., Hehl, S., 2012. Experimental and numerical investigations on adhesively bonded hardwood joints. International Journal of Adhesion and Adhesives 37, 65-69.

[14] Tannert, T., Lam, F., Vallée, T., 2011. Structural performance of rounded dovetail connections: Experimental and numerical investigations. European Journal of Wood and Wood Products 69, 471-482.
[15] Clouston, P., Lam, F., Barrett, J.D., 1998. Incorporating size effects in the Tsai-Wu strength theory for Douglas-fir laminated veneer. Wood Science and Technology 32, 215-226.
[16] Madsen, B., 1990. Size effects in defect-free Douglas fir. Canadian Journal of Civil Engineering 17, 238-242.
[17] Madsen, B., Tomoi, M., 1991. Size effects occurring in defect-free spruce-pine-fir bending specimens. Canadian journal of civil engineering 18, 637-643.
[18] Madsen, B., 1990. Length effects in 38 mm spruce-pine-fir dimension lumber. Canadian Journal of Civil Engineering 17, 226-237.
[19] Tannert, T., Lam, F., Vallée, T., 2010. Strength prediction for rounded dovetail connections considering size effects. Journal of Engineering Mechanics 136, 358-366.
[20] Vanmarcke, E., 2010. Random fields: analysis and synthesis. World Scientific.
[21] Arwade, S.R., Clouston, P.L., Krupka, M.T., 2011. Length effects in tensile strength in the orthogonal directions of structural composite lumber. Journal of Testing and Evaluation 39, 1-7.
[22] Vořechovský, M., Chudoba, R., 2006. Stochastic modeling of multi-filament yarns: II. Random properties over the length and size effect. International Journal of Solids and Structures 43, 435-458.

4 Transverse mechanical properties of clear timber: Uncertainty and size effects

4.1 Introduction

The existence of variability in the mechanical properties of timber has long been recognized [1]. This variability is related to the age, original position of the timber within the tree, structural complexity and imperfections, load history during tree growth etc. [2]. As a consequence of this variability, the statistics of the mechanical properties of timber can change with specimen size [3].

The longitudinal mechanical properties of timber have been more intensively investigated compared to the transverse properties. This is primarily because of the common applications of timber for beams and truss elements where mainly longitudinal stresses develop. On the other hand, in some applications such as mechanical and adhesively-bonded timber joints, transverse properties, such as the transverse tensile strength of clear timber which is only a few percent of its longitudinal tensile strength [4], are of critical importance.

The mean strength of timber, in its brittle failure modes such as those under longitudinal and transverse tensile loadings, decreases as its volume increases, since the probability of the occurrence of a weakest material point with a lower strength value increases. This phenomenon is referred to as the size effect on strength. Several experimental works have been devoted to the effect of size on the transverse strength of clear timber [1, 5-9], mainly focusing on glued-laminated material. The classical Weibull size effect law (CWSEL) [10] is commonly used in the literature for modeling this effect [5,6,9]. Very few works in the literature have adopted other approaches to investigate the size effect in timber, especially in the transverse direction. In the case of transverse strength, Pedersen et al. [8] and Astrup et al. [9] conducted transverse tensile tests on bulk specimens with a double symmetry and observed a large size effect in the results. They developed a deterministic model for the size effect observed from experiments. This model was based on the consideration of stress inhomogeneity caused by the anisotropic nature of timber.

The density and mechanical properties of timber are naturally correlated [2] and therefore correlation coefficients between these properties are necessary parameters to accurately perform probabilistic simulations [11]. Nevertheless, very few studies have been conducted on

the correlation between density and transverse properties. Xavier et al. [12] found a reasonably good correlation between the radial variability of transverse and shear components of the stiffness matrix of maritime pine wood, based on mechanical tests on unnotched Iosipescu specimens. Recently, Xavier [13] and Pereira et al. [14] measured the density and elastic moduli of cubic specimens cut from different radial positions and heights on the Pinus pinaster tree and concluded that "none of the studied density parameters showed a stable correlation pattern for any of the elastic properties."

Previous experiments were mostly carried out on bulk cubic or glulam specimens in order to comply with the EN standard [15], which recommends a glued laminated timber composed of solid timber blocks as the testing specimen, while the size effect on the transverse strength of small clear specimens has not been investigated. Also, it is reported in [3] that no conclusive evidence has yet been found concerning the accuracy of probabilistic strength size effect theories, like the CWSEL. Compared to the uncertainty regarding strength, the effect of the high scatter in the timber elastic properties [16] on the response of timber structures has received less attention [3,4,17]. However, a spatially variable elastic field can lead to a different stress field, compared to the case of a uniform elastic modulus. This stress field results in a different failure probability when used with a failure function, compared to the case when the spatial variability is not included. The relevant literature also provides insufficient information regarding the correlation between the density and transverse mechanical properties. Moreover, to the best of the authors' knowledge, there is no data in the literature about the correlation between the transverse strength and the transverse elastic modulus at the scale of a few millimeters, which can be important when considering the local variability in elastic modulus and strength fields in stochastic simulations.

This chapter addresses the aforementioned shortcomings in the literature by performing quasi-static experiments on specimens cut in the transverse direction with different lengths and thoroughly analyzing their mechanical behavior and failure types. In addition to the global displacement monitoring, the local deformations along the length of each specimen were measured. The mechanical behavior of specimens of different lengths cut in regular and random manners from different boards was studied. The statistics of the elastic modulus, strength and strain to failure as well as the effect of size on these properties were examined. The accuracy of CWSEL for the transverse tensile strength of small clear specimens was also evaluated, and the correlations between the mechanical properties and between the mechanical properties and the material's density were investigated.

4.2 Experimental program

4.2.1 Material used and conditioning

Norway spruce wood was used for the specimen preparation in this study. All specimens were conditioned to 12% moisture content according to the ASTM standard D143-14 and tested at the laboratory temperature of 22±3 C°. The average density of the specimens after conditioning was 441.2±14.4 kg/m3. The density was obtained by dividing the weight of each specimen by its volume, after conditioning.

4.2.2 Spruce boards

Ten boards were cut from the same batch of spruce lumbers in the radial-longitudinal plane. Seven boards were used for cutting regularly positioned specimens of a specific length, and henceforth referred to as regular boards (REBs). The remaining three boards were used for cutting randomly positioned specimens of different lengths and are designated random boards (RABs). The boards can have different average strengths, affecting the size effect investigation. Therefore randomly positioned specimens of different sizes, cut from each of the RABs, are used to eliminate this effect.

Figure 4.1a-c shows REBs used for cutting specimens of different lengths. Two boards for specimens of 8-mm length, two boards for specimens of 32-mm length and three boards for specimens of 120-mm length were used. Specimens of 8-mm and 32-mm lengths were cut in two rows from each board, and specimens of 120-mm length were cut in one row, taking into account the geometries of the specimens and boards. In Fig. 4.2, one RAB is shown.

a)

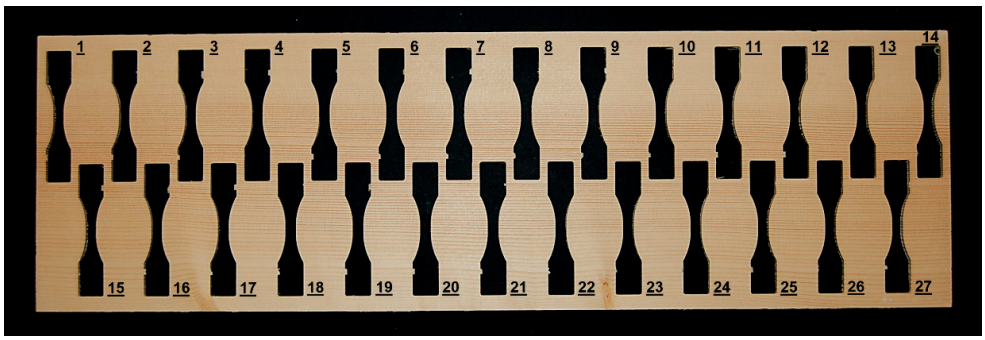

b)

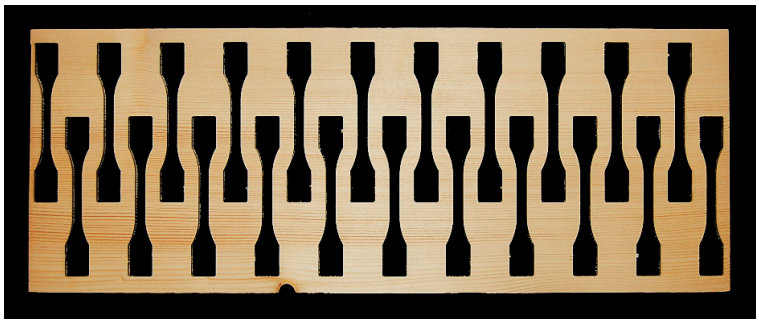

c) 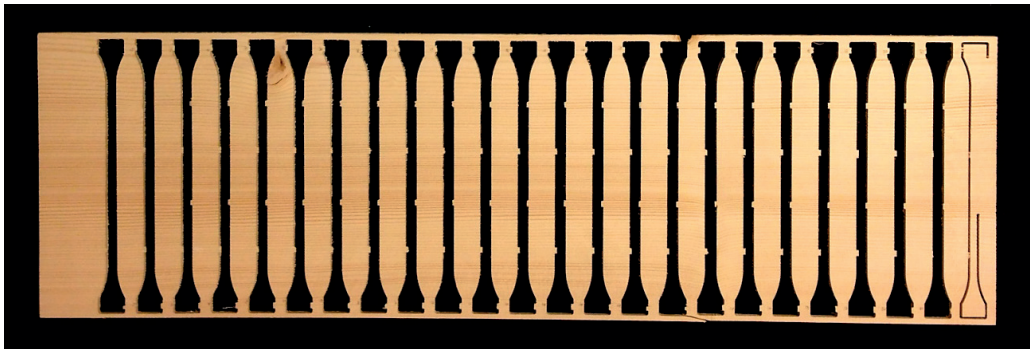

Fig. 4.1: Boards with regular arrangement of specimens. a) 8-mm specimens. b) 32-mm specimens. c) 120-mm specimens.

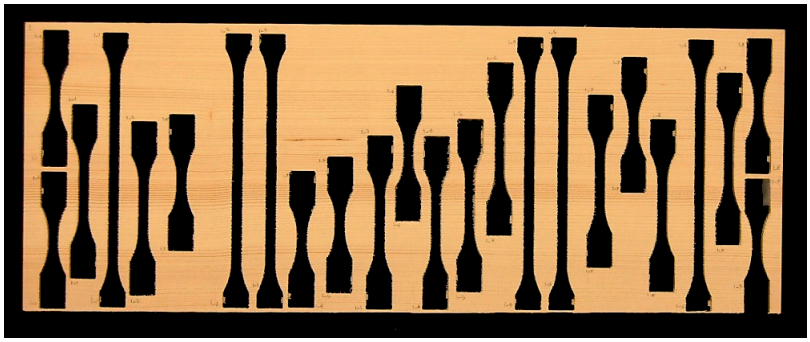

Fig. 4.2: Typical arrangement used for cutting randomly positioned specimens of different lengths.

4.2.3 Specimen description

Specimens with different lengths were fabricated by using a CNC machine. A cross-sectional area of 4×4 mm^2 was considered for all investigated specimens. Representative specimens are shown in Fig. 4.3. The length of the middle zone (nominal length) can be 8, 32 and 120 mm. After conducting a number of preliminary experiments, 226 specimens were tested during the main program and the results are reported in this chapter.

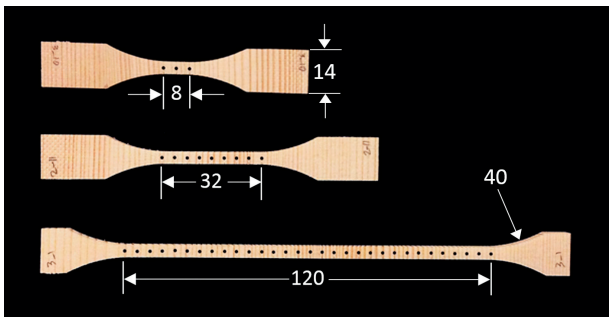

Fig. 4.3: Fabricated specimens of different lengths. Dimensions in mm.

The following system is used to refer to the specimens in this study: TT-abc-16-de-fghi where TT refers to transverse tensile, 'abc' is the specimen length in mm (008, 032, 120), 16 is the cross-sectional area in mm^2, the same for all specimens, and 'de' denotes the specimen ID number in each group of specimens with the same length. Finally, 'fghi' indicates the specific board.

4.2.4 Experimental set-up and instrumentation

All experiments were carried out on a 5 kN electromechanical Walter+Bai testing machine. Quasi-static tensile tests were performed in displacement-control mode. Stroke rates of 1 mm/min for specimens with nominal lengths of 8 and 32 mm and a stroke rate of 2 mm/min for specimens with a nominal length of 120 mm were used on the basis of previous preliminary experiments so that the final failure occurred within 180±60 s throughout the whole testing program.

A video extensometry system composed of a 10-bit Sony XCLU1000 CCD connected to a Fujinon HF35SA-1, 35-mm f 1.4-22 lens with an accuracy of ±0.005 mm was used during the experiments to measure the axial deformation. Prior to the tests, black target dots of 1.1-mm diameter were applied on the specimens' surfaces. The distance between each two consecutive dots was 4 mm for all groups of specimens. A typical specimen of 32-mm length mounted in the testing rig is shown in Fig. 4.4. The axial coordinates of the dots were recorded at a frequency of 5 Hz by the video extensometer throughout loading. Using these data, the engineering strain between each two consecutive dots was calculated, designated as the local strain. These data were used for calculation of the local elastic modulus, E_{loc}. Also, using the displacements of the first and last dots on each specimen, an overall strain for each nominal length was obtained. These data were used for calculating the effective elastic modulus, E_{eff}, for each specimen. Nominal axial stresses were calculated by using the load measurements and the initial cross-sectional areas.

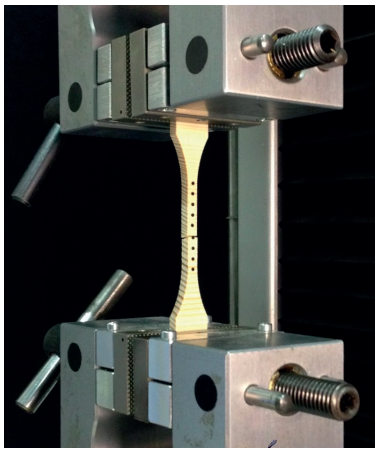

Fig. 4.4: Specimen of 32-mm nominal length with applied dots inside machine grips.

4.3 Experimental results

Tensile stress-strain curves of the 8-mm, 32-mm and 120-mm-length specimens, cut from the REBs, are shown in Figs. 4.5-4.11. In the cases of boards with two rows of specimens, the curves in each row are indicated by a different color. Maximum and minimum strengths and strain to failure are indicated by vertical and horizontal dashed lines in each figure. The overall strains are used for plotting these curves; the average slope of each curve indicates the effective elastic modulus.

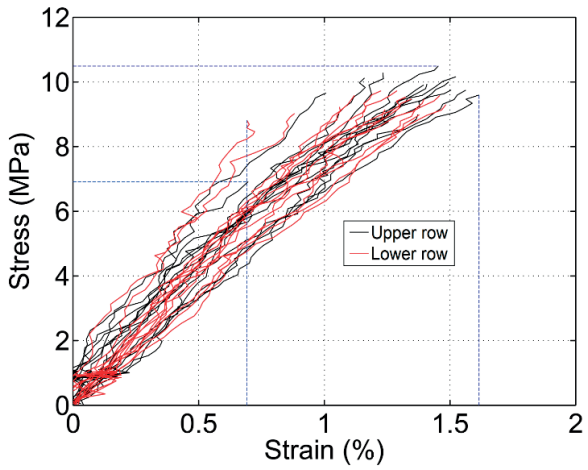

Fig. 4.5: Transverse tensile stress-strain curves of spruce wood for 8-mm specimens cut from REB1.

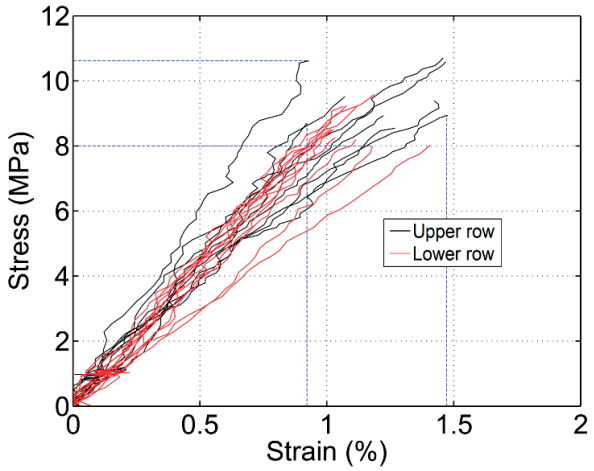

Fig. 4.6: Transverse tensile stress-strain curves of spruce wood for 8-mm specimens cut from REB2.

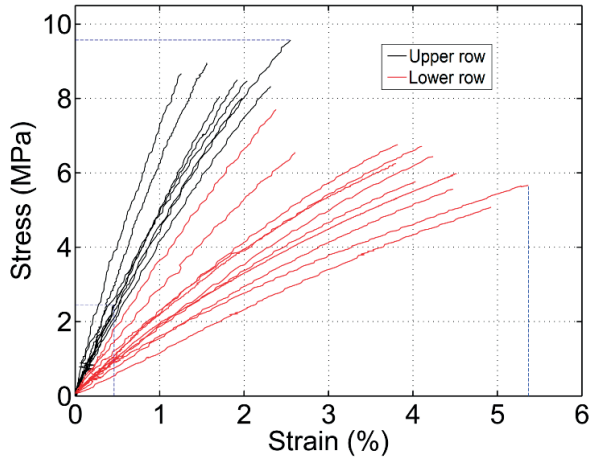

Fig. 4.7: Transverse tensile stress-strain curves of spruce wood for 32-mm specimens cut from REB1.

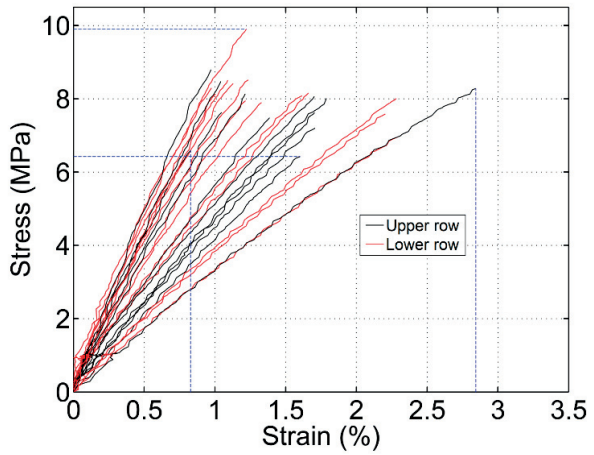

Fig. 4.8: Transverse tensile stress-strain curves of spruce wood for 32-mm specimens cut from REB2.

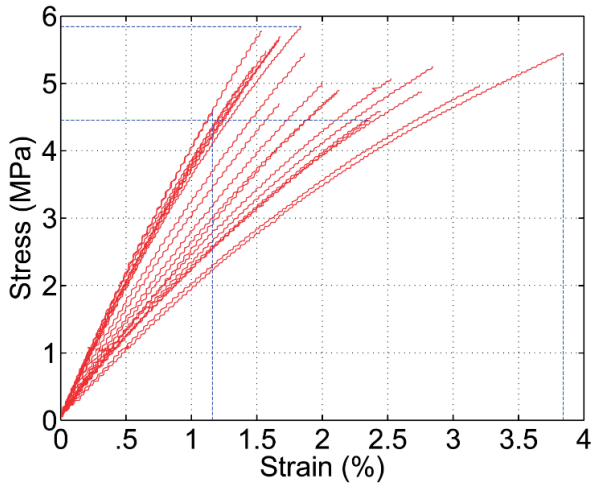

Fig. 4.9: Transverse tensile stress-strain curves of spruce wood for 120-mm specimens cut from REB1.

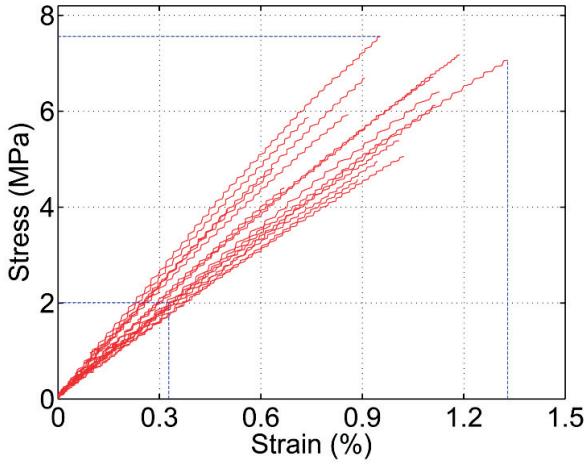

Fig. 4.10: Transverse tensile stress-strain curves of spruce wood for 120-mm specimens cut from REB2.

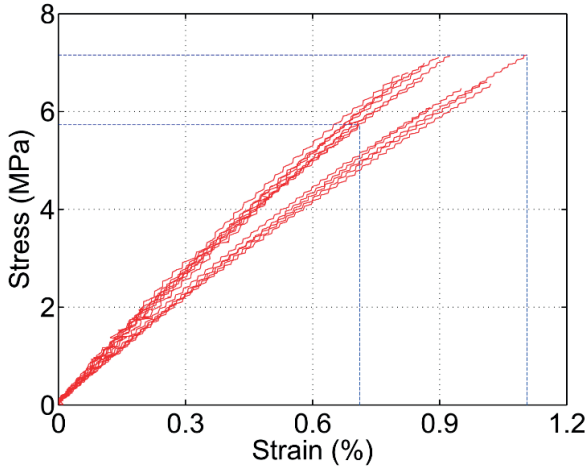

Fig. 4.11: Transverse tensile stress-strain curves of spruce wood for 120-mm specimens cut from REB3.

An almost linear stress-strain behavior is observed for most of the specimens. There is a high scatter in the effective elastic modulus, strength and strain to failure (overall strain) for each length. In a few cases, the maximum/minimum values of strength are associated with the maximum/minimum values of strain to failure, especially when the minimum strength in a board is relatively low.

Considering the specimens of 8-mm length, the results of the two rows from each board are not significantly different. The range of variation of strength and strain to failure is wider in the first board. The specimens from the first board have slightly higher strengths.

In the first board for specimens of 32-mm length, the specimens in the upper row exhibit higher moduli and strengths and lower strains to failure. However, the specimen behaviors in the two rows of the second board are not significantly different. As a result, the scatter in the mechanical

properties is higher in the first board. Also, the first board is less stiff than the second board and exhibits lower strengths but higher strains to failure. In the specimens from the first board, higher moduli values are associated with higher strengths, which is not the case for the specimens from the second board. The range of variation in the strength is wider in the first board, mainly because of one specimen that happened to have a relatively low strength.

Regarding the specimens of 120-mm length, the specimens from the first board have lower moduli and strengths. The scatter in the effective elastic modulus and strain to failure is higher in the first board. However, the second board shows higher scatter in the strength. The strength is higher for the specimens from the third board than those from the second board, and higher for the specimens from the second board than those from the first board.

Specimens of 8-mm length exhibit a lower variability in their mechanical properties, since they represent mainly the variability of the transverse modulus in the longitudinal direction. The variability of the transverse modulus in the transverse direction of the boards can be better taken into account when specimens are longer. However, a size effect is still present with shorter specimens exhibiting higher strengths.

The experimental results for the mechanical properties of specimens of different lengths in the RABs are shown in Figs. 4.12-4.14. The mechanical behavior is almost linear, similar to the REBs. The strength consistently decreases with increasing specimen length. A detailed discussion regarding the size effect is provided in Section 4.4.

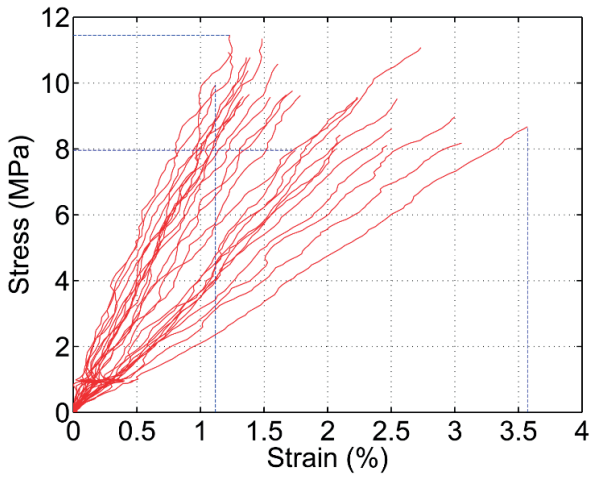

Fig. 4.12: Transverse tensile stress-strain curves of spruce wood for 8-mm specimens cut from RABs.

The mechanical properties of each specimen including the effective elastic modulus, the strength and the strain to failure as well as their maximum and minimum values in each board, along with density and failure type, are given in Tables 4.1-4.3.

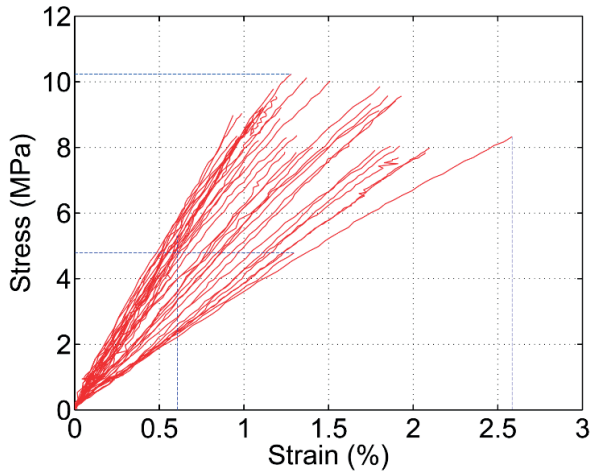

Fig. 4.13: Transverse tensile stress-strain curves of spruce wood for 32-mm specimens cut from RABs.

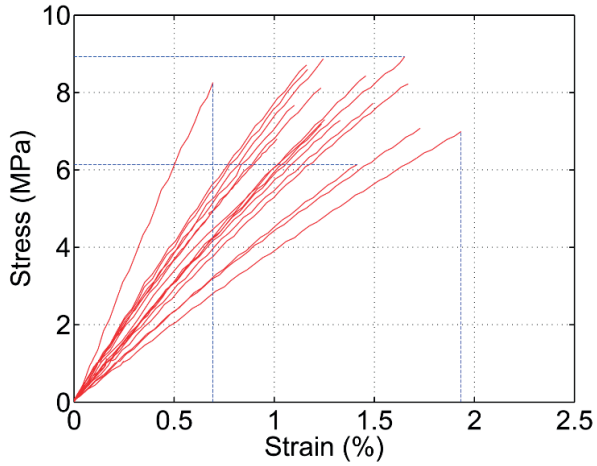

Fig. 4.14: Transverse tensile stress-strain curves of spruce wood for 120-mm specimens cut from RABs.

The failure types are discussed in Section 4.5. Those few specimen densities affected by a nearby knot (mainly in the tab of the specimen) are indicated by * in the tables and are excluded when examining the correlation between density and mechanical properties.

Table 4.1: Effective elastic modulus, strength, strain to failure, density and failure type for 8-mm specimens.

Specimen code	Effective E (MPa)	Strength (MPa)	Strain to failure (%)	Density (kg/m^3)	Failure type	Maxima and minima
TT-008-16-01-REB1	735.8	9.97	1.35	442.4	3	Max(E)=1184.3 MPa
TT-008-16-02-REB1	655.1	10.2	1.56	452.4	3	Min(E)=643.3 MPa
TT-008-16-03-REB1	643.3	9.61	1.49	464.3	1	Max(S)=10.59 MPa
TT-008-16-04-REB1	918.0	7.01	0.76	458.4	1	Min(S)=7.01 MPa

TT-008-16-05-REB1	837.8	10.40	1.24	452.5	1	Max(ε)=1.56 %
TT-008-16-06-REB1	664.4	9.82	1.48	441.4	3	Min(ε)=0.75 %
TT-008-16-07-REB1	970.8	9.77	1.01	459.0	1	
TT-008-16-08-REB1	667.6	9.073	1.36	453.4	3	
TT-008-16-09-REB1	723.5	9.52	1.32	465.6	1	
TT-008-16-10-REB1	676.1	9.80	1.45	472.7	1	
TT-008-16-11-REB1	681.6	10.06	1.46	462.4	1	
TT-008-16-12-REB1	868.7	10.19	1.17	466.5	1	
TT-008-16-13-REB1	722.4	10.59	1.47	465.8	1	
TT-008-16-14-REB1	676.8	10.09	1.49	461.3	1	
TT-008-16-15-REB1	818.7	9.84	1.20	409.3	1	
TT-008-16-16-REB1	672.9	9.52	1.41	409.7	1	
TT-008-16-17-REB1	737.7	9.50	1.29	418.0	1	
TT-008-16-18-REB1	759.7	9.20	1.21	405.3	2	
TT-008-16-19-REB1	893.9	9.17	1.03	402.6	2	
TT-008-16-20-REB1	881.6	9.64	1.09	426.4	1	
TT-008-16-21-REB1	868.7	9.31	1.07	421.2	1	
TT-008-16-22-REB1	712.1	9.61	1.35	417.0	1	
TT-008-16-23-REB1	655.5	9.43	1.44	423.1	1	
TT-008-16-24-REB1	677.7	9.09	1.34	421.2	2	
TT-008-16-25-REB1	720.4	9.67	1.34	415.4	1	
TT-008-16-26-REB1	798.3	9.84	1.23	417.5	1	
TT-008-16-27-REB1	1184.3	8.90	0.75	424.2	1	
TT-008-16-28-REB2	597.7	8.90	1.49	458.9	1	Max(E)=1121.4 MPa
TT-008-16-29-REB2	754.9	10.75	1.42	455.1	1	Min(E)=575.2 MPa
TT-008-16-30-REB2	748.4	10.60	1.42	459.5	1	Max(S)=10.75 MPa
TT-008-16-31-REB2	755.2	9.02	1.19	455.1	1	Min(S)=8.07 MPa
TT-008-16-32-REB2	642.3	9.40	1.46	453.2	1	Max(ε)=1.49 %
TT-008-16-33-REB2	707.7	8.62	1.22	458.4	1	Min(ε)=0.87 %
TT-008-16-34-REB2	917.5	9.62	1.05	459.6	1	
TT-008-16-35-REB2	1121.4	10.69	0.95	454.3	1	
TT-008-16-36-REB2	-	10.37	-	544.1*	1	
TT-008-16-37-REB2	1003.8	8.74	0.87	449.8	1	
TT-008-16-38-REB2	803.9	8.47	1.05	449.5	1	
TT-008-16-39-REB2	827.1	9.66	1.17	446.1	1	
TT-008-16-40-REB2	899.9	9.26	1.03	441.9	1	
TT-008-16-41-REB2	869.8	9.34	1.07	446.5	1	
TT-008-16-42-REB2	911.3	9.27	1.02	430.8	1	
TT-008-16-43-REB2	906.7	8.54	0.94	437.8	1	

TT-008-16-44-REB2	850.3	8.50	1.00	441.9	1	
TT-008-16-45-REB2	763.0	8.27	1.08	430.9	1	
TT-008-16-46-REB2	838.4	8.53	1.02	430.1	1	
TT-008-16-47-REB2	673.2	8.07	1.20	429.0	1	
TT-008-16-48-REB2	575.2	8.14	1.42	430.1	1	
TT-008-16-49-RAB1	559.0	9.70	1.74	458.4	1	Max(E)=773.5 MPa
TT-008-16-50-RAB1	598.3	9.68	1.62	453.5	1	Min(E)=251.9 MPa
TT-008-16-51-RAB1	773.5	10.91	1.41	446.4	1	Max(S)=10.91 MPa
TT-008-16-52-RAB1	358.9	8.71	2.43	457.3	1	Min(S)=8.10 MPa
TT-008-16-53-RAB1	595.4	9.86	1.66	454.6	1	Max(ε)=3.46 %
TT-008-16-54-RAB1	482.8	8.10	1.68	451.5	2	Min(ε)=1.41 %
TT-008-16-55-RAB1	251.9	8.72	3.46	462.7	1	
TT-008-16-56-RAB1	279.2	8.19	2.93	443.7	4	
TT-008-16-57-RAB1	329.5	8.15	2.47	424.5	3	
TT-008-16-58-RAB2	839.8	10.00	1.19	407.1	1	Max(E)=773.5 MPa
TT-008-16-59-RAB2	746.1	10.51	1.41	442.8	1	Min(E)=251.9 MPa
TT-008-16-60-RAB2	438.0	9.60	2.19	439.7	1	Max(S)=11.53 MPa
TT-008-16-61-RAB2	940.0	11.53	1.23	455.1	1	Min(S)=9.60 MPa
TT-008-16-62-RAB2	645.5	9.67	1.50	439.9	1	Max(ε)=3.46 %
TT-008-16-63-RAB2	892.7	11.05	1.24	446.1	1	Min(ε)=1.41 %
TT-008-16-64-RAB2	793.5	10.91	1.37	454.6	2	
TT-008-16-65-RAB2	765.4	11.46	1.50	547.0*	1	
TT-008-16-66-RAB3	733.8	9.73	1.33	473.7	3	Max(E)=734.5 MPa
TT-008-16-67-RAB3	393.9	8.03	2.04	424.3	1	Min(E)=312.7 MPa
TT-008-16-68-RAB3	719.6	9.44	1.31	455.6	1	Max(S)=11.17 MPa
TT-008-16-69-RAB3	734.5	9.72	1.32	446.9	3	Min(S)=8.03 MPa
TT-008-16-70-RAB3	418.1	8.46	2.02	459.5	3	Max(ε)=2.89 %
TT-008-16-71-RAB3	312.7	9.05	2.89	455.0	1	Min(ε)=1.31 %
TT-008-16-72-RAB3	380.0	9.57	2.52	461.3	1	
TT-008-16-73-RAB3	458.2	9.56	2.09	455.5	1	
TT-008-16-74-RAB3	426.1	11.17	2.62	462.4	1	
TT-008-16-75-RAB3	649.6	10.61	1.63	446.5	1	

Table 4.2: Effective elastic modulus, strength, strain to failure, density and failure type for 32-mm specimens.

Specimen code	Effective E (MPa)	Strength (MPa)	Strain to failure (%)	Density (kg/m^3)	Failure type	Maxima and Minima
TT-032-16-01-REB1	597.6	8.97	1.50	438.2	1	Max(E)=674.8 MPa
TT-032-16-02-REB1	538.2	2.48	0.46	455.0	4	Min(E)=104.3 MPa
TT-032-16-03-REB1	674.8	8.81	1.31	450.5	1	Max(S)=9.60 MPa

TT-032-16-04-REB1	441.3	8.58	1.94	446.9	1	Min(S)=2.48 MPa
TT-032-16-05-REB1	406.6	8.03	1.97	445.1	1	Max(ε)=5.42 %
TT-032-16-06-REB1	408.7	8.49	2.08	444.4	1	Min(ε)=0.46 %
TT-032-16-07-REB1	362.6	8.44	2.33	448.3	4	
TT-032-16-08-REB1	385.1	9.60	2.49	490.2	1	
TT-032-16-09-REB1	477.5	8.07	1.69	450.0	1	
TT-032-16-10-REB1	168.7	6.26	3.71	435.9	1	
TT-032-16-11-REB1	154.5	6.48	4.20	443.5	4	
TT-032-16-12-REB1	130.7	5.99	4.58	447.2	1	
TT-032-16-13-REB1	105.9	5.08	4.80	448.3	1	
TT-032-16-14-REB1	104.3	5.65	5.42	435.7	3	
TT-032-16-15-REB1	126.0	5.58	4.43	431.1	4	
TT-032-16-16-REB1	144.6	5.82	4.02	442.1	4	
TT-032-16-17-REB1	162.3	6.72	4.14	436.5	1	
TT-032-16-18-REB1	181.2	6.82	3.76	419.4	1	
TT-032-16-19-REB1	248.4	6.58	2.65	443.6	3	
TT-032-16-20-REB1	323.0	7.71	2.39	439.9	1	
TT-032-16-21-REB2	295.5	8.31	2.81	447.8	1	Max(E)=923.7 MPa
TT-032-16-22-REB2	407.8	6.46	1.58	453.1	2	Min(E)=295.5 MPa
TT-032-16-23-REB2	443.5	7.68	1.73	435.5	3	Max(S)=9.98 MPa
TT-032-16-24-REB2	448.4	8.06	1.80	436.1	1	Min(S)=6.46 MPa
TT-032-16-25-REB2	422.9	7.37	1.74	436.5	3	Max(ε)=2.81 %
TT-032-16-26-REB2	462.4	8.08	1.75	431.2	1	Min(ε)=0.86 %
TT-032-16-27-REB2	536.4	7.50	1.40	438.9	3	
TT-032-16-28-REB2	710.8	7.66	1.08	441.4	3	
TT-032-16-29-REB2	778.5	6.66	0.86	405.8	2	
TT-032-16-30-REB2	667.0	8.15	1.22	433.1	1	
TT-032-16-31-REB2	824.3	8.54	1.04	436.7	3	
TT-032-16-32-REB2	923.7	8.84	0.96	439.2	1	
TT-032-16-33-REB2	304.3	6.98	2.29	451.5	1	
TT-032-16-34-REB2	344.2	7.60	2.21	443.5	1	
TT-032-16-35-REB2	348.9	8.02	2.30	469.1	1	
TT-032-16-36-REB2	472.5	8.20	1.74	442.1	1	
TT-032-16-37-REB2	491.2	8.17	1.66	434.1	1	
TT-032-16-38-REB2	595.1	8.09	1.36	429.3	1	
TT-032-16-39-REB2	653.9	8.02	1.23	430.8	1	
TT-032-16-40-REB2	743.9	8.50	1.14	429.6	1	
TT-032-16-41-REB2	795.1	8.21	1.03	432.0	1	
TT-032-16-42-REB2	805.5	8.32	1.03	424.4	1	

TT-032-16-43-REB2	669.6	8.57	1.28	443.9	1	
TT-032-16-44-REB2	813.5	9.98	1.23	468.4	1	
TT-032-16-45-REB2	792.9	8.52	1.07	442.8	1	
TT-032-16-46-RAB1	928.9	9.04	0.97	434.4	1	Max(E)=928.9 MPa
TT-032-16-47-RAB1	867.1	9.96	1.15	438.7	1	Min(E)=321.4 MPa
TT-032-16-48-RAB1	537.9	9.50	1.77	451.5	3	Max(S)=9.96 MPa
TT-032-16-49-RAB1	428.8	8.22	1.92	449.4	3	Min(S)=4.88 MPa
TT-032-16-50-RAB1	519.4	9.69	1.87	438.7	1	Max(ε)=2.61 %
TT-032-16-51-RAB1	451.0	7.92	1.76	448.0	3	Min(ε)=0.97 %
TT-032-16-52-RAB1	492.3	9.52	1.93	438.3	3	
TT-032-16-53-RAB1	321.4	8.38	2.61	439.3	3	
TT-032-16-54-RAB1	353.9	4.88	1.38	430.8	2	
TT-032-16-55-RAB2	549.0	9.93	1.81	454.6	1	Max(E)=861.5 MPa
TT-032-16-56-RAB2	666.3	10.07	1.51	447.5	1	Min(E)=499.1 MPa
TT-032-16-57-RAB2	861.5	8.65	1.00	432.2	1	Max(S)=10.23 MPa
TT-032-16-58-RAB2	499.1	9.20	1.84	430.2	1	Min(S)=7.44 MPa
TT-032-16-59-RAB2	758.6	9.23	1.22	431.0	1	Max(ε)=1.84 %
TT-032-16-60-RAB2	747.0	9.03	1.21	423.7	1	Min(ε)=0.98 %
TT-032-16-61-RAB2	811.0	9.15	1.13	442.1	1	
TT-032-16-62-RAB2	839.0	9.51	1.13	445.6	1	
TT-032-16-63-RAB2	637.5	7.86	1.23	425.1	1	
TT-032-16-64-RAB2	662.2	8.38	1.27	404.6	2	
TT-032-16-65-RAB2	666.0	8.41	1.26	438.4	1	
TT-032-16-66-RAB2	760.0	7.44	0.98	439.3	3	
TT-032-16-67-RAB2	755.7	10.23	1.35	458.6	1	
TT-032-16-68-RAB2	816.2	9.33	1.14	435.9	1	
TT-032-16-69-RAB3	867.5	9.28	1.07	445.1	1	Max(E)=926.4 MPa
TT-032-16-70-RAB3	586.8	8.10	1.38	445.5	1	Min(E)=414.0 MPa
TT-032-16-71-RAB3	854.0	5.39	0.63	448.1	3	Max(S)=10.26 MPa
TT-032-16-72-RAB3	643.5	7.89	1.23	452.2	1	Min(S)=5.39 MPa
TT-032-16-73-RAB3	916.5	8.35	0.91	465.6	3	Max(ε)=2.12 %
TT-032-16-74-RAB3	926.4	9.07	0.98	449.1	1	Min(ε)=0.63 %
TT-032-16-75-RAB3	376.9	7.88	2.09	448.1	1	
TT-032-16-76-RAB3	378.6	8.01	2.12	452.3	1	
TT-032-16-77-RAB3	847.0	9.59	1.13	439.2	1	
TT-032-16-78-RAB3	829.5	10.26	1.24	438.8	1	
TT-032-16-79-RAB3	433.4	8.09	1.87	478.2	1	
TT-032-16-80-RAB3	740.4	8.36	1.13	446.9	3	
TT-032-16-81-RAB3	414.0	7.71	1.86	526.6*	3	

TT-032-16-82-RAB3	523.0	9.65	1.85	574.1*	1	

Table 4.3: Effective elastic modulus, strength, strain to failure, density and failure type for 120-mm specimens.

Specimen code	Effective E (MPa)	Strength (MPa)	Strain to failure (%)	Density (kg/m^3)	Failure type	Maxima and minima
TT-120-16-01-REB1	143.3	5.44	3.80	443.2	4	Max(E)=392.0 MPa
TT-120-16-02-REB1	177.2	4.87	2.75	449.7	4	Min(E)=143.3 MPa
TT-120-16-03-REB1	155.5	4.98	3.20	447.4	4	Max(S)=5.84 MPa
TT-120-16-04-REB1	183.8	5.25	2.86	456.0	4	Min(S)=4.45 MPa
TT-120-16-05-REB1	230.0	4.90	2.13	529.7*	3	Max(ε)=3.80 %
TT-120-16-06-REB1	187.5	4.45	2.37	451.1	3	Min(ε)=1.16 %
TT-120-16-07-REB1	187.2	4.59	2.45	436.3	4	
TT-120-16-08-REB1	198.4	5.07	2.56	441.7	4	
TT-120-16-09-REB1	229.06	4.86	2.12	445.6	3	
TT-120-16-10-REB1	246.8	5.01	2.03	448.4	3	
TT-120-16-11-REB1	278.4	4.70	1.69	447.9	2	
TT-120-16-12-REB1	288.5	5.45	1.89	452.2	2	
TT-120-16-13-REB1	336.7	5.64	1.68	449.5	2	
TT-120-16-14-REB1	360.8	4.85	1.34	450.0	2	
TT-120-16-15-REB1	392.0	4.53	1.16	453.1	2	
TT-120-16-16-REB1	375.1	5.78	1.54	446.9	2	
TT-120-16-17-REB1	341.2	5.69	1.67	442.5	2	
TT-120-16-18-REB1	318.7	5.84	1.83	444.7	4	
TT-120-16-19-REB1	348.7	5.48	1.57	446.6	2	
TT-120-16-20-REB1	352.8	5.25	1.49	450.3	3	
TT-120-16-21-REB1	338.7	5.59	1.65	442.3	1	
TT-120-16-22-REB2	655.2	4.40	0.67	411.3	2	Max(E)=802.6 MPa
TT-120-16-23-REB2	580.8	3.66	0.63	421.1	2	Min(E)=493.8 MPa
TT-120-16-24-REB2	556.1	2.01	0.36	420.2	4	Max(S)=7.56 MPa
TT-120-16-25-REB2	570.1	6.40	1.12	416.7	1	Min(S)=2.01 MPa
TT-120-16-26-REB2	513.8	4.95	0.96	429.7	3	Max(ε)=1.32 %
TT-120-16-27-REB2	493.8	5.06	1.02	437.1	2	Min(ε)=0.36 %
TT-120-16-28-REB2	533.1	7.06	1.32	429.5	3	
TT-120-16-29-REB2	510.0	4.57	0.90	429.9	2	
TT-120-16-30-REB2	530.2	5.39	1.02	426.5	2	
TT-120-16-31-REB2	547.2	6.12	1.12	429.0	3	
TT-120-16-32-REB2	603.7	7.17	1.19	452.0	2	
TT-120-16-33-REB2	606.9	6.72	1.11	430.8	3	

TT-120-16-34-REB2	696.8	5.93	0.85	431.2	2	
TT-120-16-35-REB2	743.5	6.69	0.90	437.0	1	
TT-120-16-36-REB2	744.7	4.81	0.65	427.6	1	
TT-120-16-37-REB2	802.6	7.56	0.94	430.5	1	
TT-120-16-38-REB2	793.8	5.87	0.74	427.6	1	
TT-120-16-39-REB2	768.2	3.95	0.51	428.3	2	
TT-120-16-40-REB3	652.0	7.16	1.10	426.0	3	Max(E)=848.5 MPa
TT-120-16-41-REB3	654.5	6.59	1.01	431.2	mixed	Min(E)=641.2 MPa
TT-120-16-42-REB3	641.2	6.56	1.02	439.4	mixed	Max(S)=7.16 MPa
TT-120-16-43-REB3	695.6	6.07	0.87	431.5	mixed	Min(S)=5.73 MPa
TT-120-16-44-REB3	680.3	6.47	0.95	428.1	1	Max(ε)=1.10 %
TT-120-16-45-REB3	783.4	7.13	0.91	435.3	2	Min(ε)=0.72 %
TT-120-16-46-REB3	784.0	6.69	0.85	429.0	2	
TT-120-16-47-REB3	799.4	5.73	0.72	426.3	3	
TT-120-16-48-REB3	801.6	5.97	0.74	431.6	2	
TT-120-16-49-REB3	848.5	6.73	0.79	439.0	2	
TT-120-16-50-REB3	800.4	7.10	0.89	425.7	2	
TT-120-16-51-REB3	815.3	6.99	0.86	424.0	1	
TT-120-16-52-REB3	842.7	6.79	0.81	433.6	2	
TT-120-16-53-RAB1	579.9	7.45	1.28	440.7	4	Max(E)=585.8 MPa
TT-120-16-54-RAB1	585.8	8.63	1.47	454.4	1	Min(E)=362.0 MPa
TT-120-16-55-RAB1	584.7	7.31	1.25	449.8	2	Max(S)=8.63 MPa
TT-120-16-56-RAB1	438.4	6.28	1.43	446.1	3	Min(S)=6.28 MPa
TT-120-16-57-RAB1	408.2	7.08	1.73	444.0	3	Max(ε)=1.95 %
TT-120-16-58-RAB1	362.0	7.05	1.95	441.6	3	Min(ε)=1.25 %
TT-120-16-59-RAB2	1214.7	8.84	0.73	577.2*	1	Max(E)=1214.7 MPa
TT-120-16-60-RAB2	740.7	8.82	1.19	433.6	1	Min(E)=663.5 MPa
TT-120-16-61-RAB2	759.4	7.90	1.04	424.2	1	Max(S)=8.99 MPa
TT-120-16-62-RAB2	694.5	8.21	1.18	424.8	1	Min(S)=6.84 MPa
TT-120-16-63-RAB2	663.5	8.99	1.35	425.0	1	Max(ε)=1.35 %
TT-120-16-64-RAB2	717.2	6.84	0.95	428.5	3	Min(ε)=0.73 %
TT-120-16-65-RAB3	666.0	7.82	1.17	434.5	3	Max(E)=666.0 MPa
TT-120-16-66-RAB3	517.1	7.43	1.44	441.0	3	Min(E)=501.5 MPa
TT-120-16-67-RAB3	547.2	8.29	1.51	434.9	1	Max(S)=9.03 MPa
TT-120-16-68-RAB3	501.5	9.03	1.80	438.2	1	Min(S)=7.43 MPa
TT-120-16-69-RAB3	542.0	7.45	1.37	460.2	1	Max(ε)=1.17 %
						Min(ε)=1.80 %

4.4 Statistics of mechanical properties and size effects

4.4.1 Statistics of effective elastic modulus

The statistics of the effective elastic modulus for the three specimen lengths, cut from the REBs and RABs, are given in Table 4.4. First, test results for specimens cut from the REBs are considered. It can be seen that the mean value for specimens of 8-mm length is considerably higher than those for 32-mm- and 120-mm-length specimens; however, the standard deviation (SD) is lower. Consequently, the coefficient of variation (COV) for the 8-mm-length specimens is also much lower. This is because the elastic moduli values of the 8-mm-length specimens mainly represent the scatter in the transverse elastic modulus along the longitudinal paths from which they were cut. This is also true for the mean value of the modulus for the 8-mm-length specimens from the REBs. However, in the case of the 32-mm- and 120-mm-length specimens, a wider range in the transverse direction is covered and therefore the variability of the transverse elastic modulus in the transverse direction can be appropriately investigated.

Table 4.4: Statistics of the transverse mechanical properties for specimens of different sizes.

Property	Length (mm)	Mean REB (MPa)	Mean RAB (MPa)	COV REB (%)	COV RAB (%)
Effective elastic modulus	8	787.0	574.7	14.65	35.24
	32	464.3	655.9	49.90	28.54
	120	513.8	581.8	44.06	20.53
Strength	8	9.41	9.71	8.18	10.88
	32	7.57	8.68	17.57	13.43
	120	5.63	7.79	19.01	10.49
Strain to failure	8	1.23	1.88	15.54	32.78
	32	2.16	1.43	55.26	30.21
	120	1.39	1.38	52.52	19.63

Considering the RABs, the mean value of the modulus slightly increases from 8-mm to 32-mm-length specimens and then decreases for 120-mm-length specimens, indicating that the mean value does not change significantly as size changes. On the other hand, the COV decreases consistently as specimen lengths increase.

4.4.2 Statistics of longitudinal tensile strength

The statistics of strength are also given in Table 4.4 for specimens cut from both the random and the regular boards. The mean strength decreases with increasing length in all cases.

Concerning the variability in the REBs, the COV of the 8-mm-length specimens is considerably lower than the other COVs. Similar to the case of the elastic modulus, this is because the COV of the 8-mm-length specimens from the REBs mainly represents the variability of the transverse tensile strength in the longitudinal direction. Considering the specimens of each length from the RABs, the COVs are similar, as shown in Table 4.4. However a sound conclusion cannot be drawn for the specimens cut from the REBs, since each specimen group (different lengths) comes from a different board and the COV is therefore increased as it includes the variability resulting from different boards.

According to the classical Weibull size effect law (CWSEL), the strength changes linearly with specimen size on the logarithmic scale. The slope of this line depends only on the shape factor of the corresponding Weibull distribution. In turn, this shape factor is only a function of COV. Therefore, using each three COVs from the RABs, the COVs of the strength data for specimens of 8-, 32- and 120-mm lengths were calculated and used to obtain an average value for the line slope. This slope, equal to -0.095, was used to fit a line to the experimental data, labeled as CWSEL in Fig. 4.15. The variability between the different boards is also shown in this figure as the mean values of strength obtained for each one of the RABs per specimen length is also indicated by solid symbols. This figure shows the experimental data on the logarithmic scale. It is seen that this line can well describe the size effect on the transverse strength of clear timber. The R-squared value for the fitting line is 0.972. This result is in contrast to the case of the longitudinal tensile strength, studied in Chapter 3.

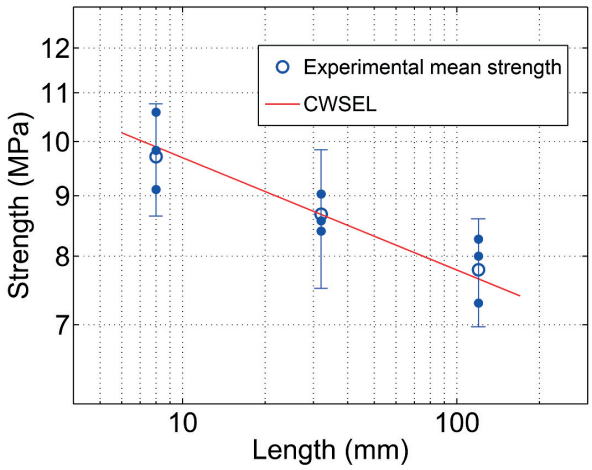

Fig. 4.15: Evaluation of accuracy of CWSEL against experimental data. Each hollow circle shows mean strength values for specimens of specific lengths cut from RABs. Solid circles show strength mean values in individual boards for specimens of specific lengths.

It should be noted that the above analysis is not carried out for specimens from the REBs since specimens of different sizes are cut from different boards and, as shown in Fig. 4.15, variability between boards can affect the resulting average strengths.

4.4.3 Statistics of strain to failure

The statistics of the strain to failure are given in Table 4.4, for the REBs and RABs. Both mean value and COV decrease with increasing length in the RABs, because the mean elastic modulus does not change significantly, but the strength significantly decreases with length. When examining the specimens from the REBs, however, the COV of the 8-mm-length specimens is considerably lower than those of specimens with different lengths, similar to the case of the elastic modulus and strength.

4.4.4 Statistical distributions for transverse modulus and strength

For stochastic simulations of timber structures/components, it is necessary to know the statistical distributions governing the mechanical properties. The three most commonly used statistical distributions for mechanical properties, i.e. normal, lognormal and Weibull, were fitted to the experimental data for the transverse modulus and strength. The results of the goodness-of-fit tests, Anderson-Darling (AD) and Kolmogorov-Smirnov (KS), at a significance level of 0.05 are given in Table 4.5. A 'zero' denotes that sampled data are taken from the corresponding distribution, while 'one' rejects the presumed distribution. KS test support the three statistical distributions for all the specimen lengths in REBs and RABs. However, the AD test rejects the statistical distributions in some cases.

Table 4.5: Results of goodness-of-fit tests for the transverse modulus and strength.

Property	REB/RAB	Specimen length (mm)	Normal		Lognormal		Weibull	
			AD	KS	AD	KS	AD	KS
Transverse elastic modulus	REB	8	1	0	0	0	1	0
		32	0	0	1	0	0	0
		120	1	0	1	0	1	0
	RAB	8	0	0	0	0	0	0
		32	1	0	1	0	1	0
		120	0	0	0	0	0	0
Transverse strength	REB	8	0	0	0	0	0	0
		32	1	0	1	0	1	0
		120	0	0	1	0	0	0
	RAB	8	0	0	0	0	0	0
		32	0	0	0	0	0	0
		120	0	0	0	0	0	0

4.5 Specimen failures

Here the term 'grain angle' is defined as the angle between latewood and the axis perpendicular to the load direction. Four types of fracture were observed in the specimens, as shown in Fig. 4.16 where characteristic failure photos of full cross sections are presented: 1) Earlywood 2) Earlywood-border 3) Growth ring border 4) Crossing growth rings. In the first type, failure occurs mostly in the radial direction of the earlywood and the failure plane is approximately perpendicular to the loading direction. The second failure type occurs in both earlywood and growth ring borders. The failure plane is often not perpendicular to the loading direction. The failure path is mostly along radial bonds. In the third type, failure occurs in the ring border between earlywood and latewood, and the failure plane is not perpendicular to the loading direction. In the fourth type, the failure plane is approximately perpendicular to the loading direction and the fracture path crosses the ring border.

Fig. 4.16: Different failure types observed in specimens: a) Earlywood failure b) Earlywood-border failure c) Growth ring border failure d) Crossing growth ring failure. Vertical dimension is 4mm (specimen width). Load is applied in horizontal direction.

The grain angle increases from the first type to the fourth, and the mean strength decreases accordingly, since timber is stronger in the radial direction than in the tangential direction. The statistics of strength of all specimens from the REBs and the RABs, grouped according to their failure types, are given in Table 4.6.

Table 4.6: Statistics of strength for all specimens when grouped according to failure types and statistics of local elastic modulus at failure zone.

Failure type	Number of specimens	Mean strength (MPa)	Mean local elastic modulus (MPa)
1	134	8.85±1.26	634.1±246.1
2	42	7.42±1.58	614.1±284.9
3	32	6.34±1.71	546.2±308.6
4	15	5.50±1.77	179.0±119.0

In order to investigate whether or not the above classification also implies a significant difference between the mean strengths of the four groups, an analysis of variance (ANOVA), at a significance level of 5%, was performed. The null hypothesis states that samples in different data sets are taken from the same population. In this procedure, the variability of the means of data sets around the grand mean (between-set), which is the mean of all the raw data, is compared to the variability of the raw data around their respective means (within-set). By dividing the "between-set" variability by the "within-set" variability, an F-value is obtained which, along with the number of data sets and sample sizes, can be used for the estimation of the p-value from the F-distribution. The lower the p-value, the lower the probability that the raw data in the data sets are taken from the same population. Information regarding the calculation of the p-value is given in [18, 19]. A p-value of 1.11e-16, which is far less than 0.05, was obtained for the examined pool of data sets, suggesting that one or more data sets were significantly different from the others. To identify the sets with significantly different mean values, the Scheffe's test [20] was used. The results of this test are given in Table 4.7. Any comparison whose associated p-value is less than 0.05 indicates a significant difference between the related data set mean values. All the estimated p-values, except the p-value of the pair 3 and 4, which is 3.21e-1, are less than 0.05. All comparisons, except that between the third and the fourth groups, show that specimen groups with different failure types have statistically significantly different mean strengths. Although the difference between the mean strength values of the third and fourth groups is similar to the differences between the first and second, or second and third groups, the limited fourth group sample size may have masked the significant statistical difference between these groups.

Table 4.7: Results of Scheffe's test for two-by-two comparisons between failure types.

Pair	1 vs 2	1 vs 3	1 vs 4	2 vs 3	2 vs 4	3 vs 4
p-value	1.51e-6	1.13e-14	8.67e-14	1.71e-2	2.56e-4	3.21e-1

4.6 Correlations

The correlations between the local elastic modulus and strength, the effective modulus and density and between the strength and density were examined. Fig. 4.17 shows the tensile strength of each specimen vs the corresponding local elastic modulus measured at the failure zone. The data from each of the specimen groups are indicated by a different symbol. Also, the centroid of each group is indicated by a larger symbol of the same type. Since here the correlation between local properties is considered, all specimen strengths and their corresponding local modulus can be used for estimation of a single correlation coefficient. It can be seen that both mean local elastic moduli and mean strengths decrease as length increases.

The linear correlation coefficient was found to be 0.610. For example, when a value is randomly assigned to the local elastic modulus or strength at a material point, the uncertainty of the other property value at that material point is decreased due to this correlation between them. If a low value were randomly assigned to the first parameter, due to the correlation between them, it would be more probable that a low value would also be assigned to the second parameter at that material point. From a mechanical point of view, lower elastic moduli are associated with higher grain angles, because timber is stiffer in the radial direction than in the tangential direction [8]. This can also be seen in Table 4.5 in which the mean values of the local moduli at the failure zones, corresponding to specimen sets with different failure types, are given. The mean value decreases from the first set to the fourth set. The decrease from the third set to the fourth set is more obvious, but this can be attributed to the low sample size of the fourth set. Similarly, as the grain angle increases, the failure type changes and strength decreases. This explains the reason for the correlation between the modulus and the strength. For example, in the case of the first failure type, "Earlywood", the grain angle has the lowest values and the strength has the highest of all examined cases.

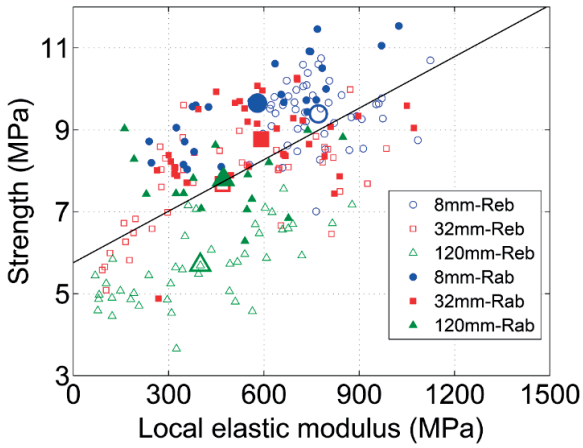

Fig. 4.17: Correlation between local elastic modulus and tensile transverse strength.

In Fig. 4.18, the scatter plot of the effective elastic modulus of specimens versus their densities is given. There is no significant correlation in this case. One reason for this is that the variability of the effective elastic modulus is very high, mainly due to the change in the grain angle, much larger than that due to the density. Therefore, the variability in the effective elastic modulus caused by density variability cannot be easily quantified. A detailed study measuring the local densities could possibly provide a more comprehensive result. These results are compatible with observations revealed in [13] where no consistent correlation between density and transverse elastic parameters was reported.

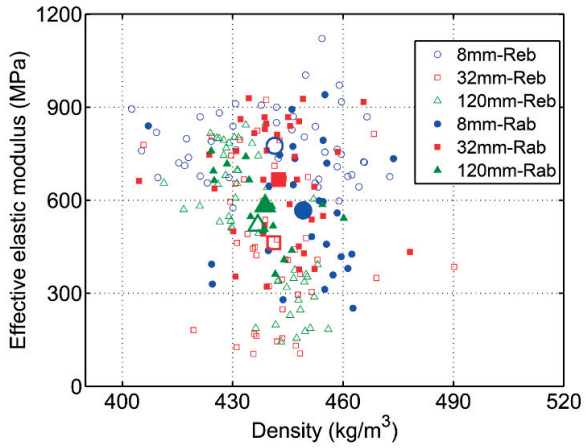

Fig. 4.18: Correlation between density and effective elastic modulus.

The scatter plot of the specimens' strengths versus their densities is given in Fig. 4.19 showing a relatively weak correlation in this case. The correlation coefficient is 0.21, when all the data points in the figure are taken into account. The reason for the correlation being higher compared to the previous case is that the variability of the strength is much less than the variability of the effective elastic modulus, and therefore the effect of the density change on the strength is more obvious, although the change in the grain angle has a still larger effect.

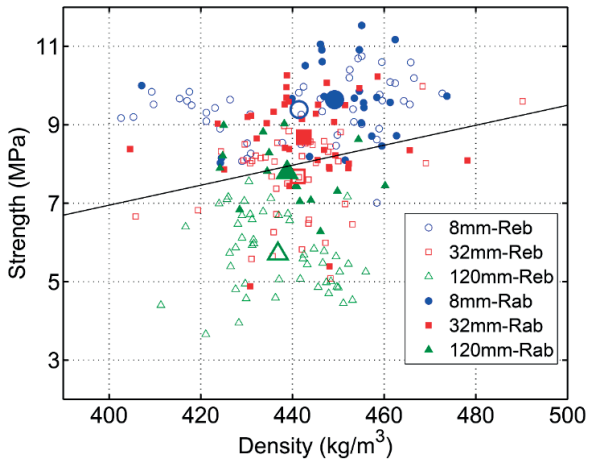

Fig. 4.19: Correlation between density and tensile transverse strength.

4.7 Conclusions

In this chapter, an experimental campaign consisted of transverse tensile quasi-static experiments on specimens of different lengths made of spruce wood was conducted. A total number of 226 valid experimental results were obtained. The cross-sectional area was the same for all specimens and reasonably small, so as to exclude the effect of the variability of the

properties in the cross section. The nominal length of specimens varied from 8 mm to 120 mm in order to investigate the size effect on the mechanical properties. The following main conclusions were drawn:

- A cutting plan with regularly positioned specimens can lead to underestimation of the randomness in the mechanical properties, as especially shown in the case of the 8-mm-length specimens from the REBs.
- A significant variability was observed in the effective transverse elastic modulus of clear spruce wood. This variability decreases as length increases.
- Four types of failure were observed in the specimens. The strengths were higher when the grain angle was lower.
- The CWSEL is sufficiently accurate for modeling the size effect on the transverse tensile strength of clear timber. This is in contrast to the case of longitudinal tensile strength, studied in Chapter 3.
- A significant correlation was found between the local elastic modulus and the strength. The correlation between the specimen density and the strength was less significant, and the correlation between the specimen density and effective elastic modulus was negligible.

With recent progress in computational power, stochastic analyses of timber structures are receiving more attention. The results presented in this chapter can be used for taking into account the statistical variability of the transverse mechanical properties and their correlation, especially when local mechanical properties are concerned. This is of paramount importance in applications such as adhesively-bonded timber joints, where the transverse mechanical properties play a critical role in determining the load-bearing capacity of the structure.

4.8 References

[1] Barrett, J.D., 1974. Effect of size on tension perpendicular-to-grain strength of Douglas-fir. Wood and Fiber 6, 126-143.

[2] Dinwoodie, J.M., 2000. Timber: Its nature and behaviour. Taylor & Francis Group.

[3] Tannert, T., Lam, F., Vallée, T., 2010. Strength prediction for rounded dovetail connections considering size effects. Journal of Engineering Mechanics 136, 358-366.

[4] Tannert, T., Vallée, T., Hehl, S., 2012. Probabilistic strength prediction of adhesively bonded timber joints. Wood Science and Technology 46, 503-513.

[5] Barrett, J.D., Foschi, R.O., Fox, S.P., 1975. Perpendicular-to-grain strength of Douglas-Fir. Canadian Journal of Civil Engineering 2, 50-57.

[6] Fox, S.P., 1974. Strength and stiffness of laminated Douglas-fir blocks in perpendicular-to-glueline tension. Wood and Fiber 6, 156-163.

[7] Norlin, L.P., Lam, F., 1998. Fatigue behaviour and size effects perpendicular to the grain of laminated Douglas fir veneer. Materials and structures 32, 298-303.
[8] Pedersen, M.U., Clorius, C.O., Damkilde, L., Hoffmeyer P., 2003. A simple size effect model for tension perpendicular to the grain. Wood Science and Technology 37, 125-140.
[9] Astrup, T., Clorius, C.O., Damkilde, L., Hoffmeyer P., 2007. Size effect of glulam beams in tension perpendicular to grain. Wood Science and Technology 41, 361-372.
[10] Weibull, W., 1939. A statistical theory of strength of materials. In: Proceedings of the Royal Swedish Institute. Research No. 151, Stockholm, Sweden.
[11] Wang, Y.T., Lam, F., 1998. Computational modeling of material failure for parallel-aligned strand based wood composites. Computational Materials Science 11, 157-165.
[12] Xavier, J., Avril, S., Pierron, F., Morais, J., 2009. Variation of transverse and shear stiffness properties of wood in a tree. Composites Part A: Applied Science and Manufacturing 40, 1953-1960.
[13] Xavier, J., 2007. Characterisation of the wood stiffness variability within the stem by the virtual fields methods: Application to P. Pinaster in the LR plane. PhD thesis, Arts et Métiers ParisTech, Châlons-en-Champagne, France.
[14] Pereira, J., Xavier J., Morais J., Lousada J., 2014. Assessing wood quality by spatial variation of elastic properties within the stem: Case study of Pinus pinaster in the transverse plane. Canadian Journal of Forest Research 44, 107-117.
[15] EN-408, 2012. Timber structures – Structural timber and glued laminated timber – Determination of some physical and mechanical properties.
[16] Forest Product Laboratory, 1999. Wood handbook: Wood as an engineering material, USDA, Madison, Wis, USA.
[17] Tannert, T., Vallée, T., Hehl, S., 2012. Experimental and numerical investigations on adhesively bonded timber joints. Wood Science and Technology 46, 579-590.
[18] Walpole, R.E., Myers, R.H., S.L. Myers, Ye, K., 2012. Probability and statistics for engineers and scientists. Pearson Education, Inc.
[19] Devore, L.J., Berk, K.N, 2012, Modern mathematical statistics with applications. Springer.
[20] Lawal, B., 2014. Applied statistical methods in agriculture, health and life Sciences. Springer.

5 Spatial variability in transverse mechanical properties of clear timber

5.1 Introduction

Timber as a natural composite is highly variable in terms of its mechanical properties [1]. Some of the influencing factors are the age of the tree, the original position of timber within the tree, the structural complexity and imperfections, the load history etc. This random and spatial variability is also observed in other materials such as synthetic composites and is usually called the "random spatial variability" [2-3].

The transverse tensile strength of clear timber is low compared to the longitudinal tensile strength [4]. Therefore, consideration of the transverse strength can be important even in a stress field with small transverse stress components. Moreover, in some applications such as adhesively bonded timber joints, normally made up of clear wood, the transverse stress is very important concerning the failure [5,6], and the contribution of the transverse strength in the determination of the load-bearing capacity of the structure is more significant than the longitudinal strength.

The statistical variability in the mechanical properties of timber has been examined in many works. In the case of transverse properties, a range of 10% to 30% for the coefficient of variation of the transverse elastic modulus and the tensile transverse strength has been reported [5-8]. On the other hand, a few experimental works have been devoted to the characterization of the spatial variability in the transverse mechanical properties of timber and timber products. Regarding the clear timber, Xavier et al. [9] used the unnotched Iosipescu test for the study of the radial variability of stiffness parameters of maritime pine wood. Pereira et al. [10] conducted tensile tests on cubic specimens cut in different radial positions and heights of Pinus pinaster tree. The results show that the radial transverse modulus and the shear transverse modulus decrease from tree center outwards. Also, Brandner and Schickhofer [7] used EN standard-type specimen (cubic bulk material) to investigate the spatial correlation in the transverse tensile strength and elastic modulus along the tree stem.

The mesostructure of clear wood is mainly characterized by earlywood-latewood arrangements. Concerning the transverse plane, the mechanical properties are superior in the radial direction

[11]. Therefore, when the latewoods are locally perpendicular to the nominal axis of a specimen, which is cut in the transverse plane, the local mechanical properties are higher.

The characterization of spatial variability in the transverse local strength and local elastic modulus at mesoscale (a few millimeters) has not been studied in detail in the literature. Consequently, the spatial variability is frequently neglected in the probabilistic simulations of timber structures [12-14]. The knowledge of the random spatial variability in elastic parameters can lead to predicting more accurate stress fields within the material. This along with data for the spatial variability of strength parameters can improve structural designs with a required reliability levels. Also, in this chapter, attempt has been made to find a reasonable qualitative correlation between timber mesostructural patterns and local variations of the transverse elastic modulus. This can be an aid for visually evaluating the local elastic modulus.

In this chapter, the RSV in the transverse mechanical properties of clear timber is investigated based on the results of the mechanical tests explained in the previous chapter. The spatial variability in the transverse elastic modulus, transverse strength and transverse strain to failure in both longitudinal and transverse directions was characterized. Also, the effect of the mesostructure of the clear timber on the local elastic modulus was studied. Finally, the effect of some defects on the timber properties were examined.

5.2 Clear timber mesostructure

The mesostructure of the clear spruce wood is mainly characterized by the earlywood-latewood patterns. The main local mesostructural characteristics are shown in Fig. 5.1. The darker parts of the growth rings are latewood that have superior mechanical properties, hereafter called ‘strips of latewood’. Although the boards were cut in the radial-tangential, in terms of the common terminology of timber production, not all the specimens were exactly in the radial direction due to the positioning of specimens along each board’s thicknesses. This along with the natural variability of the timber structure cause the variability in the timber local mesostructure. Figure 5.1a illustrates the change in the angle between the tangential direction and the axis perpendicular to the nominal axis of the specimen. The local mechanical properties are higher when the angle is closer to 0°. It is seen in Fig. 5.1b that in some growth rings, the latewood thickness is higher than the others which also influences the local mechanical properties. Finally, Fig. 5.1c shows the change in the growth ring thickness. These local microstructural changes are the main origin of random spatial variability in the mechanical properties.

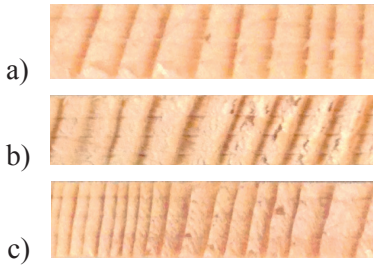

Fig. 5.1: Mesostructural characteristics of spruce wood in the transverse plane: a) Change in the angle between the tangential direction and the transverse axis of the specimen b) Latewood thickness change c) Growth ring thickness change.

5.3 Spatial variability in the mechanical properties

5.3.1 Transverse elastic modulus

The spatial variability of the transverse elastic modulus along the transverse and the longitudinal axes of the boards are examined here. Specimens of 120 mm length in REBs are best suited for this purpose. Fig. 5.2 shows the variability of the modulus in the transverse direction in the three used REBs. The average variability of the modulus in these boards has also been provided in Fig. 5.3 for a better comparison between boards. The three boards are different in terms of local elastic modulus variations. On average, the third board is stiffer than the second board and the second board is stiffer than the first board. In most specimens cut from these boards, the local modulus value gradually increases from the one side, reaches a maximum value somewhere in the middle, and then decreases. Also, the scatter in the results is more significant in the second board compared to the other two boards.

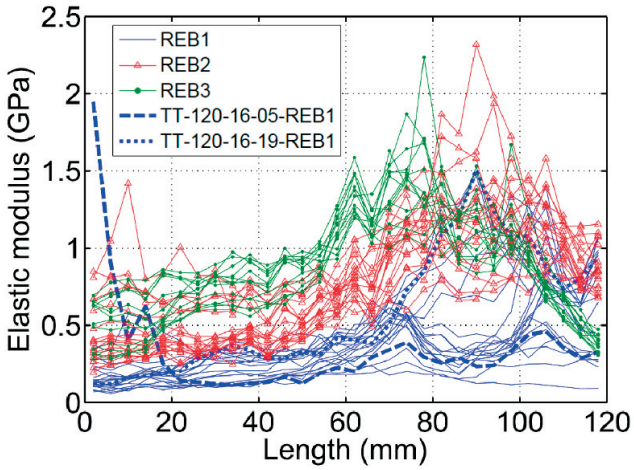

Fig. 5.2: Spatial variability of the transverse elastic modulus in the transverse direction for specimens of 120 mm length in REBs.

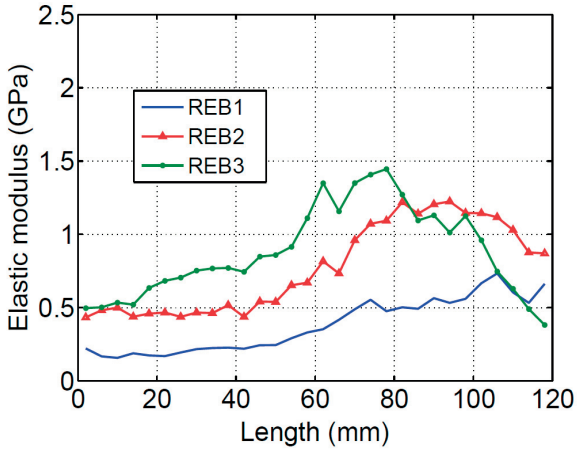

Fig. 5.3: Average Spatial variability of the transverse elastic modulus in the transverse direction in REBs for 120 mm specimens.

There are major changes in the trend of the modulus variability in the first board in a few specimens compared to the others, such as the highlighted dashed and dotted curves (TT-120-16-05-REB1 and TT-120-16-19-REB1) in Fig. 5.2. These are discussed in Section 5.4.2 with regard to the mesostructure of the wood.

Although the statistical aspects of the results of the current experimental campaign have been studied in the previous chapter, here a discussion is made on the contributions of the variability of the local elastic modulus due to changing the spatial position within individual specimens (within-specimen variability or WSV) and the variability of the local elastic modulus due to switching between specimens (between-specimen variability or BSV) to the total variability of the local elastic modulus. Results of specimens of 120 mm in REBs are used again, as they are more suitable for examining the spatial variability of the local elastic modulus. In Table 5.1, the COVs are given. It is seen that the contribution of the WSV is higher than that of the BSV. Also, the effective moduli of specimens of 120 mm in REBs and the corresponding COVs have been shown in Figs. 5.4 and 5.5, respectively. In Fig. 5.4, it is seen that the BSV becomes more influential when specimens from different boards are considered together, compared to the case of individual boards. The sudden changes in the effective elastic moduli between boards is obvious. The three boards have also different behaviors in terms of the variation of the COVs of local moduli. The odd COV of the specimen 5 is due to the surprisingly high value of the local elastic modulus at the first few segments of this specimen, as mentioned above. The REB2 has the highest variation in COV of its specimens, among the three boards, from 15.6 % to 73.3 %.

Table 5.1: Statistics of local and effective elastic moduli of 120mm-specimens cut from REBs.

	Data set size	COV (%)
Local modulus (total variability)	1560	60.65
Local modulus of individual specimens (WSV)	30 (each specimen)	48.02 (average)
Effective modulus (BSV)	52	44.06

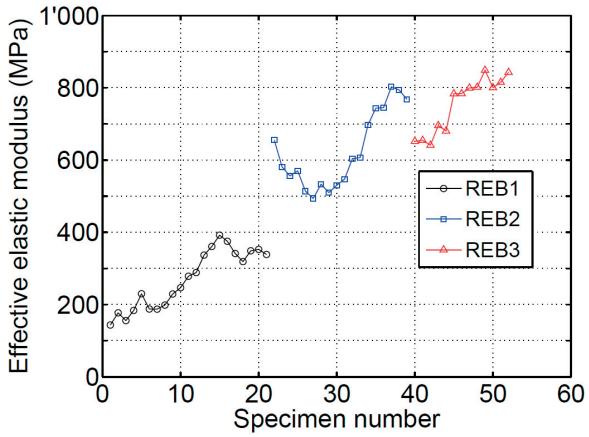

Fig. 5.4: Variation of the effective elastic modulus in the REBs for 120 mm specimens.

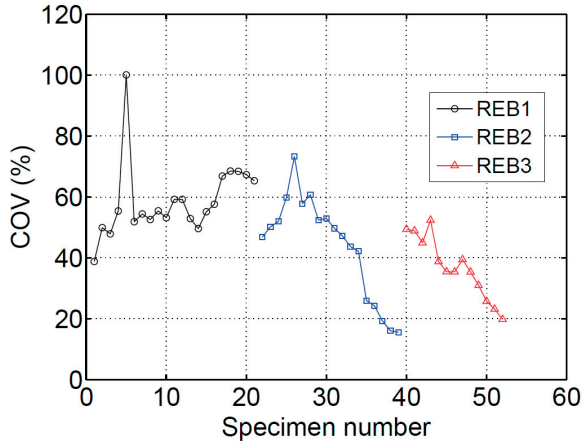

Fig. 5.5: Variation of the COV in the REBs for 120 mm specimens.

Variability of the transverse modulus in the longitudinal direction in the three REBs is plotted in Figs. 5.6-5.8. Four curves have been highlighted in each figure in order to show how the longitudinal variability of the transverse modulus differs from lower paths to upper paths. The average longitudinal variations in the three boards have been provided in Fig. 5.9. On average, the longitudinal variability is higher in the first board.

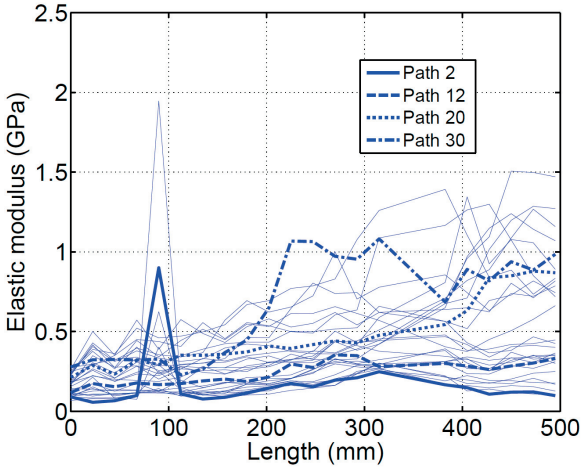

Fig. 5.6: Spatial variability of the transverse elastic modulus in the longitudinal direction in REB1 used for 120 mm specimens.

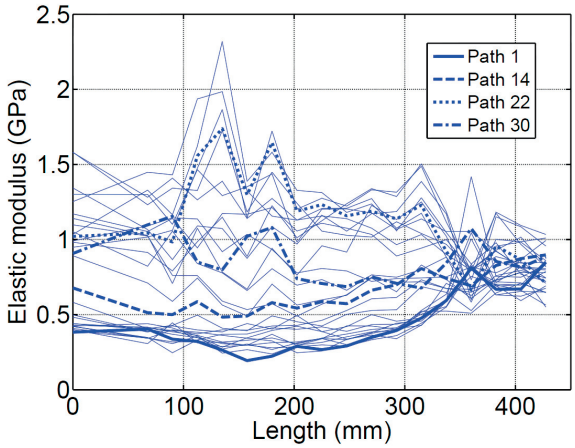

Fig. 5.7: Spatial variability of the transverse elastic modulus in the longitudinal direction in REB2 used for 120 mm specimens.

As a general trend in REB1 (Fig. 5.6), the upper paths have higher values of the modulus compared to the lower paths. The paths are closer to each other in the left half length (lower scatter) of the board compared to the right half length (higher scatter). The unusual increase in the value of the transverse modulus, in the first few path, at the longitudinal position of 90 mm, is explained in Section 5.4.2. Excluding this unusual variation at 90 mm position, the variability within individual paths ranges from 183.4 MPa to 1340.5 MPa, , with a mean value of 581.3 MPa. The corresponding values for the transverse paths in this board are 208.9, 1372.8 and 869.0 MPa. The mean variability in the longitudinal direction is considerably lower than in the transverse direction. This becomes even more critical when noting that the length of the transverse path is only 24.2% (120/495) of the length of the longitudinal path.

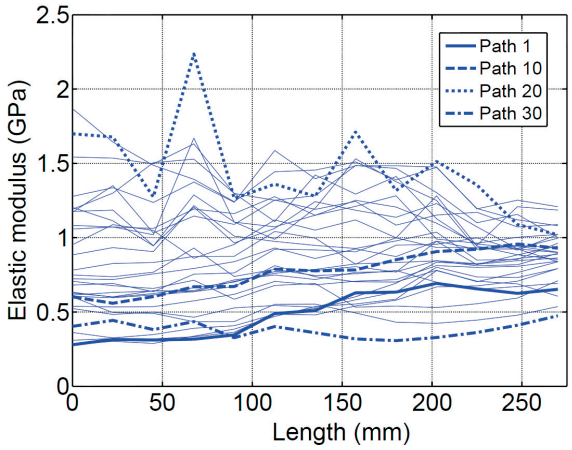

Fig. 5.8: Spatial variability of the transverse elastic modulus in the longitudinal direction in REB3 used for 120 mm specimens.

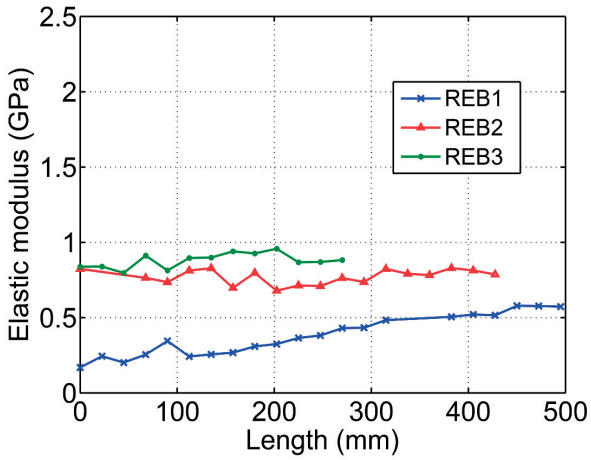

Fig. 5.9: Average spatial variability of the transverse elastic modulus in the longitudinal direction in three REBs used for 120 mm specimens.

In the second board, the upper paths have again higher values. The difference between paths after the position of 320 mm from the left side is considerably lower than before that position. The minimum and maximum variability in the individual paths are 394.1 MPa and 1650.8 MPa, with a mean value of 686.4 MPa. These values for transverse paths are 484.0 MPa, 2075.5 MPa and 1064.5 MPa, respectively. Again, the mean variability in the transverse direction is higher than in the longitudinal direction. In this case, the longitudinal path is longer by a factor of 3.56.

In the third board, the longitudinal variability of the transverse elastic modulus is more uniformly distributed, although the scatter is slightly reduced from left to right. Generally, middle paths are stiffer. In this case, the minimum, the maximum and the mean variability in individual paths are 167.0 MPa, 1216.1 MPa and 421.9 MPa, respectively, which are

considerably lower than the corresponding values for the transverse paths, namely 733.6 MPa, 1918.5 MPa and 1205.4 MPa. Similar to previous cases, the mean variability in the transverse direction is significantly higher than in the longitudinal direction, although the transverse distance is only 44.44% of the longitudinal distance.

The spatial variation of the transverse elastic modulus in the three boards are shown in Fig. 5.10 as 2D contours. The same range for the colorbar has been used for all contours. In order to compare the degree of the variability in the boards, three coefficients are defined for each board. The first is the ratio between the mean variability in the transverse direction and the transverse distance, the second is the ratio between the mean variability in the longitudinal direction and the longitudinal distance and the third is the ratio of these two coefficients, designated as anisotropy ratio, in the sense of different levels of variability in different directions. These values are provided in Table 5.2. It can be seen that the longitudinal variability coefficients are much lower than the transverse variability coefficient. The longitudinal variability coefficient is higher in the second board followed by the third board. However, the transverse variability coefficient is higher in the third board followed by the second board. Compared to these two coefficients, the difference between the anisotropy ratios of the boards is less significant, with the third board being the most anisotropic followed by the first board.

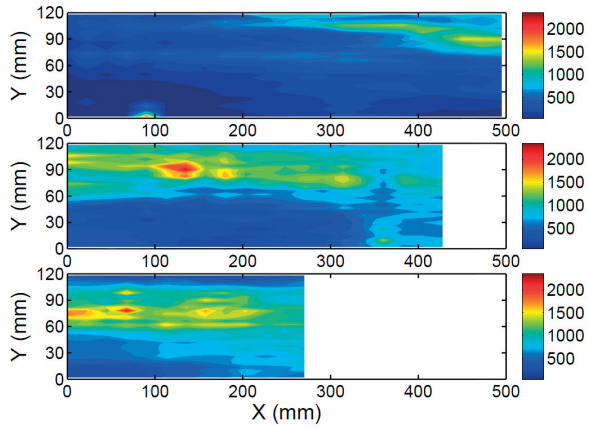

Fig. 5.10: 2D contours of the spatial variability of the transverse elastic modulus in the three board.

Table 5.2: Longitudinal variability coefficient, transverse variability coefficient and anisotropy ratio for the three REBs with 120 mm-specimens.

Board number	Longitudinal variability coefficient (MPa/mm)	Transverse variability coefficient (MPa/mm)	Anisotropy ratio
1	1.17	7.24	6.19
2	1.61	8.87	5.51
3	1.56	10.0	6.41

5.3.2 Transverse strength

The variability of the transverse tensile strength in the longitudinal direction is shown in Figs. 5.11a and b. These are based on the results of the 8 mm-specimens cut from REBs, since the failures for these specimens occurred approximately at the same transverse positions for specimens at the same row. The distance between the two rows was 75 mm in each board. It can be seen that variability of the transverse strength in the longitudinal direction is far less significant than that of the transverse elastic modulus. The difference between minimum and maximum values along each path and their longitudinal variability coefficients are given in Table 5.3. The definition of these coefficients is similar to that of the elastic modulus. The longitudinal variability coefficients of the two rows in each board are very different.

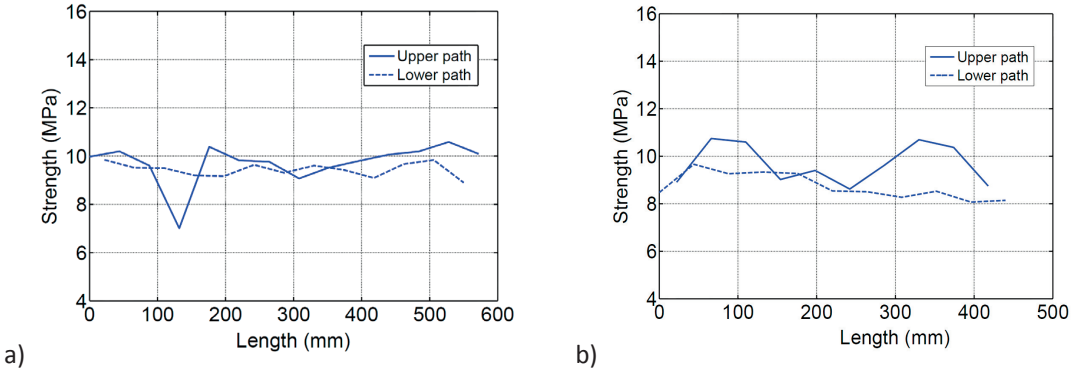

Fig. 5.11: Spatial variability of the transverse strength in the longitudinal direction from results of the 8 mm-specimens cut from REBs.

Table 5.3: Transverse Strength variability in the longitudinal direction.

Board	Path	Maximum difference in the path (MPa)	Longitudinal variability coefficient (MPa/mm)
1	Upper	3.58	6.26e-3
	Lower	0.95	1.80e-3
2	Upper	2.13	5.38e-3
	Lower	0.40	9.09e-4

In order to examine the variability of the transverse strength in the transverse direction, the test results from RAB1 and RAB2 were used. In these boards, specimen failures at different transverse positions can be found, however, with different longitudinal positions. The strength values at different transverse positions in a limited longitudinal range would give an idea of the

variability of the transverse strength in the transverse direction, approximately. Two such transverse paths for the transverse strength are shown in Fig. 5.12. The longitudinal range is 276 mm for the path in the first board and 253 mm for the path in the third board. Maximum variabilities and transverse variability coefficients for these paths are given in Table 5.4. Compared to the longitudinal variability coefficient, transverse variability coefficients are higher.

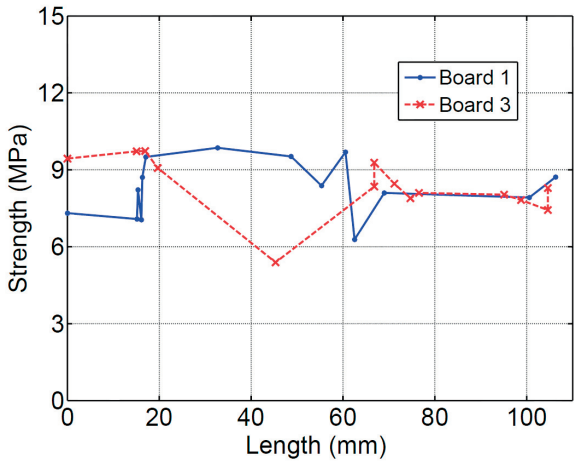

Fig. 5.12: Spatial variability of the transverse strength in the transverse direction in first and third random boards.

Table 5.4: Transverse Strength variability in the transverse direction.

Board	Maximum difference in the path (MPa)	Transverse variability coefficient (MPa/mm)
1	3.58	1.42e-2
3	4.34	1.57e-2

5.3.3 Transverse strain to failure

Longitudinal variability of the transverse strain to failure is shown in Figs. 5.13a and b. Once again, the results from 8 mm specimens are used for this purpose. Maximum variabilities and longitudinal variability coefficients are given in Table 5.5. The coefficients are closer to each other compared to the cases of the strength and the modulus.

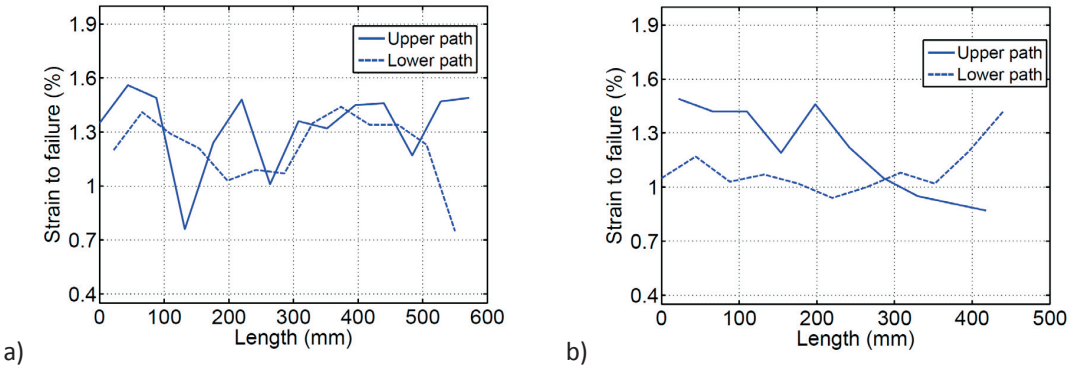

Fig. 5.13: Spatial variability of the transverse strain to failure in the longitudinal direction from results of the 8 mm-specimens cut from REB1 and REB2.

Table 5.5: Strain to failure variability in the longitudinal direction.

Board	Path	Maximum difference in the path (%)	Longitudinal variability coefficient (%/mm)
1	Upper	0.80	1.40e-3
	Lower	0.69	1.25e-3
2	Upper	0.62	1.48e-3
	Lower	0.48	1.09e-3

The transverse variability of the transverse strain to failure is shown in Fig. 5.14. Transverse variability coefficients have also been provided in Table 5.6. The transverse variability is much more significant the longitudinal variability.

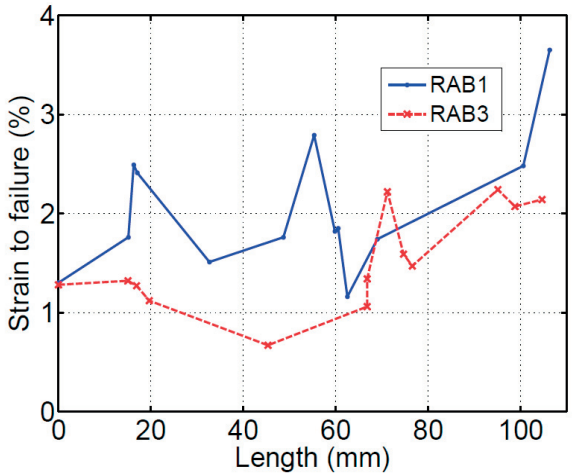

Fig. 5.14: Spatial variability of the transverse strength in the transverse direction in first and third random boards.

Table 5.6: Transverse Strength variability in the transverse direction.

Board	Maximum difference in the path (%)	Transverse variability coefficient (%/mm)
1	2.49	2.34e-2
3	1.57	1.50e-2

5.3.4 Failure paths

Failure paths for specimens of 120 mm length in REBs are shown in Fig. 5.15. These paths show how the position of the weakest cross-section changes from one specimen to the next. The dotted lines in Fig 5.15a indicate the alternative failure path. This is because in a few specimens of 120 mm length, the failure happened at two different cross-section at the same time, which indicates close strengths values at those sections. The failure position in each board changes in a rather random manner, except for the middle part of the RAB1.

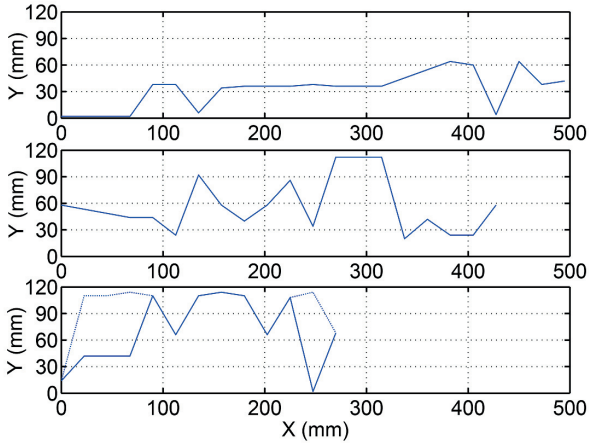

Fig. 5.15: Failure paths in REB1 (a), REB2 (b) and REB3 (c) for specimens of 120 mm length.

5.4 Effect of timber mesostructure on mechanical properties

5.4.1 Local elastic modulus

Typical examples of the correspondence between the local elastic modulus and the local mesostructure of spruce wood are given in Fig. 5.16, considering three specimens of 120mm length. In specimen the TT-120-16-11-REB1 starting from the left, the angle between the tangential direction and the transverse axis of the specimen decreases up to 70 mm of the length. This is associated by a gradual increase in the local elastic modulus. The angle increases from

70 mm to 95 mm and after that decreases again, causing the local modulus to decrease and then increase, as a general trend. The maximum value happened to be at end of the specimen, where the angle between the tangential direction and the transverse axis of the specimen has its lowest value. There is also a localized decrease in the value of the elastic modulus in the part of the specimen between 110 mm and 115 mm which is attributed to a decrease in the thickness of the latewood strips in this zone.

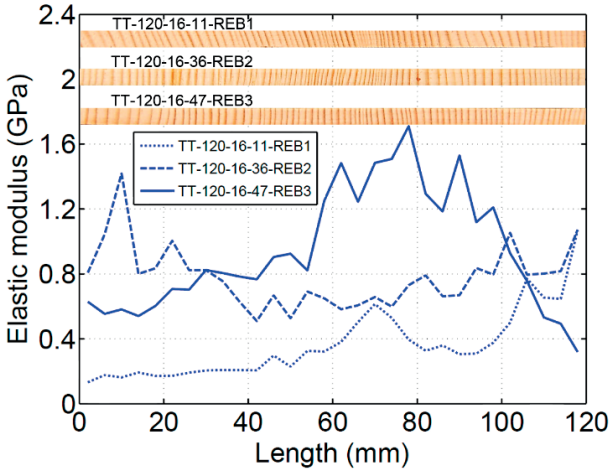

Fig. 5.16: Correspondence between mesostructure of spruce and local transverse elastic modulus.

In specimen the TT-120-16-36-REB2, over the first 10 mm of the specimen length, there is a decrease in the angle between the tangential direction and the transverse axis of the specimen, then from 10 mm to about 60 mm the angle increases and after that the angle decreases. Correspondingly, the value of the elastic modulus first increases, then decreases and finally increases again, as a general trend. The effect of the angle between the tangential direction and the transverse axis of the specimen on the local elastic modulus is even clear at the last 20 mm of the specimen length. In this segment of the specimen, the angle first increases a little and then decreases a little and, accordingly, there is a localized minimum in the value of the local elastic modulus in the middle of this segment. Also, a local maximum for the local modulus has happened in about 80 mm from the left end of the specimen. The angle between the tangential direction and the transverse axis of the specimen has a local minimum in this position of the specimen length.

The local elastic modulus in specimen TT-120-16-47-REB3 has generally higher values compared the other two discussed specimens. The main reason is that, in this specimen, the angle between the tangential direction and the transverse axis of the specimen has generally lower values. Only, in the first 30 mm and last 20 mm of the specimen length where the angle

has higher values, the value of the modulus of this specimen is less than those of the other specimens. Also, in this specimen, latewood strips are thicker.

The presence of higher volume fractions of latewood tends to increase the value of the local elastic modulus. This can either happen by presence of a higher number of latewood strips or thicker latewood strips. For example, in both specimens TT-120-16-11-REB1 and TT-120-16-47-REB3 in the segment from 60 mm to 80 mm the number of latewood strips are higher than in the rest of segments in the corresponding specimens. Consequently, the transverse elastic modulus has a local peak in those segments.

5.4.2 Effects of defects

Although this chapter is focused on the RSV of the clear timber mechanical properties, a few cases of the effects of the structural imperfections on the properties are examined in this section. Figure 5.17a and b show the initial part of specimen TT-120-16-05-REB1 where the first four 4 mm-segments have been affected by the presence of a knot. The curve showing the spatial variability of the local elastic modulus in this specimen has been highlighted as a dashed line in Fig. 5.2. It can be seen that the first part of this curve is obviously different from those of the other specimens in the first board. The value of the local modulus at the first segment is 1946.4 MPa in the specimen, but the maximum value at this transverse position for other specimens in the board is 300.5 MPa. The effect of this change of behavior is also obvious in the first few longitudinal paths shown in Fig. 5.4. Also, there was a crack near the first black dot; however, the failure occurred somewhere in the middle of the specimen. This indicates the higher strength values in the area affected by the knot.

Fig. 5.17: A part of the specimen TT-120-16-05-REB1. a) Front view b) Top view.

The second case is related to the highlighted dotted line in Fig. 5.2. This curve, which belongs to specimen 19, and a few other curves have obviously different trends compared to the rest of

the specimens in the board, when the range between 70 mm to 120 mm is considered. This is because of the presence of a small knot in the board between the specimens 15 and 16, which changed the mesostructure of the specimens 16 to 21 at that range, compared to specimens with a lower number. The mesostructure of the TT-120-16-14-REB1, TT-120-16-15-REB1 and TT-120-16-16-REB1 are compared with each other in Fig. 5.18. The difference in the mesostructure of the specimen TT-120-16-16-REB1 and the two other specimens, between 70 mm and 120 mm, is easily noticed. The angle between the tangential direction and the transverse axis of the specimen is lower in the specimen 16, hence increasing the local elastic modulus in that range.

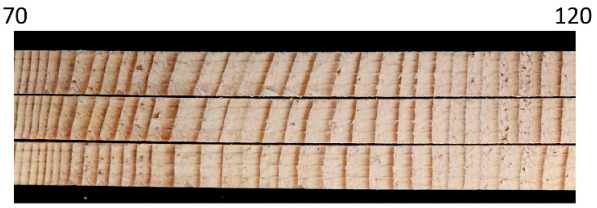

Fig. 5.18: Mesostructure of specimens TT-120-16-14-REB1 (top), TT-120-16-15-REB1 (middle) and TT-120-16-16-REB1 (bottom).

In Fig. 5.19, specimen TT-120-16-59-REB2 is shown which has several knots along its length. The effective elastic modulus and the density of this specimen were 1214.7 MPa and 577.2 kg/m3 which were considerably higher than average values of the other five specimens of 120 mm length in the same board, i.e. 715.1 MPa and 427.2 kg/m3. These values were not used in the statistical analyses of Chapter 3.

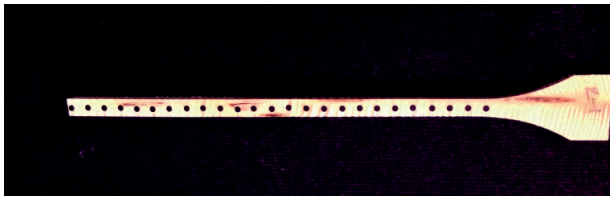

Fig. 5.19: Specimen TT-120-16-59-RAB2.

A specimen with a resin check (TT-032-16-02-REB1) is shown in Fig. 5.20, after testing. The strength of this specimen was excluded from statistical analyses. The cross section of this specimen in the position of the check has been also provided. The strength of this specimen was very low, 2.48 MPa, compared to the average of the strengths of the two neighboring specimens, 8.89 MPa. Therefore, the crack caused by the resin check reduced the strength by approximately 72.1%. This specimen was not considered in the analyses of Chapter 3.

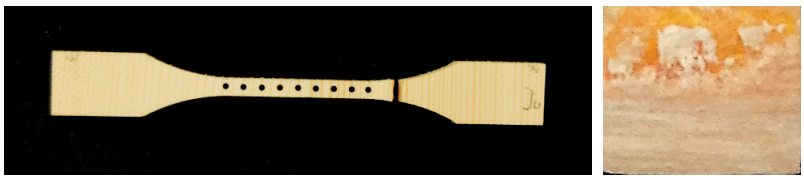

Fig. 5.20: Specimen TT-032-16-02-REB1 with a resin check.

5.5 Conclusions

The spatial variability in the mechanical properties of clear timber was studied in this chapter. The following main conclusions were drawn:

- A highly significant spatial variability was observed in the transverse tensile elastic modulus of clear spruce wood. A difference of more than 1000% for the local elastic modulus was observed within some specimens.
- Variability of the transverse mechanical properties is higher in the transverse direction than its variability in the longitudinal direction.
- Spatial variability in the transverse strength and the transverse strain to failure is lower than it is in the local elastic modulus.
- Transverse position of the failure section changes randomly in the each board.
- Main reason for the spatial variability of the local elastic modulus is irregular changes in the mesostructure of the wood. The change in the angle between the tangential direction and the transverse axis of the specimen is the most important factor influencing the local elastic modulus.
- Knots can substantially change the mechanical properties of the clear wood around them.

Due to the low transverse mechanical properties of timber, in-depth research on the naturally existing random spatial variability is of particular importance, especially for those applications where the transverse stress component is relatively high such as timber joints. The results of this study can be considered as part of establishing advanced stochastic models capable of handling different kind of variability in the solid timber properties.

5.6 References

[1] Barrett, J.D., 1974. Effect of size on tension perpendicular-to-grain strength of Douglas-fir. Wood and Fiber 6, 126-143.

[2] Vořechovský, M., 2007. Interplay of size effects in concrete specimens under tension studied via computational stochastic fracture mechanics. International Journal of Solids and Structures 44, 2715-2731.
[3] Sriramula, S., Chryssanthopoulos, M.K., 2013. An experimental characterisation of spatial variability in GFRP composite panels. Structural Safety 42, 1-11.
[4] Dinwoodie, J.M., 2000. Timber: Its nature and behaviour. Taylor & Francis Group.
[5] Tannert, T., Vallée, T., Hehl, S., 2012. Probabilistic strength prediction of adhesively bonded timber joints. Wood Science and Technology 46, 503-513.
[6] Tannert, T., Vallée, T., Hehl, S., 2012. Experimental and numerical investigations on adhesively bonded timber joints. Wood Science and Technology 46, 579-590.
[7] Brandner, R., Schickhofer, G., 2014. Spatial correlation of tensile perpendicular to grain properties in Norway spruce timber. Wood Science and Technology 48, 337-352.
[8] Pedersen M.U., Clorius C.O., Damkilde, L., Hoffmeyer P., 2003. A simple size effect model for tension perpendicular to the grain. Wood Science and Technology 37, 125-140.
[9] Xavier J., Avril S., Pierron F., Morais J., 2009. Variation of transverse and shear stiffness properties of wood in a tree. Composites: Part A 40, 1953-1960.
[10] Pereira, J., Xavier J., Morais J., Lousada J., 2014. Assessing wood quality by spatial variation of elastic properties within the stem: Case study of Pinus pinaster in the transverse plane. Canadian Journal of Forest Research 44, 107-117.
[11] Forest Product Laboratory, 1999. Wood handbook: Wood as an engineering material, USDA, Madison, Wis.
[12] Clouston, P.L., Lam, F., 2002. A stochastic plasticity approach to strength modeling of strand-based wood composites. Composites Science and Technology 62, 1381-1395.
[13] Clouston, P.L., Lam, F., 2001. Computational modeling of strand-based wood composites. Journal of Engineering Mechanics 127, 844-851.
[14] Tannert, T., Lam, F., Vallée, T., 2010. Strength prediction for rounded dovetail connections considering size effects. Journal of Engineering Mechanics 136, 358-366.

6 A non-intrusive stochastic finite element framework: Application to bonded timber joints

6.1 Introduction

Behavior of engineering systems is significantly affected by the presence of uncertainties [1]. Concerning engineering structures, uncertainties mainly exist in external loading, environmental conditions, geometry, and material properties. When structures made of composite and timber are concerned, the quantification of uncertainty in the material properties and evaluation of its effect on the structural response has received more attention by researchers [1-8]. This is because the level of uncertainty in the properties of these materials is so high that it usually acts as the main factor causing the uncertainty in the structural response. The material properties are random in a spatial manner and this is referred to as the random spatial variability (RSV).

By taking advantage of the recent fast growing computational power, more realistic numerical models, capable of evaluating the uncertainty in the structural response, are developing. One of the most powerful tools for this purpose is the stochastic finite element (SFE) method, which is the combination of the traditional finite element method and stochastic analyses [4]. Recently, it has been shown that consideration of the spatial variability in probabilistic analysis of structures has a major impact on the final stochastic structural response [6,9-10]. In these studies, it is noted that taking into account the spatial variability effect can lead to a more efficient use of materials and reliability estimations with higher accuracy. A recent comprehensive review on different aspects of SFEM can be found in [4].

The main drawback of this method is that it is computationally highly expensive. This becomes more critical noting that in the majority of the previous works in this field, the developed SFE framework is intrusive, meaning that the core procedures of the traditional finite element method needs to be modified [11]. For examples, new terms should be added to the global stiffness matrix of the problem. This can also lead to the dependency of the random field discretization to the finite element discretization, which can increase the time needed for the generation of realizations. This is especially true when a coarser mesh suffices for accurately discretizing the random field. For these reasons, the intrusive approach makes it very difficult to take advantage of the fast finite element algorithms developed in the powerful third party

finite element packages, such as ABAQUS, to examine the effect of RSV on the behavior of structural systems.

A very limited amount of previous works have implemented the SFE to study the stochastic response of the timber structures [12,13]. However, no previous study in the literature has been devoted to investigate the effect of the RSV on the stochastic response of clear solid timber structures. A very recent review on the stochastic finite element approaches for wood-based products can be found in [14].

In this chapter, the efficient spectral representation method was used in connection with the commercial finite element software ABAQUS to evaluate the stochastic response of the structures with spatially random material properties. Also, for the first time, an SFE framework was used to model the behavior of a clear solid timber component with random spatial variability. The realizations of the material properties, taking into account the correlations between the elastic and strength parameters as well as size effects, were generated in MATLAB, based on the spectral representation scheme. These realizations were imported into ABAQUS via UEL subroutine, specifying the material properties at each element integration point. Adhesively bonded double-lap timber joints with different overlap lengths were selected to demonstrate the potential of the established framework for solving real world stochastic problems. The Monte Carlo method was used to determine the stochastic elastic response of the structure. The Norris criterion was used to obtain the failure index at each element Gauss point. The maximum failure index in each sample joint was used to calculate the failure load of that sample. With sufficient number of sample joints, the statistics of the load-bearing capacity of the joint was estimated. This estimation was compared to the available experimental data from the literature.

6.2 Modeling procedure

The detailed procedure of the developed SFE framework is presented in this section. The procedure is illustrated in the flowchart shown in Fig. 6.1. The stochastic data and random field discretization data are needed to start the modeling. The stochastic data include statistical distributions for elastic and strength parameters, linear correlation coefficients between elastic and strength parameters and random field correlation lengths and correlation functions. The discretization data is a set of coordinates of points at which the values of the random field are needed, for example the element integration points in a finite element model. However, depending on the correlation length/lengths, a smaller set of coordinates may also be chosen, without reducing the accuracy of discretization.

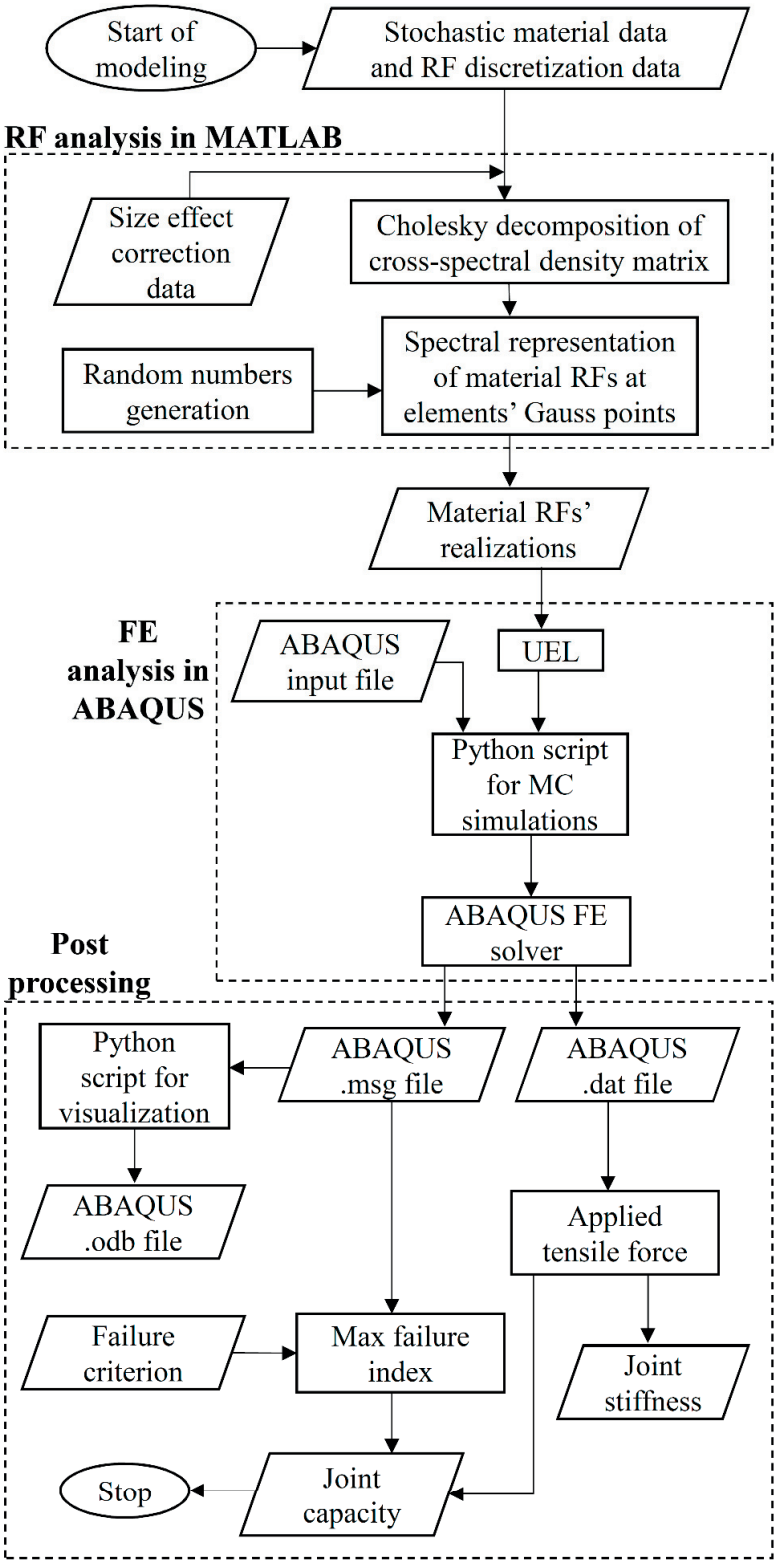

Fig. 6.1: Flowchart of developed stochastic finite element framework.

The spectral representation scheme is used for modeling the material properties as 2D random fields which is the most accurate and efficient method for generating realizations of random fields [15]. The detailed procedure of generating realizations of multivariate stochastic fields can be found in [16] for Gaussian fields and in [17] for non-Gaussian fields. In the present study, the realizations represent the values of material parameters at element in integration points. Each integration point, in turn, represents a part of the corresponding element surrounding the point. The experimental input data for the statistics of strength parameters are normally from mechanical tests on specimens with specific sizes. The specimens' sizes are usually different from the size of the material surrounding the integration points. Therefore, a size effect adjustment should be applied to these statistics before generating the realizations. The 2D version of size effect model proposed in Chapter 2 is used for this purpose. In this size effect model, the mean value is changed considering the related sizes, while the COV remains constant. To keep COV constant, the standard deviation should also be modified. These modifications were considered in this study.

For cross-correlated/multivariate random fields, for example longitudinal modulus and longitudinal tensile strength of timber which are normally correlated, a cross-spectral density matrix, containing power spectral density functions, has to be constructed. Since, in the current study, only pair-wise correlations between each elastic modulus and its related strength were considered, the matrix dimensions were 2×2. These matrices were decomposed following the Chelosky method [16] and, along with random numbers generated by 'rand()' function in MATLAB, used to generate the realizations. The total number of realizations depend on the total number of simulations for the chosen finite element model and the number of parameters involved. For the case study of this chapter, six realizations, corresponding to elastic and strength parameters of clear timber, for each simulation were generated.

A python script was written and used in ABAQUS to conduct the Monte Carlo simulations for the finite element model that receives information from ABAQUS input file and ABAQUS user-defined element subroutine (UEL) . For each simulation, the input file defines the geometry, element type, finite element meshing and boundary conditions for the finite element model. Also, the UEL subroutine was written for a 4-node quadrilateral element in a plane stress state that reads the values for the material parameters for each element integration point from the generated realizations. The python script sends these information to the ABAQUS finite element solver.

The results of each finite element simulation are stored in a .msg file for stresses, strains and displacements and in a .dat file for boundary reaction forces. A python script was also written in ABAQUS for the visualization of the results which can also be used to visualize the realizations. The rest of the post processing shown in Fig. 6.1 is focused on the case study of Section 6.3. The necessary explanations are given in that section.

6.3 Case study on an adhesively-bonded timber joint: Geometry and properties

As a real world structure, a double-lap adhesively-bonded timber joint was chosen to illustrate the capability of the developed SFE framework. The behavior of the joint was investigated under tensile loading. The parameters used for the joint dimensions and also boundary conditions are shown in Fig. 6.2 which is not the scale. To be able to compare the simulation results to the available experimental results in the literature, the tested joints in [18] were selected. The dimensions are as follows: $a = 38\,\text{mm}$, $b = 19\,\text{mm}$, $c = 10\,\text{mm}$, $d = 1\,\text{mm}$. Three values for the overlap length L were considered: 80 mm, 160 mm and 320 mm. A small fillet of 0.5 mm radius was also considered for the adhesive at the corners. Tensile displacement boundary conditions were applied to the two ends. A uniform element size of 0.5×0.5 mm^2 was considered for meshing the joint. Preliminary finite element modeling showed that this mesh is sufficiently fine for the high stress gradient near the joint corners.

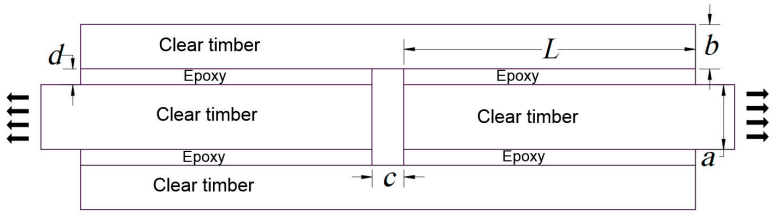

Fig. 6.2: Nomenclature and boundary conditions of bonded joint.

The joint is made of clear beech adherends connected by epoxy adhesive with elastic modulus $E_{ep} = 4.56\,\text{GPa}$ and Poisson ratio $\nu_{ep} = 0.37$. The statistics of the material parameter of beech as an orthotropic material, needed for modeling the joint are given in Table 6.1 [18,19]. S_x and S_y are tensile strengths. A linear correlation coefficient of 0.7 was also considered for each pair of elastic modulus and its corresponding strength parameter. Since no information regarding the type of the statistical distributions for the material parameters were available, the normal distribution was used.

Table 6.1: Statistics of material parameters for clear beech.

	E_x (GPa)	E_y (GPa)	ν_{xy}	G_{xy} (GPa)	S_x (MPa)	S_y (MPa)	S_{xy} (MPa)
Mean	14.5	0.79	0.37	1.3	95.9	13.76	15.8
COV	12.0	10.0	-	10.0	21.5	10.0	10.0

Since there are no values available in the literature for the correlation lengths of beech material parameters, as random fields, it was assumed that all the parameters have the same correlation length, independent of the fiber direction. An approach similar to that of Chapter 2 was used for estimation of the correlation length. By extensive numerical experimentation on joint with 160 mm overlap length, assuming different values for the correlation length, i.e. trial and error approach, the appropriate value was found to be 16.0 mm. This value was also used for modeling joints with other overlap lengths. Using this value, a fairly good agreement between the simulation results for the joint capacity and the experimental data was obtained, as discussed in Section 6.4. For higher correlation lengths, the agreement was lower. For the lower correlation lengths, however, often occurred non-realistically extremely high failure indices at one or more element integration points. The reason was that, due to the high COV of S_x, there were often extremely low values for S_x in each realization. Using the written Python script, a realization of the longitudinal tensile elastic modulus for the bonded joint is visualized in Fig. 6.3.

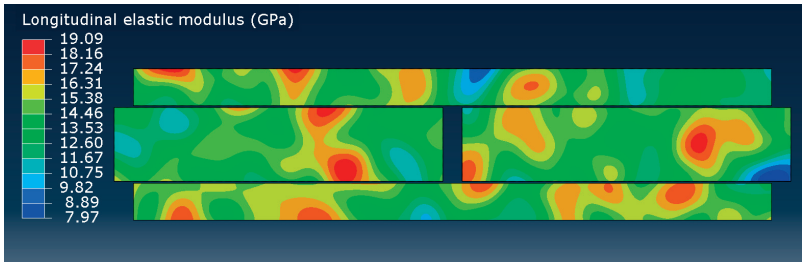

Fig. 6.3: A realization of longitudinal elastic modulus for bonded joint of 160 mm overlap length.

In the process of obtaining the joint capacity in each simulation, first the 2D Norris criterion, given in Eq. (6.1), was used to calculate the failure index, *FI*, in all the element integration points. It was found that the maximum *FI* always occurs in the joint corners. The square root of the maximum *FI* was used for the normalization of the applied tensile loading, noting that there is a linear relationship between the applied loading and the square root of the maximum *FI*. In simpler words, the failure tensile load was determined by setting the square root of the maximum *FI* to 1.0.

$$FI = \max\left\{\left(\frac{\sigma_x}{S_x}\right)^2 - \left(\frac{\sigma_x\sigma_y}{S_xS_y}\right) + \left(\frac{\sigma_y}{S_y}\right)^2 + \left(\frac{\tau_{xy}}{S_{xy}}\right)^2;\ \left(\frac{\sigma_x}{S_x}\right)^2;\ \left(\frac{\sigma_y}{S_y}\right)^2\right\} \tag{6.1}$$

6.4 Results and discussions

Two hundred simulations were conducted to estimate the statistics of the bonded joint capacity under tensile loading for each overlap length. In two of the simulations for the case of 160 mm overlap length, extremely high failure indices were found inside the inner adherends due to very low values of longitudinal tensile strength, S_x, at a few element integration points. This was because the variability of S_x is higher than the other strength parameters, as given in Table 6.1. Therefore, the probability of occurrence of lower values was higher for this parameter which lead to extremely high failure indices in two of the simulations. In two other simulations, maximum failure indices in the joint were obviously separate from the rest of the population of maximum failure indices and were deleted as outliers. Therefore, the results of the remaining 196 simulations are presented in this section. The failure locations as well as the total number of failures at each location are shown in Fig. 6.4. The failure always occurred at the corners: In 154 simulations, at the outer corners and in 42 simulations at the inner corners. In [18], it is reported that in the experiments, the joints almost always failed at the outer corners. This might be due to limited number of tests performed (21 in total for different overlap lengths). In simulations, it was observed that the stresses at the inner corners were slightly lower than outer corners; therefore, due to the random spatial variations of the mechanical properties, failure occurred at the inner corners in almost 20% of simulations. In cases of 80 mm and 240 mm overlap lengths, there were 2 and 5 outliers in the simulations, respectively, that were discarded.

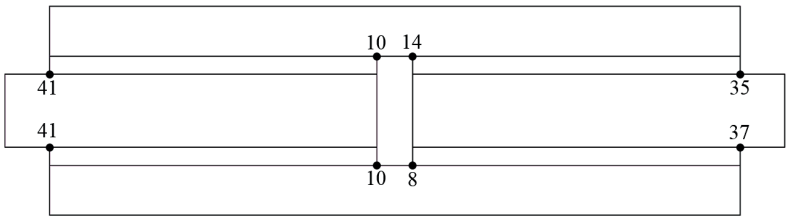

Fig. 6.4: Failure locations for bonded joint of 160 mm overlap length under tensile loading and number of failures occurred at each location.

The joint stiffness is defined as the applied force per unit change of joint total length. Figure 6.5 shows the histograms for the stiffness of the bonded joint of 160 mm overlap length from numerical simulations along with fitted probability density functions (PDFs). The PDFs of three common statistical distributions, normal, lognormal and Weibull, have been fitted to the simulation results. The difference between the PDFs of normal and lognormal distributions is negligible and both are better fitted than the PDF of Weibull distribution. A mean value of 98.44 kN/mm and a COV of 1.96 % was obtained for the joint stiffness. It is seen that the ca. 10% COV of the elastic moduli of the clear beech lead to ca. 2% COV for the joint stiffness. This is

due to the fact that in each sample joint, the elastic moduli at all the integration points contribute to the joint stiffness, reducing its COV. However, the type of the statistical distribution for the joint stiffness remained the same as that of the elastic moduli.

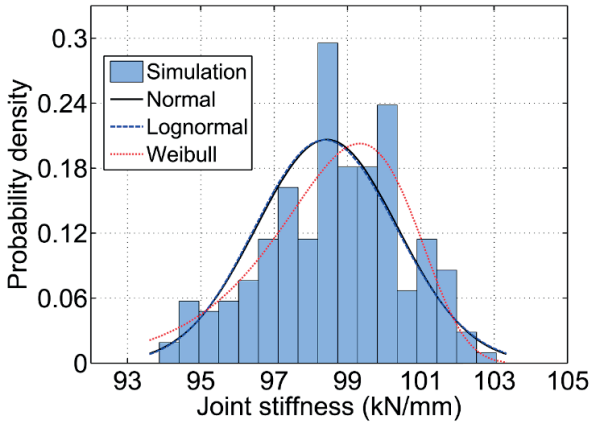

Fig. 6.5: Probability density functions fitted to simulation results for joint stiffness.

Mean joint stiffnesses for different overlap lengths are shown in Fig. 6.6. Error bars indicate standard deviations. The stiffness is reduced significantly as overlap length increases. This is simply because a longer joint will deform more than a shorter joint under the same loading. Figure 6.7 shows the force need to impose 1% strain in the joints. It is seen that, in this way of representing joint elastic resistance, the required force increases and gradually levels off.

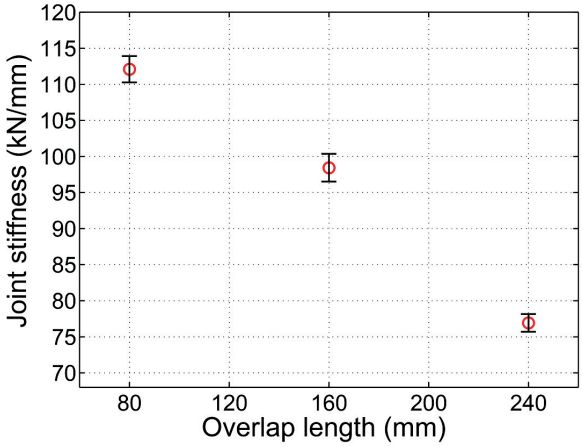

Fig. 6.6: Joint stiffness versus overlap length.

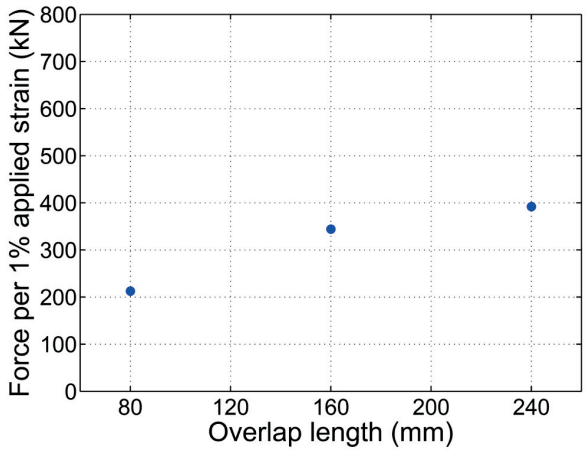

Fig. 6.7: Tensile force required for imposing 1% tensile strain in joints for different overlap lengths.

The bonded joint capacity from numerical simulations are shown in Fig. 6.8 for overlap length of 160 mm. The same type of statistical distributions were also fitted to the joint capacity results. Interestingly, the Weibull distribution was found to be the best fitted statistical distribution in this case, in spite the assumption of normal distribution for the input parameters. This can be due to the brittle failure considered for the joint.

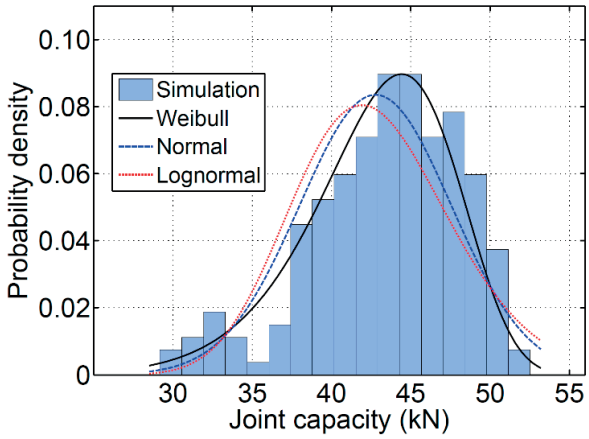

Fig. 6.8: Probability density functions fitted to the simulation results for the capacity of joint with 160 mm overlap length.

The joint capacity from the numerical simulations for different overlap lengths are presented in Fig. 6.9. The error bars indicate the standard deviations. The numerical and experimental results from [18] are also shown for comparison purposes. The statistics of the current simulations and the experiments from [18] are given in Table 6.2. It is seen that there is a fairly good agreement

between the experimental results in [18] and current simulations. In the current simulations, there is a significant increase in the joint capacity from 80 mm to 160 mm overlap length. From 160 mm to 240 mm, there is a slight increase in the joint capacity and the capacity levels off. The same trend exists in the finite element results from [18], but with a large bias in the results. The average error in the current simulations compared to the experiments is 18.9 %. This is a major improvement in modelling accuracy compared to the modeling results reported in [18] for the same joint, where the average prediction error for the mean value of the joint capacity was 73 %.

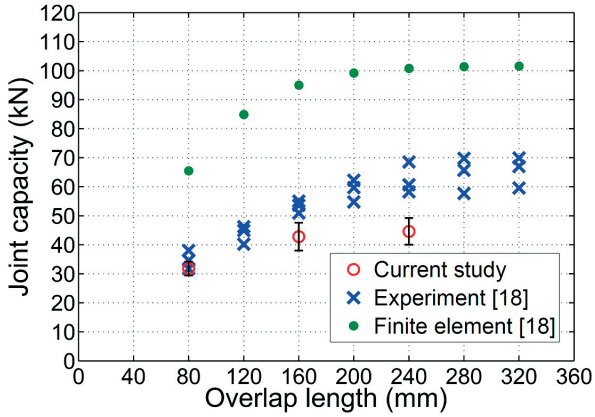

Fig. 6.9: Joints capacities versus overlap lengths for conducted simulations and comparison with experimental and numerical results from [18].

Table 6.2: Statistics of bonded joint capacity for different overlap lengths from current simulations and experiments in [18].

Overlap length	Mean value from simulations (kN)	COV from simulations (%)	Mean value from experiments (kN) [18]	COV from experiments (%) [18]
80	31.8	7.58	34.8	9
160	42.8	11.2	53.2	4
240	44.6	10.3	62.5	9

The joint stiffness and capacity results from simulations were further examined for the possibility of a correlation. The scatter plot for the joint capacity versus joint stiffness is shown in Fig. 6.10, for overlap length of 160 mm. A linear correlation coefficient of 0.38 was obtained between the joint stiffness and joint load-bearing capacity, indicating a relatively weak linear relationship between the two parameters.

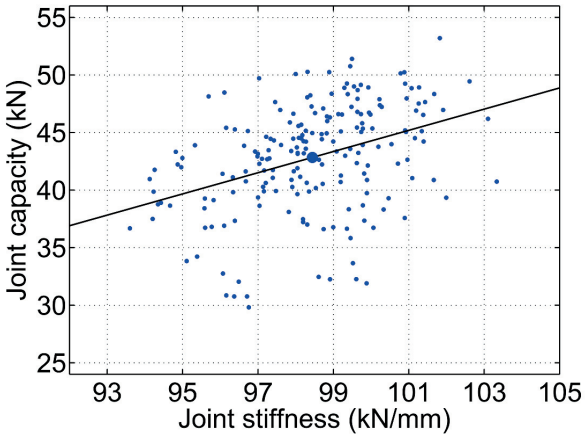

Fig. 6.10: Correlation between capacity and stiffness of joint with 160 mm overlap length.

6.5 Conclusions

A stochastic finite element framework for structural analysis was developed that, for the first time, combines the efficient spectral representation scheme, for generating realizations, with the powerful commercial finite element software ABAQUS in a non-intrusive manner. Also, for the first time, the effect of RSV in clear timber on the structural response of solid clear timber structures was studied in this chapter. The case study was performed for an adhesively-bonded double-lap timber joint under tensile loading. The main conclusions drawn from this chapter are summarized as follows:

- The developed SFE framework facilitates the transferring of the realizations of the material properties to the element integration points due to its non-intrusive feature.
- The case study of the bonded timber joint based on the Monte Carlo method demonstrated the applicability of the SFE framework to real world structural problems. The mean value of the joint capacity predicted in this work was in fairy good agreement with experimental results. It was also a major improvement compared to the existing model used for analyzing the same joint in the literature. The Weibull distribution was fitted very well to the simulation results for the joint capacity.
- The mean joint stiffness decreased with increase in the overlap length. The predicted COV of the modelled joint stiffness were significantly lower than the COV of the elastic moduli of the clear timber. A weak correlation of 0.38 was obtained between the joint stiffness and capacity.

The development of accurate stochastic modeling frameworks, as in this thesis, can significantly reduce the cost of conducting a large number of experiments on new structures/components exhibiting significant randomness in their response under external loadings. Application of the developed framework in ABAQUS to other real

structures/components will help the development of SFE simulations into industrial design analyses.

6.6 References

[1] Chiachio, M., Chiachio, J., Rus, G., 2012. Reliability in composites - A selective review and survey of current development. Composites Part B: Engineering 43, 902-913.
[2] Sriramula, S., Chryssanthopoulos, M. K., 2009. Quantification of uncertainty modelling in stochastic analysis of FRP composites. Composites Part A: Applied Science and Manufacturing 40, 1673-1684.
[3] Lekou, D.J., Philippidis, T.P., 2008. Mechanical property variability in FRP laminates and its effect on failure prediction. Composites Part B: Engineering 39, 1247-56.
[4] Stefanou, G., 2009. The stochastic finite element method: Past, present and future. Computer Methods in Applied Mechanics and Engineering 198, 1031-51.
[5] Spanos, P., Kontsos, A., 2008. A multiscale Monte Carlo finite element method for determining properties of polymer nanocomposites. Probabilistic Engineering Mechanics 23, 456-70.
[6] Noh, H-C., 2011. Stochastic finite element analysis of composites plates considering spatial randomness of material properties and their correlations. Steel and Composite Structures 11, 115-30.
[7] Carbillet, S., Richard, F., Boubakar, L., 2009. Reliability indicator for layered composites with strongly non-linear behaviour. Composites Science and Technology 69, 81-7.
[8] Sriramula, S., Chryssanthopoulos, M.K., 2013. An experimental characterisation of spatial variability in GFRP composite panels. Structural Safety 42, 1-11.
[9] Rollet, Y., Bonnet, M., Carrere, N., Leroya, F-H., Maire, J-F., 2009. Improving the reliability of material databases using multiscale approaches. Composite Science Technology 69, 73-80.
[10] Shaw, A.J., Sriramula, S., Gosling, P.D., Chryssanthopoulos, M.K., 2010. A critical reliability evaluation of fibre reinforced composite materials based on probabilistic micro and macro-mechanical analysis. Compos Part B Engineering 41, 446-53.
[11] Sudret, B., der Kiureghian, A., 2000. Stochastic finite element methods and reliability: a state-of-the-art report, Rep. No. UCB/SEMM-2000/08, University of California at Berkeley, USA.
[12] Wang, Y.T., Foschi, R.O., 1992. Random field stiffness properties and reliability of laminated wood beams. Structural Safety 11, 191-202.
[13] Jeong, G.Y., Park, M.J., Park, J.S., Hwang, K.H., 2012. Predicting load-carrying capacity of dovetail connections using the stochastic finite element method. Wood and Fiber Science 44 430-439.

[14] Kandler, G., Füssl, J., Eberhardsteiner, J., 2015. Stochastic finite element approaches for wood-based products: theoretical framework and review of methods. Wood Science and Technology 49 1055-1097.

[15] Stefanou, G., Papadrakakis, M., 2007. Assessment of spectral representation and Karhunen-Loève expansion methods for the simulation of Gaussian stochastic fields. Computer Methods in Applied Mechanics and Engineering 196, 2465-2477.

[16] Deodatis, G., 1996. Simulation of ergodic multivariate stochastic processes. Journal of Engineering Mechanics 122, 778-787.

[17] Shields, M.D., Deodatis, G., 2013. A simple and efficient methodology to approximate a general non-Gaussian stationary stochastic vector process by a translation process with applications in wind velocity simulation. Probabilistic Engineering Mechanics 31, 19-29.

[18] Tannert, T., Vallee, T., Hehl, S., 2012. Experimental and numerical investigations on adhesively bonded hardwood joints. International Journal of Adhesion and Adhesives 37, 65-69.

[19] Niemz, P., 2011. Ermittlung elastomechanischer Kennwerte von Rotbuchenholz, Projektnummer: 2010.09, ETH Zurich, Switzerland.

7 Conclusions and future research

7.1 Conclusions

A stochastic analysis of the variability of the mechanical properties of clear timber and the associated variability in the response of clear timber joints was performed in this thesis. The random spatial variability in the longitudinal and transverse tensile properties and the correlations between elastic and strength parameters were experimentally investigated at the mesoscale. Size effects were also experimentally studied. A random field-based size effect model for clear timber strength was developed. A stochastic finite element framework was established for the stochastic analysis of clear timber structures. This stochastic finite element framework was used together with the size effect model to simulate the behavior of a double-lap adhesively-bonded timber joint, and a comparison was made with the experimental data available in the literature. The main conclusions drawn from the experimental and theoretical results are summarized in this section.

7.1.1 Experimental investigations

- A new, simple specimen geometry was proposed for longitudinal tensile tests on clear timber and used for the characterization of the random spatial variability of the longitudinal mechanical properties. Using this geometry, the failure in almost all specimens occurred in their middle part that had a constant cross-sectional area. For the characterization of spatial variability in the longitudinal elastic modulus, the longest specimens, i.e. 128 mm, were used, since they better represented the spatial variability of the modulus. A change in the longitudinal local elastic modulus of more than 100% was observed along the length of certain specimens. The contribution of the between-specimen variability to the total/ensemble variability was greater than that of the within-specimen variability. The main reason for this spatial variability of the longitudinal local elastic modulus was found to be irregular changes in the mesostructure of the wood, including fiber misalignment, fiber waviness and variable growth ring thickness.
- The coefficient of variation of the effective elastic modulus in the longitudinal direction was also thoroughly investigated. The coefficient of variation reached values as high as 12.7% for the longer specimens of 128-mm length, while it attained the maximum value of ca. 20% for the short specimens. The mean value of the modulus does not change significantly with specimen length. Also, a maximum value of 113.0 MPa was obtained

for the mean value of the longitudinal tensile strength for very small specimen nominal lengths. The mean value decreased to 103.8 MPa for a length of 128 mm. The change in the coefficient of variation of the tensile strength with specimen length was negligible, with an average value of 15.1%. The variation of the mean strength with specimen size cannot be appropriately modeled by the classical Weibull size effect law.

- Timber boards with regularly positioned and randomly positioned specimens were used for the probabilistic characterization of transverse mechanical properties. The statistical analyses revealed that a cutting plan with regularly positioned specimens could lead to an underestimation of the coefficient of variation of the mechanical properties. This was particularly shown in the case of 8-mm-long specimens with a regular arrangement in the respective boards. A difference of more than 1000% was observed in the effective transverse elastic moduli of clear spruce wood specimens. The coefficient of variation of the effective transverse elastic modulus decreases as length increases.
- The classical Weibull size effect law was sufficiently accurate for describing the size effect observed in results for the transverse tensile strength of clear timber specimens of different lengths. This was in contrast to the case of the longitudinal tensile strength. Four types of failure were observed in the specimens cut in the transverse direction, exhibiting different mean transverse strengths. The strengths were higher when the grain angle was lower. The analysis of variance confirmed that the differences were statistically significant. Also, the transverse position of the failure section changed randomly in each board.
- The spatial variability of the transverse mechanical properties is higher in the transverse direction than in the longitudinal direction. The spatial variability in the transverse strength and transverse strain to failure is lower than in the local elastic modulus. The change in the grain angle is the most important factor for creating the random spatial variability in the case of the local elastic modulus. It was also shown, in a few cases, that knots can substantially change the mechanical properties of the clear wood surrounding them.

7.1.2 Theoretical investigations

- The application of the classical Weibull size effect law to the experimental data for the longitudinal tensile strength in the literature showed a very high level of error. A random field-based numerical size effect model was proposed and used to predict the effect of size on the longitudinal tensile strength. Good agreement with the experimental data was obtained. An analytical formula for the size effect on the strength was also proposed that closely approximates the numerical results and facilitates the application of the current model.

- The proposed size effect model for clear timber strength predicts an upper bound for the timber strength as specimen dimensions approach zero. On the other hand, when the dimensions are sufficiently large compared to the correlation length of the strength field of the timber, the result obtained by the current model approaches that of the classical Weibull size effect law. Using experimental data from the literature, values of 62 mm and 225 mm for the correlation lengths of the strength fields of spruce and Japanese larch were obtained. These values can be used in the stochastic simulation of timber structures under different loading conditions such as bending. Also, this indicates that the correlation length of the strength field in timber can vary significantly between different species.
- The developed stochastic finite element framework takes advantage of the fast algorithms of the spectral representation scheme for generating realizations. It also allows independent meshing for finite element and random field discretization, which is easier to handle. It can also lead to less CPU time for generating each realization, if a coarser mesh suffices for random field discretization. Another advantage is that it enables the use of powerful third party finite element codes, such as ABAQUS.
- The stochastic finite element framework was used for modelling double-lap adhesively-bonded timber joints with different overlap lengths. The model response for the load-bearing capacity of the joint agreed fairly well with the available experimental data and was a major improvement compared to the model used in the literature to predict the capacity of the same joints. A linear correlation coefficient of 0.38 was obtained between the joint stiffness and joint load-bearing capacity, showing a relatively weak linear relationship between the two parameters. The development of accurate stochastic modelling frameworks, as in this thesis, can significantly reduce the cost of conducting a large number of experiments on timber structures/components exhibiting considerable randomness in their response under external loadings. In traditional designs, safety factors are applied to the characteristic values of strength parameters to obtain the design values. Sufficiently high safety factors are normally chosen to guarantee the safety of structures in different working conditions. However, this safety factor is a rough value and can be too conservative, or it can even significantly overestimate structure reliability. The accurate determination of the spatial variability effect on the stochastic response of timber structures can result in more reliable timber designs for different structures and loading conditions.

7.2 Original contributions

The original contributions of the thesis to the topic and the respective research field are listed below:

- A random field-based model was proposed to investigate the size effect on the strength of clear timber and validated. It was shown that this model is much more accurate than the classical Weibull size effect law when small clear specimens are concerned. A new reversed approach, based on the experimental size effect results, was used for estimation of the correlation length of the strength field.
- The random spatial variability of the longitudinal elastic modulus of clear timber was experimentally characterized. The size effect was also investigated. It was experimentally proved that there is an upper bound for the longitudinal mean strength when the specimen length diminishes. The correlation between the longitudinal modulus and strength at mesoscale was also obtained.
- The random spatial variability of the transverse mechanical properties of clear timber was experimentally characterized. The experimental data relating to the size effect on the clear timber strength for small volumes of material were provided. Experimental data concerning the correlation between the transverse strength and transverse elastic modulus at the mesoscale were provided.
- A stochastic finite element framework was developed for clear timber components. The framework was used to model the behavior of adhesively-bonded timber joints under tensile loading and the applicability of the model was demonstrated.

7.3 Recommendations for future research

Although a major experimental campaign was conducted in this work, several aspects of the topic still need to be addressed by further experimental research. The developed numerical models can also be enhanced/extended. The recommendations for further research to continue the current study are discussed below.

- In the current study, the experimental characterization of the random spatial variability of the mechanical properties of clear timber was performed under longitudinal and transverse tensile quasi-static loading. More experiments are needed to characterize the random spatial variability of the shear modulus and strength. The random spatial variability of the compressive mechanical properties is also important in cases with dominant compressive loadings.
- In addition to quasi-static behavior, the plastic behavior, creep behavior and fatigue behavior of timber structures can be important for practical applications. In these cases, the random spatial variability of the respective material parameters is required in order to evaluate the effect of the random spatial variability on the stochastic structural response.

- The random spatial variability in spruce wood, which is widely used for construction purposes, was investigated in this thesis. The characterization of the random spatial variability for other species could also form the subject of further research.
- With further analyzing the experimental data regarding the random spatial variability in the current study, the correlation lengths of the longitudinal and transverse elastic moduli of spruce wood can directly be obtained.
- In modelling the random spatial variability, the same correlation length in the longitudinal and transverse directions was assumed for the material properties as a simplification. In practice, the correlation length is likely to be different for different directions and further investigation is needed. Research is also necessary to determine which correlation function can best characterize the correlation in the material property fields of clear timber.
- The commonly used transversely isotropic behavior was adopted for modelling timber in this thesis. With the extension of the stochastic finite element framework to three dimensions, it is possible to consider the difference in timber behavior in the radial and tangential directions and thus improve the accuracy of the model.
- The established stochastic finite element framework is applicable to clear timber structures or structures in which knots have no effect on failure initiation. This framework can be used as a basis and extended for modelling timber structures in which knots play an important role in the determination of the load-bearing capacity of the structure, such as frames made of industrial lumbers in which bending loads are present.
- More investigations are required to examine the efficiency of the stochastic finite element framework in modelling timber structures other than adhesively-bonded timber joints. Also, to facilitate the use of the model for non-experts, the entire modeling procedure, as explained in Chapter 6, can be included in software. The inputs and outputs would also be the same as for the case examined in Chapter 6.

Curriculum Vita

Alireza FARAJZADEH MOSHTAGHIN

EPFL
ENAC-CCLAB
BP 2222, Station 16
CH-1015 Lausanne, Switzerland
Tel: +41 78 880 14 96
Email: a.f.moshtaghin@gmail.com

Strengths

- Composite and Timber Structures
- Numerical Simulation for Solid Structures
- Stochastic and reliability Analyses
- Micro- and Nanomechanics

Education

- PhD: Ecole Polytechnique Federale de Lausanne, Lausanne, Switzerland — 11.2012-present
- MSc: Sharif University of Technology, Tehran, Iran — 09.2009-11.2011
- BSc: Iran University of Science and Technology, Tehran, Iran — 09.2005-09.2009

Research and Teaching Interests

- Composite materials
- Timber structures
- Nanostructured materials
- Design of experiments
- Damage and fracture mechanics
- Stochastic simulations
- Reliability analysis
- Finite element and Multiscale simulations
- Micromechanics and Nanomechanics
- Nonlinear continuum mechanics(plasticity, …)

Research Experience

Research Assistant
*Composite Construction Laboratory, EPFL, Lausanne, Switzerland (**07.2013-present**)*

- Designing a new geometry for clear timber specimens for tensile tests
- Preparation of tensile, compressive and shear specimens made of timber and testing under quasi static loading. Measuring the material deformations with video-extensometry and strain-guages
- Establishing a model for size effects on the clear timber strength based on the random field theory and validating with experimental results
- Experimental characterization of the random spatial variability in the timber mechanical properties
- Establishing a stochastic finite element scheme for timber structures. A case study for adhesively bonded timber joints and validating with experimental results

Research Assistant
*Timber and Composite Construction, Bern University of Applied Sciences, Biel, Switzerland (**11.2012-06.2013**)*

- Literature review of the available stochastic studies on timber structures
- Studying wood as a material for construction
- Developing a research plan for probabilistic analysis of clear timber structures
- Conducting mechanical tests on timber specimens

Research Assistant
*Computational Mechanics Laboratory, Sharif University of Technology, Tehran, Iran (**09.2010-11.2011**)*

- Establishing a method to investigate the effect of the size of the nanostructure on the elastic and plastic properties of metal-based nanostructured materials based on surface elasticity theory
- Study of the effects of surface residual stress and surface elasticity on the elastic moduli and initial yield surface of nanoporous Aluminum
- Study of the interface effects on the elastic moduli, initial yield surfaces and non-linear hardening behavior of Aluminum-Carbon nanotube composites
- Simulation of the buckling of Carbon nanotubes and multilayer graphene sheets with non-linear van der Waals interactions under different boundary conditions

Research Assistant
*Advanced Composites Laboratory, Iran University of Science and Technology, Tehran, Iran (**09.2008-07.2009**)*

- Development of a hybrid finite element-molecular mechanics model based on the unit-cell concept for polymer-Carbon nanotube composites
- Study the effects of Carbon nanotube waviness and misalignment on the effective elastic moduli of polymer-Carbon nanotube composites

Teaching Experience

- Assistant for Advanced Composites for Engineering Structures at EPFL (2013-2015).
- Assistant for Strength of Materials Lab at Sharif University of Technology (2010-2011)
- Assistant for Engineering Mechanics, Statics, at Sharif University of Technology (2010-2011)
- Assistant for Mechanics of Nanostructures at Sharif University of Technology (2010- 2011)

Industrial Experience

Saipapress Company, Tehran, Iran (3-month internship **2007**)
A major car company, produces car frames

- Working as an engineer for quality control of car body and frames using mechanical and optical tools and filling out check sheets
- Working as an engineer for maintenance and repairing heavy metal forming presses

Iran Composites Institute, Tehran, Iran (3-month internship **2009**)
An institute for conducting industrial projects based on composite materials

- Getting familiar with practical fabrication processes for composite materials such as hand lay-up and filament winding and fabricating glass fiber-polymer composite plates
- Fabricating glass fiber-polymer composite plates

Iran Composites Institute, Tehran, Iran (Part-time job **2011-2012**)

- Worked as an assistant for design and fabrication of a set-up for compression test
- Worked on a project for measuring residual stresses in composite tubes using strain gages and a CNC machine for cutting grooves on the outer surface of the tubes

Publication

Journal Papers

1. **Moshtaghin, A.F.**, Naghdabadi, R., Asghari, M., 2012. Effects of surface residual stress and surface elasticity on the overall yield surfaces of nanoporous materials with cylindrical nanovoids. Mechanics of Materials 51, 74-87. **doi:10.1016/j.mechmat.2012.04.001**
2. **Moshtaghin, A.F.**, Naghdabadi, R., Asghari, M., 2013. A study on the plastic properties of unidirectional nanocomposites with interface energy effects. Acta Mechanica 224, 789-809. **doi:10.1007/s00707-012-0780-3**
3. **Moshtaghin, A.F.**, Franke, S., Keller, T., Vassilopoulos, A.P., 2016. Random field-based modeling of size effect on the longitudinal tensile strength of clear timber. Structural Safety 58, 60-68. **doi:10.1016/j.strusafe.2015.09.002**

4. **Moshtaghin, A.F.**, Franke, S., Keller, T., Vassilopoulos, A.P., February 2015. Experimental characterization of longitudinal mechanical properties of clear timber: Random spatial variability and size effects. Submitted to Construction and Building materials.
5. **Moshtaghin, A.F.**, Franke, S., Keller, T., Vassilopoulos, A.P., December 2015. Transverse mechanical properties of clear timber: Uncertainty and size effects. Submitted to Wood and Science Technology.

Selected Conference Proceedings

1. **Moshtaghin, A.F.**, Franke, S., Keller, T., Vassilopoulos, A.P., 2015. Spatial variability in longitudinal elastic modulus of clear Timber, Euromech Colloquium 556, Dresden, Germany.
2. **Moshtaghin, A.F.**, Franke, S., Keller, T., Vassilopoulos, A.P., 2016. Quantification of spatial variability for transverse elastic modulus of spruce wood, Eccomas Congress, Greece. Accepted.

Computer Skills

- ANSYS
- ABAQUS
- MATLAB
- Mathematica
- SolidWorks
- Fortran
- Python
- C++

Languages

- English: Fluent
- German: Pre-intermediate proficiency
- Persian: Native
- Arabic: Basic understanding

Academic Honors and Awards

- Selected as an exceptional talent for continuing education at Ph.D. level (without any entering exam) at Sharif University of Technology, Tehran, Iran, 2011.
- Ranked 1st among all the graduated M.Sc. students in applied design major (47 people) of Mechanical Engineering Department, Sharif University of Technology, Tehran, Iran, 2011.
- Ranked 1st among all the graduated B.Sc. students (87 people) of Mechanical Engineering Department, Iran University of Science and Technology, Tehran, Iran, 2009.
- Ranked 8th among more than 12,000 participants in M.Sc. entrance exam, Tehran, Iran, 2009.
- Ranked 8th in the final stage of National Mechanical Engineering Olympiad, Tehran, Iran, 2009.
- Honored as an exceptional student, Iran University of Science and Technology, Tehran, Iran, 2007 and 2008.

Extracurricular activities

- Playing football, Ping-Pong and chess
- Reading Persian and English novels
- Participating in Toastmasters EPFL club (A leadership and public-speaking training club)

Personal Information

28, Single, Iranian citizenship, Permit B.